U.S. Department of Transportation

Federal Railroad Administration

Seismic Testing for Track Substructure Assessment

Office of Research,
Development
and Technology
Washington, DC 20590

DOT/FRA/ORD-18/30

Final Report
August 2018

NOTICE

This document is disseminated under the sponsorship of the Department of Transportation in the interest of information exchange. The United States Government assumes no liability for its contents or use thereof. Any opinions, findings and conclusions, or recommendations expressed in this material do not necessarily reflect the views or policies of the United States Government, nor does mention of trade names, commercial products, or organizations imply endorsement by the United States Government. The United States Government assumes no liability for the content or use of the material contained in this document.

NOTICE

The United States Government does not endorse products or manufacturers. Trade or manufacturers' names appear herein solely because they are considered essential to the objective of this report.

REPORT DOCUMENTATION PAGE

Form Approved
OMB No. 0704-0188

1. AGENCY USE ONLY (Leave blank)	2. REPORT DATE	3. REPORT TYPE AND DATES COVERED
	August 2018	Technical Report 08/15/2012 to 02/4/2016

4. TITLE AND SUBTITLE
Seismic Testing for Track Substructure Assessment

5. FUNDING NUMBERS:
FR-RRD-0046-12-01-00

6. AUTHOR(S)
Timothy D. Stark, Carlton L. Ho, Soheil Nazarian, and Stephen T. Wilk

7. PERFORMING ORGANIZATION NAME(S) AND ADDRESS(ES)
University of Illinois
Office of Sponsored Programs & Research Administration
1901 South First Street, Suite A
Champaign, IL 61820

8. PERFORMING ORGANIZATION REPORT NUMBER
Final Report #1

9. SPONSORING/MONITORING AGENCY NAME(S) AND ADDRESS(ES)
U.S. Department of Transportation
Federal Railroad Administration
Office of Railroad Policy and Development
Office of Research, Development and Technology
Washington, DC 20590

10. SPONSORING/MONITORING AGENCY REPORT NUMBER
DOT/FRA/ORD-18/30

11. SUPPLEMENTARY NOTES
COR: Hugh B. Thompson

12a. DISTRIBUTION/AVAILABILITY STATEMENT
This document is available to the public through the FRA Web site at http://www.fra.dot.gov.

12b. DISTRIBUTION CODE

13. ABSTRACT (Maximum 200 words)

The University of Illinois at Urbana-Champaign (UIUC) presented equipment, test procedure, and interpretation techniques to rapidly, non-invasively, and quantitatively measure the engineering properties of track substructure (ballast and subgrade). In particular, seismic surface wave testing with the Spectral Analysis of Surface Waves (SASW) approach was used to estimate the shear-wave velocity, shear modulus, and Young's modulus profiles with depth for track ballast, sub-ballast, and subgrade materials. Seismic wave testing was successfully performed on revenue and non-revenue service track and showed that the average shear-wave velocity of clean ballast varies from 750 to 820 ft/sec (230 to 250 m/sec), which corresponds to a Young's modulus of 30 to 40 ksi (210 to 275 MPa). Due to the general knowledge of a track loading environment, Young's modulus can be inputted into numerical analyses to estimate the stresses and deformations induced in the track structure.

If only the ballast and sub-ballast are of interest, i.e., shallow depth (~1 foot or 0.3 meters), the Ballast Seismic Property Analyzer (BSPA), a hand-held device, can be used to estimate Young's modulus. Additional studies are recommended to modify the BSPA to span two ties to measure the modulus under two adjacent ties to evaluate tie support and load distribution.

14. SUBJECT TERMS
Seismic testing, Spectral Analysis of Surface Waves, SASW, shear-wave velocity, Young's modulus, stiffness, ballast, sub-ballast, track geometry

15. NUMBER OF PAGES
129

16. PRICE CODE

17. SECURITY CLASSIFICATION OF REPORT	18. SECURITY CLASSIFICATION OF THIS PAGE	19. SECURITY CLASSIFICATION OF ABSTRACT	20. LIMITATION OF ABSTRACT
Unclassified	Unclassified	Unclassified	

NSN 7540-01-280-5500
Standard Form 298 (Rev. 2-89)
Prescribed by ANSI Std. 239-18
298-102

METRIC/ENGLISH CONVERSION FACTORS

ENGLISH TO METRIC	METRIC TO ENGLISH
LENGTH (APPROXIMATE)	**LENGTH (APPROXIMATE)**
1 inch (in) = 2.5 centimeters (cm)	1 millimeter (mm) = 0.04 inch (in)
1 foot (ft) = 30 centimeters (cm)	1 centimeter (cm) = 0.4 inch (in)
1 yard (yd) = 0.9 meter (m)	1 meter (m) = 3.3 feet (ft)
1 mile (mi) = 1.6 kilometers (km)	1 meter (m) = 1.1 yards (yd)
	1 kilometer (km) = 0.6 mile (mi)
AREA (APPROXIMATE)	**AREA (APPROXIMATE)**
1 square inch (sq in, in^2) = 6.5 square centimeters (cm^2)	1 square centimeter (cm^2) = 0.16 square inch (sq in, in^2)
1 square foot (sq ft, ft^2) = 0.09 square meter (m^2)	1 square meter (m^2) = 1.2 square yards (sq yd, yd^2)
1 square yard (sq yd, yd^2) = 0.8 square meter (m^2)	1 square kilometer (km^2) = 0.4 square mile (sq mi, mi^2)
1 square mile (sq mi, mi^2) = 2.6 square kilometers (km^2)	10,000 square meters (m^2) = 1 hectare (ha) = 2.5 acres
1 acre = 0.4 hectare (he) = 4,000 square meters (m^2)	
MASS - WEIGHT (APPROXIMATE)	**MASS - WEIGHT (APPROXIMATE)**
1 ounce (oz) = 28 grams (gm)	1 gram (gm) = 0.036 ounce (oz)
1 pound (lb) = 0.45 kilogram (kg)	1 kilogram (kg) = 2.2 pounds (lb)
1 short ton = 2,000 pounds (lb) = 0.9 tonne (t)	1 tonne (t) = 1,000 kilograms (kg)
	= 1.1 short tons
VOLUME (APPROXIMATE)	**VOLUME (APPROXIMATE)**
1 teaspoon (tsp) = 5 milliliters (ml)	1 milliliter (ml) = 0.03 fluid ounce (fl oz)
1 tablespoon (tbsp) = 15 milliliters (ml)	1 liter (l) = 2.1 pints (pt)
1 fluid ounce (fl oz) = 30 milliliters (ml)	1 liter (l) = 1.06 quarts (qt)
1 cup (c) = 0.24 liter (l)	1 liter (l) = 0.26 gallon (gal)
1 pint (pt) = 0.47 liter (l)	
1 quart (qt) = 0.96 liter (l)	
1 gallon (gal) = 3.8 liters (l)	
1 cubic foot (cu ft, ft^3) = 0.03 cubic meter (m^3)	1 cubic meter (m^3) = 36 cubic feet (cu ft, ft^3)
1 cubic yard (cu yd, yd^3) = 0.76 cubic meter (m^3)	1 cubic meter (m^3) = 1.3 cubic yards (cu yd, yd^3)
TEMPERATURE (EXACT)	**TEMPERATURE (EXACT)**
[(x-32)(5/9)] °F = y °C	[(9/5) y + 32] °C = x °F

QUICK INCH - CENTIMETER LENGTH CONVERSION

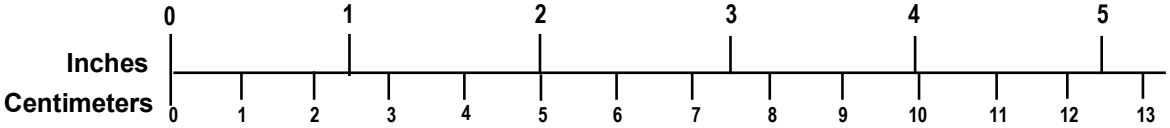

QUICK FAHRENHEIT - CELSIUS TEMPERATURE CONVERSIO

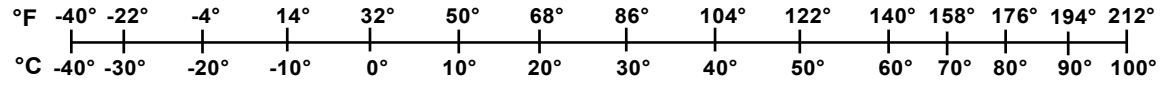

For more exact and or other conversion factors, see NIST Miscellaneous Publication 286, Units of Weights and Measures. Price $2.50 SD Catalog No. C13 10286

Updated 6/17/98

Acknowledgements

The authors would like to acknowledge Amtrak and Steven Chrismer; Paducah & Louisville Railway and Tom Garrett and Gerald Gupton; Transportation Technology Center, Inc. and Colin J. Basye; Union Pacific Railroad and Samuel C. Douglas for providing the track access for field testing of seismic surface waves. The authors also acknowledge the Federal Railroad Administration's Program Manager Mr. Hugh B. Thompson, II, and the U.S. Department of Transportation's John A. Volpe National Transportation Systems Center's Dr. Theodore R. Sussmann, Jr. for their excellent insights and suggestions for modifying the hand-held seismic wave testing device to measure track and ballast properties.

Contents

Illustrations

Tables

Executive Summary

The Federal Railroad Administration (FRA) funded a project performed by the University of Illinois at Urbana-Champaign (UIUC) to evaluate the applicability of seismic surface waves for measuring shear-wave velocity and shear modulus profiles in track structures. The work was executed between August 15, 2012, and February 4, 2016, with testing conducted on revenue and non-revenue service tracks that represented a range of railroad environments.

Test results indicated that seismic surface waves can be used to measure shear modulus to assess track substructure (ballast and subgrade) engineering properties and condition of the track substructure. UIUC presented equipment, test procedure, and interpretation techniques to rapidly, non-invasively, and quantitatively measure the engineering properties of track substructure. In particular, seismic surface wave testing with the Spectral Analysis of Surface Waves (SASW) approach was used to estimate the shear-wave velocity, shear modulus, and Young's modulus profiles with depth for track ballast, sub-ballast, and subgrade materials. Seismic wave testing was successfully performed on revenue and non-revenue service track and showed an average shear-wave velocity of clean ballast varying from 750 to 820 ft/sec (230 to 250 m/sec), which corresponds to a Young's modulus of 30 to 40 ksi (210 to 275 MPa). Due to the general knowledge of a track loading environment, Young's modulus can be inputted into numerical analyses to estimate the stresses and deformations induced in the track structure.

Seismic surface wave principles were used to estimate the shear-wave velocities of different layers under the track structure. In the last 30 years, these principles were implemented in several different approaches, such as the Spectral Analysis of Surface Waves (SASW) and multichannel analysis of surface waves (MASW) to evaluate transportation infrastructure. The common goal in these approaches is to take advantage of the dispersive characteristics of surface waves in a multi-layered structure, such as railroad substructures. When an energy source is coupled to the ground surface, the following three types of waves are generated: shear, compression, and Rayleigh.

Surface wave interpretation techniques focus on Rayleigh waves that propagate radially from the energy source. The depth of penetration of surface wave energy decreases exponentially with distance from the free surface and exhibits meaningful motion energy only to a depth of approximately one wavelength of the energy imparted on the ground surface. Surface waves have been commonly employed to a depth of about 100 ft. (30 m) for seismic site classifications based on the average shear-wave velocity or V_{s30}. For railroad applications, the depth of interest is around 20 ft. (6 m) or less which is within the commonly used range. In general, the distances between the receivers and the energy source control the maximum and minimum depths of investigation. Based on that general framework, the distance between the source and last receiver, e.g., accelerometer or geophone, equals the maximum depth of investigation. Therefore, the initial receiver spacings are recommended as follows: one-half ballast thickness, ballast thickness, maximum depth of sub-ballast, and maximum depth of subgrade.

The field equipment required for seismic wave testing consisted of an energy source, two or more seismic wave receivers (e.g., accelerometers or geophones), placed along a line on the ground surface to record the Rayleigh waves, with a computer-based data acquisition system. To couple the accelerometers to the ballast layer, a 3-inch (75 mm) long stake was driven in the ballast and the accelerometer attached to the top of the stake with a high strength magnet. A

small sledgehammer was used to strike a circular metal plate to generate the seismic energy source. For ballast and sub-ballast layers, i.e., shallow depth (~1 foot or 0.3 meters), the handheld device termed Ballast Seismic Property Analyzer (BSPA) will used. Additional studies are recommended to modify the BSPA to span two ties to measure the modulus under two adjacent ties to evaluate tie support and load distribution. The modified BSPA system will also be able to assess concrete and wood tie integrity, but must undergo field calibration before it can be implemented.

An analysis of the seismic testing results obtained from revenue and non-revenue service track provided results in the following ranges of Young's modulus (E) for different ballast conditions as shown in Table 1:

Table 1: Young's Modulus on Revenue and Non-Revenue Service Tracks

Component	Range of Young's Modulus (ksi)	Range of Young's Modulus (MPa)
Dry and wet, clean ballast	30 to 40	205 to 275
Dry fouled ballast	50 to 55	345 to 380
Wet fouled ballast	20 to 25	135 to 170

These results show there is little difference between the Young's modulus of wet and dry clean ballast. However, the difference between the Young's modulus of wet and dry fouled ballast is significant because the fouling material softens due to the increased moisture. These results confirm the importance of the moisture content in fouled ballast and can be used in dynamic finite element analyses to simulate the loading environment in railroad track.

1. Introduction

The testing for this project was conducted by the University of Illinois Urbana-Champagne (UIUC) on revenue and non-revenue service track that represented a range of railroad environments. This section provides a comprehensive overview of the project and project deliverables.

1.1 Background

The substructure of a railroad is a multi-layered system, and the efficiency of a track-supported structure can decrease with time due to a variety of loads, stress redistribution, and sudden impacts that cause deterioration of ties, ballast, and/or foundation soils. Ballast degradation causes ballast fouling, i.e., filling of ballast voids with fine material, due to ballast degradation, breakage, and/or infiltration of other materials from the ballast surface or foundation soil and is a common problem for track performance. Monitoring and identifying changes in ballast and foundation soil properties in a track system are important for determining transient and permanent track displacements. Currently there is no tool available that can quantitatively measure the mechanics-based properties (e.g., shear-wave velocity and modulus) of the layers in a track structure. These properties are usually inferred from direct or indirect measurements, such as ground penetrating radar (GPR). This report describes the use of seismic surface-wave testing to directly measure the mechanics-based properties of track substructure layers quickly and non-invasively.

The equipment, test procedure, and interpretation techniques developed during this study to perform seismic surface-wave testing on revenue and non-revenue service track are presented along with results from the field sites tested during this study. Seismic wave testing was successfully performed and shows an average shear-wave velocity of clean ballast varying from 750 to 820 ft/sec (230 to 250 m/sec), which corresponds to a Young's modulus of 30 to 40 ksi (210 to 275 MPa). Young's modulus can be inputted into numerical analyses to estimate the stresses and deformations induced in the track structure.

1.2 Objectives

The research objective during this study was to determine whether or not seismic surface wave testing can be used on railroad track to measure the shear-wave velocity and modulus profiles with depth of the ballast, sub-ballast, and subgrade materials. Seismic surface wave testing has been used extensively on soils and pavements but the complexity and non-uniformity of track structure posed many complications due to the presence of rails, different types of crossties and spacing, ballast, sub-ballast, and variation of subgrade materials. This complexity resulted in more variability in shear-wave velocity and modulus with trackbed depth than experienced on soils and pavements.

As a result, the main objective of this project is to develop a track substructure (ballast and subgrade) condition assessment system using the seismic surface wave testing method that could accommodate the various track components. Seismic surface wave testing is desirable because it is non-invasive, low cost, and can quickly assess areas of track in a few hours. The substructure condition is characterized by shear-wave velocity profiles from which shear modulus and the Young's modulus can be calculated using measured or reasonably assumed values of mass

density and Poisson's ratio for the materials being tested. This report explains the surface wave method, equipment, interpretation techniques, software, results from laboratory and field tests, and several technical difficulties encountered during the system development and implementation.

1.3 Overall Approach

The overall approach of this project was to conduct small-scale laboratory tests to determine the optimal configuration of the seismic surface wave system to capture meaningful shear-wave velocity profiles along a section of railroad track in a short period of time. Some of the issues that were addressed in the initial laboratory experimental testing are as follows:

- Device size, location, and coupling of the excitation source with available types of crossties, tie spacing, and fastening systems
- Type, location, and coupling of the receivers placed along the track with different types of crossties, spacing, and fastening systems
- Receiver orientation, e.g., perpendicular vs. parallel to the rails or both, optimal spacing, the number of receivers for various surface wave systems

To initially investigate these issues, a laboratory ballast test section was constructed to demonstrate and refine the surface wave testing equipment before utilizing it on a revenue railroad. Based on the outcome, the surface wave system was tested on the following revenue and non-revenue service tracks to further demonstrate and refine the surface wave testing equipment, procedure, and data interpretation:

- Amtrak near South Kingstown, RI
- High Tonnage Loop (HTL) at Transportation Technology Center (TTC) in Pueblo, CO
- Jobe Materials, Inc. facility in El Paso, TX
- Paducah & Louisville Railway (PAL) near Gilbertville, KY
- Union Pacific Railroad (UP) near Ogallala, NE

In parallel with these activities, a dynamic finite element analysis was conducted that modeled the propagation of seismic surface waves passing through a railroad track structure. The numerical modeling was used to investigate the direction of wave propagation, e.g., under or parallel to a tie, and to investigate the optimal configuration of the energy source and receivers to yield the best results of shear-wave velocity with depth. The numerical modeling was also used to verify values of shear modulus estimated from the Spectral Analysis of Surface Waves (SASW) technique.

1.4 Scope

To achieve the project objectives, the following main tasks were completed:

1. Several numerical analyses took place to model seismic waves propagating through typical railroad track to understand the behavior of seismic wave propagation with an emphasis on the effects of crossties on seismic surface wave travel. This task was

primarily performed at UIUC.

2. The development of a surface wave testing system for railroads assessed the engineering properties of surface and subsurface layers, e.g., ballast and soil subgrade materials. This task was primarily performed at the University of Texas at El Paso (UTEP) and consists of several practical considerations including the testing approach, receiver type (geophone or accelerometer), frequency range of receivers, coupling mechanisms of the receivers to ballast, and transferring of seismic energy to ballast via impact energy sources.
3. Small-scale laboratory and field-testing took place in El Paso, TX, to optimize the selections made in the initial development of the system described above.
4. Based on the laboratory and field testing, the surface-wave testing system improved by adjusting or modifying the existing hardware and software for a condition assessment of track substructure.
5. To further evaluate and verify the feasibility of the surface wave method and the workability of the testing system and to document its limitation, full scale tests occurred on several revenue and non-revenue service tracks.

1.5 Organization of the Report

This report consists of the following seven sections, which contain:

Section 1: The background, objective, and scope of work for the project.

Section 2: A review and assessment of the numerical modeling of seismic wave techniques performed at UIUC.

Section 3: A description of the development of a seismic surface wave system for testing railroad track substructure. The best approaches are investigated for adapting existing soil and pavement testing equipment for track substructure assessments, including optimal configuration of system components and interpretation of surface wave test results to capture meaningful shear-wave velocity profiles in a short period of time. In addition, this section presents:

- A recommended seismic approach (SASW or Multichannel Analysis of Surface Waves [MASW]) and test setup for railroads
- The size, location, type, and coupling of excitation with different types of crossties and spacing
- The orientation (parallel or perpendicular to rails), optimal spacing, quantity, and coupling of the accelerometers and/or geophones to the ballast
- The testing protocol for using surface wave methods for track substructure assessment, e.g., number of excitations per tests, number of tests, geophone optimal locations, data recorded and graphical display, etc.
- The documentation of the necessary interpretation techniques and software that can be used to evaluate the recorded field data, e.g., acceleration time histories
- A generated list of practical and technical difficulties encountered during tests and best alternatives to result and address the issues

- The specifications to acquire the desired system components that can perform a seismic surface wave for assessing track substructure.

Section 4: The presentation of results from the initial laboratory and field testing to modify and improve the existing pavement related equipment to perform cost-effective and rapid track substructure assessments using seismic surface wave method. The results of this testing were used to fabricate the necessary instrumentation (primarily geophone and excitation systems) for conducting surface wave measurements on railroads. This section also discusses the following:

- How surface wave test setup was customized to assess railroad track substructures, which consisted of detailed information on the components of the system (e.g., receivers, excitation systems, computer, data acquisition software, AD converter, etc.), with sufficient detail to enable railroad personnel to purchase their own system.
- How to operate the system to obtain meaningful data using extensive information and documentation.
- How to interpret the data to obtain profiles of shear-wave velocity and shear modulus with depth using extensive information and documentation on.

Section 5: Presents the results from full-scale testing on several revenue and non-revenue service tracks using the seismic wave system described above. In addition, the following items are discussed in this section:

- The collection of data from full-scale or revenue service testing, including shear-wave velocity, shear strength, and shear modulus profiles vs. depth at the HTL at TTC in Pueblo, CO
- A comparison of the shear-wave velocity, shear strength, and shear modulus data with the actual conditions installed at the test locations using available GPR and other obtained data at the HTL
- Documentation of a realistic evaluation of the surface wave system and means of further improving the testing methodology for the surface wave techniques to develop innovative testing equipment and protocols to advance the newly acquired testing technique

Section 6: Presents the specifications and possible vendors for acquiring a fully functional seismic testing system for the Federal Railroad Administration (FRA) and railroad personnel and the sources that can provide the necessary items to create a prototype SASW system. In addition, this section discusses:

- How to operate the seismic testing system, interpret the results for track substructure assessments, and how to interpret the data to obtain profiles of shear-wave velocity and shear modulus vs. depth. A detailed operation manual is presented in Section 6.

Section 7: Contains a summary of the findings, recommendations, and conclusions drawn from this important research project.

Further information can be found in the report appendices, which contain the following:

- Appendix A provides the specifications for purchasing a prototype system for FRA and railroad personnel, which is similar to Section 6.1 and included as an appendix so it can be easily removed and given to purchasing personnel.

- Appendix B presents a user's guide on how to operate the SASW system for track substructure assessments and how to interpret the collected data to obtain profiles of shear-wave velocity and shear modulus vs. depth, which is similar to Section 6.2 and included as an appendix so it can be easily removed and given to railroad personnel.
- Appendix C provides the results in the form of shear modulus and Young's modulus profiles vs. depth from full-scale testing at several railroad test sites tested during this study for comparison purposes and as a check for future measurements.

2. Modeling of Seismic Surface Waves for Railroads

This section describes the numerical modeling of seismic surface waves in railroad track substructure. This section is intended to give the reader an overview of the finite element model, input parameters, boundary conditions, and typical results of the numerical modeling of seismic surface waves in railroads. Most importantly, the results show the seismic waves will propagate under concrete and wood ties, which indicate that the modulus of the ballast directly underneath the tie can be estimated using seismic wave testing. This is important for determining appropriate remedial measures for the ubiquitous tie-ballast gap or void that develops under some of the ties. Depending on the magnitude of ballast modulus under the ties, additional ballast compaction may or may not need be necessary to support the applied wheel loads.

2.1 Modeling of Seismic Waves for Track Substructure Assessment

LS-DYNA, a non-linear transient dynamic finite element program, was used to model the track structure to determine the migration of surface waves and confirm the modulus values estimated using the SASW techniques. This section describes the finite element model, input parameters, boundary conditions, and typical results of the numerical modeling of seismic surface waves in railroad.

2.1.1 LS-DYNA Software

The Livermore Software DYNA (LS-DYNA) is a three-dimensional finite element method (FEM) software package distributed by Livermore Software Technology Corporation (LSTC) that specializes in non-linear transient dynamic finite element analyses. LS-DYNA originated from the three-dimensional finite element program DYNA3D developed by Dr. John O. Hallquist at Lawrence Livermore National Laboratory in 1976. LS-DYNA is capable of modeling the entire track structure and behavior along with the inclusion of train cars and wheel systems. Other researchers have used LS-DYNA to investigate the effect of freight trains on track structures, e.g., Nicks (2009) and Lundqvist and Dahlberg (2005). LS-DYNA was used in a companion study to model the entire track structure, e.g., train bogey or cart, rail, tie, ballast, and subgrade, and their coupled interaction to understand the behavior of railway bridge transitions [33].

LS-DYNA is being used to replicate the train/track systems including the train bogey, rails, ties, tie fasteners, ballast, sub-ballast, and various subgrade layers [33]. As a result, LS-DYNA is able to simulate the mechanisms that increase the applied loads on the ballast due to a tie-ballast gap. Another important aspect of LS-DYNA is the estimation of modulus values for the various layers at each field instrumentation site, e.g., ballast, sub-ballast, and subgrade layers, using Linear Variable Differential Transformers (LVDT) and high-speed video cameras [33]. LS-DYNA has been used to perform an inverse analysis to estimate modulus values for the various subsurface layers using measured applied loads and transient vertical displacements. As a result, the use of LS-DYNA for other railway modeling would be suitable for modeling of seismic surface waves through the track substructure.

2.1.2 LS-DYNA Surface Wave Model

The LS-DYNA model developed for the analysis of seismic surface waves is shown in Figure 1 and serves as the basis for several models used to assess the effects of the accelerometer orientation and spacing, modulus, types of crossties and spacing, and subsurface conditions. Figure 2 is a close-up of the LS-DYNA model, which shows the details of the track structure. The three layers in the model are ballast (grey), sub-ballast layer (green), and subgrade layer #1 (tan).

This base model was calibrated using surface wave field data obtained from a revenue railroad test site in El Paso, TX, which is described in detail in section 4. This railroad is located inside the northwest yard of Jobe Materials, L.P. facility in El Paso, TX. The track in this test area consists of a 12-inch (0.3 m) thick ballast bed, 12-inch (0.3 m) thick sub-ballast layer, and two subgrade layers below the sub-ballast with thickness of 1 foot (0.3 m) and 6 feet (1.8 m) for a total depth of about 9 feet (2.7 m). The layer underneath the 6-foot thick subgrade layer has a thickness of 7 feet (2.1 m) and is modeled as rock to avoid boundary condition effects. The ballast at the site was slightly fouled at the time of testing and is modeled accordingly. In comparison with the ballast materials used for small-scale testing and large-scale testing, the ballast in this track was considerably coarser. The dimensions and material properties of the track system used in the LS-DYNA analysis described below are intended to replicate the conditions at this site in El Paso, TX.

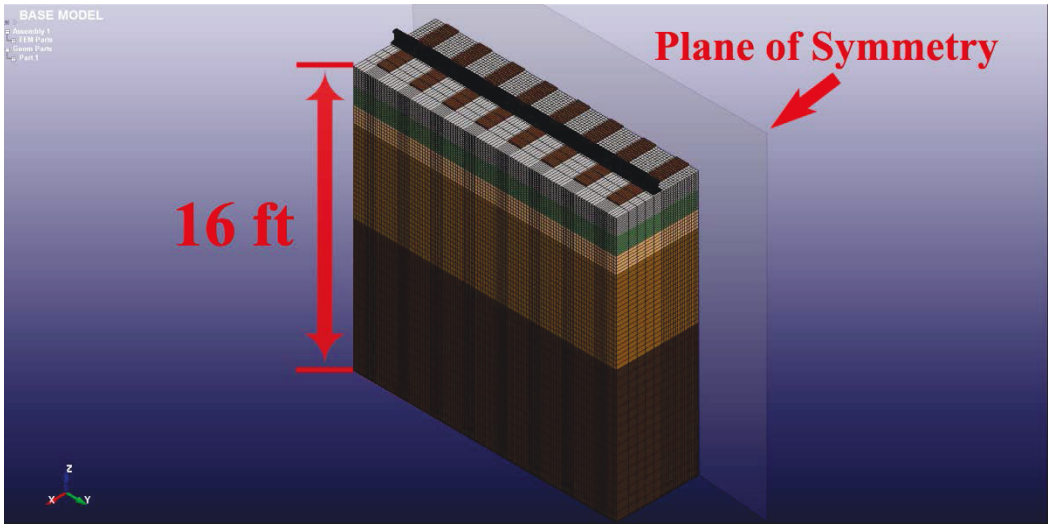

Figure 1. Symmetric Mesh for Base Model Used in LS-DYNA Analysis

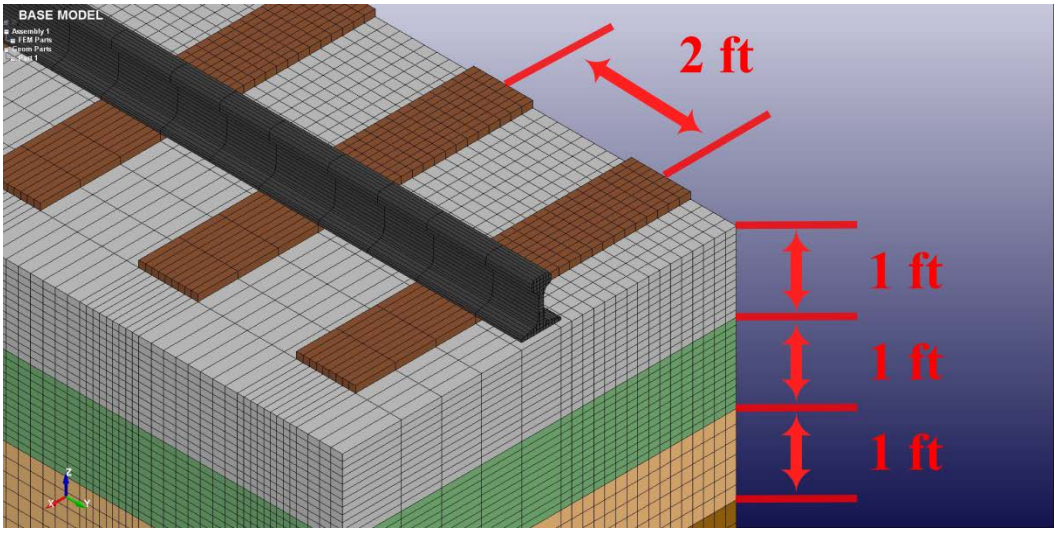

Figure 2. Mesh Details of Base Model Used in LS-DYNA Analysis

2.1.3 Track

In the base model, the steel rails were dimensioned per American Railway Engineering and Maintenance-of-Way Association (AREMA) standards for 136 lb/yd-rail, which is used at the El Paso site. The crossties were assigned the material properties of white oak using the LS-DYNA database and are spaced 2 feet center-to-center, not the standard 19.5-inch spacing, based on field measurements and observations. During further analyses, concrete crossties of various strengths were used, e.g., 4,000 psi through 8,000 psi (27, 6 and 55.2 MPa), and different crib widths to investigate the migration of the surface waves. Due to the relatively small displacements imparted to the track system by the hammer-induced waves, elastic material properties, i.e., mass density (ρ), Young's modulus (E), and Poisson's ratio (ν), were assigned to the rails and crossties and are shown in Table 2. Both the rails and crossties were modeled using solid elements.

Table 2. Track Material Properties

Track Component	Material Density, ρ (slugs/ft^3)	Young's Modulus, E, (ksi)	Poisson's Ratio, ν
Rail (Steel)	15.2	30,000	0.30
Crosstie (White Oak)	1.32	128	0.43

For a homogeneous, isotropic, and linear elastic solid medium, Young's modulus or elastic modulus (E), from point-receiver land/surface-seismic data (e.g., reflection or refraction or surface wave data) can be calculated using the following equations:

$$E = 2 * G(1 + \upsilon) \quad (1)$$

Where G is the shear modulus, υ is Poisson's ratio, and

$$G = \rho * V_s^2 \quad (2)$$

Where ρ is the mass density and V_s is the shear-wave velocity.

If the properties of only the topmost layer of a structure, e.g., a pavement, bridge deck, tunnel liner, or railroad ballast, are of interest, the SASW approach can be further simplified. For these applications, at wavelengths less than or equal to the thickness of the uppermost layer or its top portion, the phase velocity of propagation of surface waves is essentially independent of wavelength depending on how uniform the layer is. As a result, the average shear-wave velocity (V_s) can be easily calculated (without using an inversion process, which is discussed below) from the average phase velocity of the fundamental mode Rayleigh waves (V_r), measured by a two-channel system and using Equation (3) below.

$$V_s = V_r * (1.13 - 0.16 * \nu) \quad (3)$$

For a Poisson's ratio of 0.25, the shear wave velocity can be calculated as:

$$V_s = 1.09 * V_r \quad (4)$$

The modulus calculated from point-receiver surface-seismic data is a low-strain modulus ($<10^{-4}$ strain) and its value is, in general, significantly larger than that measured at a high-strain ($>10^{-4}$ strain) condition. Some quantitative relationships between this modulus and the moduli measured with other types of tests have been well or fairly defined for different pavement materials such as hot mixed asphalt, granular base and subgrade [3] [17].

Conversely, unfouled railroad ballast is a heterogeneous and loose material with many air voids (non-solid). The void space in clean ballast can be as high as 37 percent but only about 5 percent when it is fouled [33] [43]. Therefore, one of the issues addressed in this section is how effectively the modulus of the ballast can be calculated using the above expressions and how to relate the resulting modulus to other parameters used for track design.

2.1.4 Substructure

The track substructure consists of the ballast, sub-ballast, and subgrade comprised of natural soil. In the base model, the natural soil was divided into three sublayers to capture the change in stiffness, i.e., Young's modulus (E), with depth. Further divisions may be readily applied if necessary. The ballast and sub-ballast were each modeled as 12-inch (0.3 m) thick layers using solid, elastic elements in the LS-DYNA model shown in Figure 2. The natural soil extends to a depth of 16 ft (4.9 m) from the top of the ballast layer. This is a sufficient distance for the waves produced by the instrumented hammer to attenuate and induce negligible displacements at the base of the model. For larger input sources, which are needed to characterize the lower layers, a deeper model is necessary and was developed.

In general, soil does not behave elastically. However, the relatively small displacements induced by the surface waves allow for accurate modeling of the soil behavior using elastic elements. Mass densities were obtained using typical unit weights for granular and clayey soils, and Poisson's ratio was taken as 0.30 for each substructure layer as shown in Table 3.

Table 3. Substructure Material Properties

Component	Material Density, ρ (slugs/ft^3)	Poisson's Ratio (ν)
Substructure Layer 1 (Ballast)	4.19	0.30
Substructure Layer 2 (Sub-Ballast)	3.26	0.30
Substructure Layer 3 (Subgrade)	3.26	0.30

2.1.5 Boundary Conditions

Given sufficient attenuation of seismic surface waves from the source to the base of the model, pin supports are imposed on the latter. Symmetric boundary conditions were applied on the sides of the model containing the source node as to reduce the size of the mesh (i.e., the top-most corner of the mesh shown in Figure 3). For example, the symmetric part of the mesh in the yz-plane was only restricted from displacing in the x-direction (see Figure 3). As is common for many geomechanic problems, the size of the mesh was further reduced by imposing non-reflecting boundary conditions on every side of the substructure except for the top of the ballast layer. Finally, roller supports allowing only vertical movement were applied to the nodes contained by the non-symmetrical sides.

2.2 Model Calibration

The LS-DYNA finite element model was calibrated to the Jobe Materials test site before use for parametric or sensitivity studies. Given the load time history obtained from the instrumented hammer and the mass density and Poisson's ratios of the substructures materials in Table 3, the primary unknowns in the analysis are the Young's modulus and Rayleigh damping coefficients for each substructure layer. Thus, these parameters were varied until a reasonable match to the field measured acceleration time histories were obtained. The results of the calibration analyses show the Rayleigh damping coefficients for each subgrade layer did not have a significant impact on matching or calibrating the acceleration time histories obtained from LS-DYNA.

The LS-DYNA base model is calibrated using ground accelerations induced by an instrumented hammer and the resulting surface waves measured by accelerometers oriented parallel to the rails at 2-foot (0.6 m) center-to-center spacing. The time series obtained from the instrumented hammer was applied to the top-most node of the base model (see node 15,163 in Figure 3), and acceleration time histories were output at the nodes corresponding to the location of the four accelerometers locations installed in the field (see nodes 10,428 and 12,336 in Figure 3). Figure 4 presents a photograph of the test setup and track geometry at the Jobe Materials test site that is the basis of the LS-DYNA model. In this test setup, the accelerometers are installed 2, 4, 8, and 16 ft. (0.61, 1.2, 2.4, and 4.8 m) from the energy source along a line between the two rails in the cribs. The energy source also consists of a small sledgehammer and a metal strike plate, which is near the top of the photograph in Figure 4.

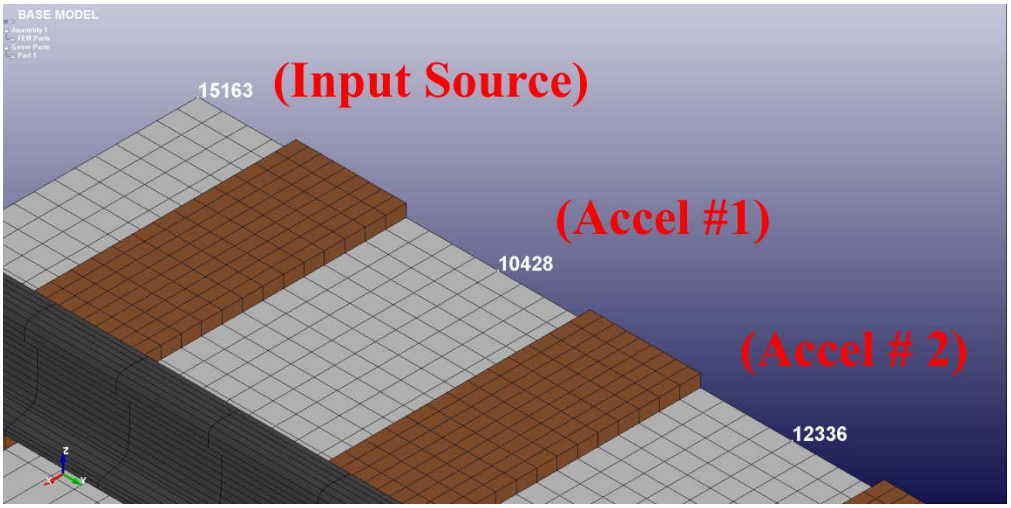

Figure 3. Location and Number of Nodes for Input Source and Two Output Acceleration Locations

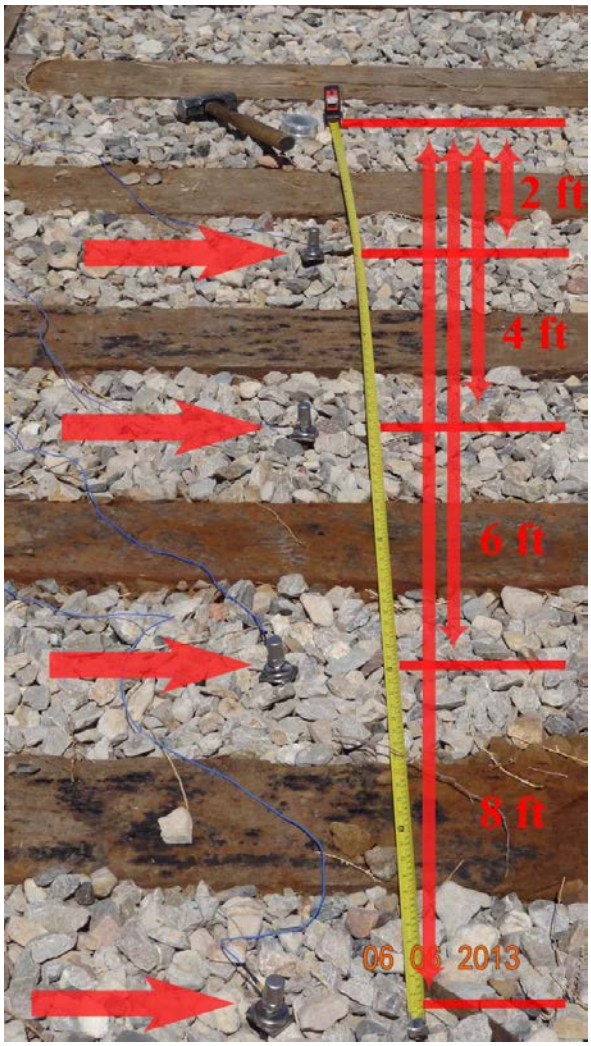

Figure 4. Photograph of Seismic Surface Wave Test Setup with Four Accelerometers (See Arrows) and Hammer and Metal Strike Plate at Jobe Material in El Paso

Figure 5 presents the measured acceleration time histories from these accelerometers, which were used in the model calibration. The values of the Young's modulus and the Rayleigh damping coefficients for the ballast, desiccated clayey sublayer, and typical clayey subgrade varied until a reasonable match of the field measured acceleration time histories were obtained.

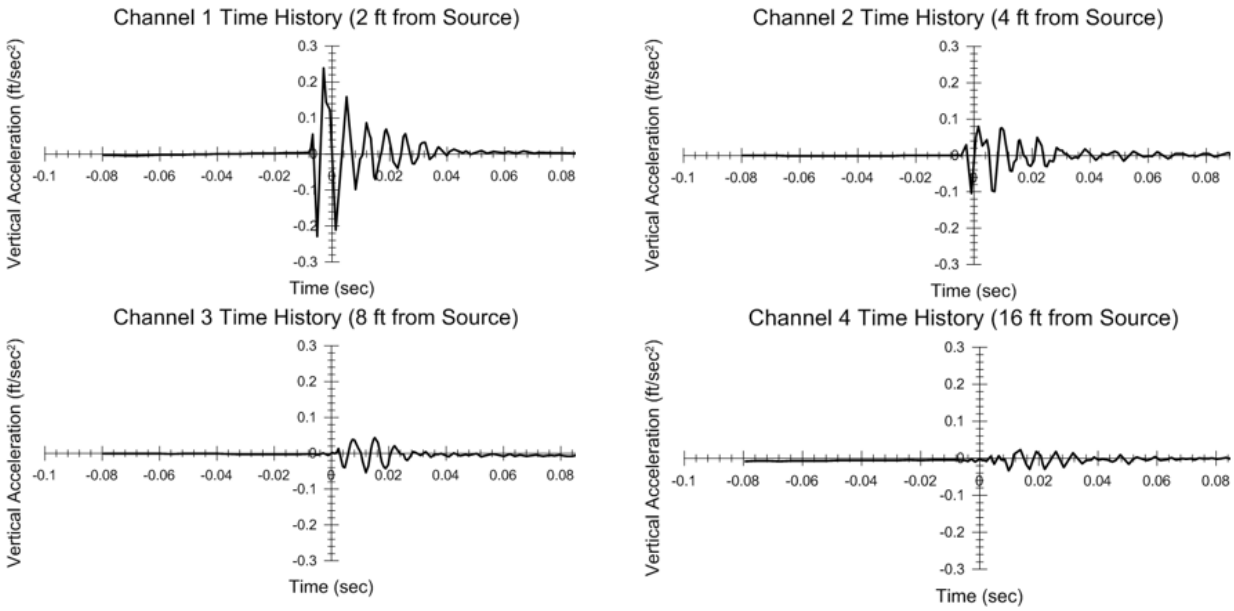

Figure 5. Acceleration Time Histories Obtained at 2, 4, 8, and 16 ft. (0.61, 1.2, 2.4, and 4.8 m) from the Energy Source for Jobe Materials Track Testing

After several trials, the base LS-DYNA model was able to accurately capture the first two maxima and the first minimum of the acceleration time history obtained from the first channel in the field as shown in Figure 6. Multiple changes, such as using softer material at the crosstie-ballast interface, were implemented in the base model to capture the latter portions of the measured time histories at different distances from the energy source, which resemble an "echo" of the initial response.

The time history obtained from LS-DYNA shown in Figure 6 uses the Young's moduli of 40 ksi (201 kPa) and 30 ksi (275 kPa) for the ballast and sub-ballast, respectively. As expected, the subgrade layers beneath the ballast and sub-ballast have negligible influence on the accelerations recorded at the first receiver, i.e., receiver closest to the energy source, because that receiver is separated from the source by only 2 feet (0.6 m). The results of the parametric study that show the elastic parameters for the subgrade layers below the ballast have a greater influence as the spacing between accelerometers increased because the Raleigh wave have sufficient time to reach greater depths past a spacing of 2 feet (0.6 m).

With this calibrated base model, values of shear-wave velocity and Young's modulus for the ballast at this site were estimated to be 600 to 720 ft/sec (180 to 220 m/sec) and 28 to 40 ksi (195 to 275 MPa), respectively. The calibrated base model was then used to estimate the shear-wave velocity profile with depth at the Jobe Materials test site and is shown in Figure 7. The shear-wave velocity profile is estimated by modeling the calculated shear-wave velocities from 2, 4, 8, and 16 ft. (0.6, 1.2, 2.4, and 4.8 m) along with the known site location soil profile described above. Using the relationships between shear-wave velocity, shear modulus, and the Young's Modulus shown above, the profile of the Young's modulus with depth at the Jobe Materials test site was developed and is shown in Figure 8.

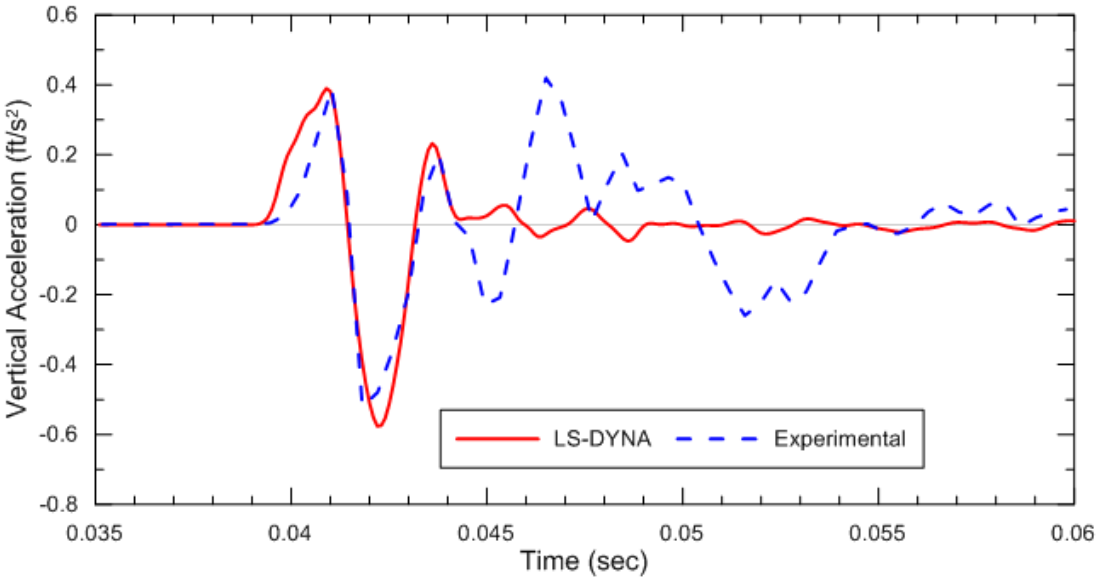

Figure 6. Comparison of Experimental and LS-DYNA Time Histories for First Channel

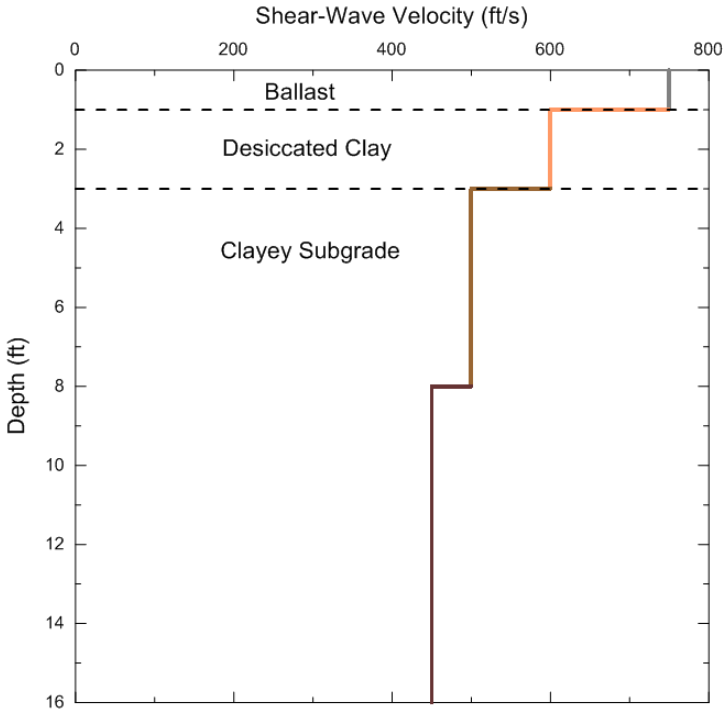

Figure 7. Profile of Shear-Wave Velocity, V_s, Obtained from Measured Acceleration Time Histories at 2, 4, 8, and 16 ft. (0.6, 1.2, 2.4, and 4.8 m) from the Energy Source for Ballast, Desiccated Clayey Subgrade, and Typical Clayey Subgrade Material at Jobe Materials Track Test Site

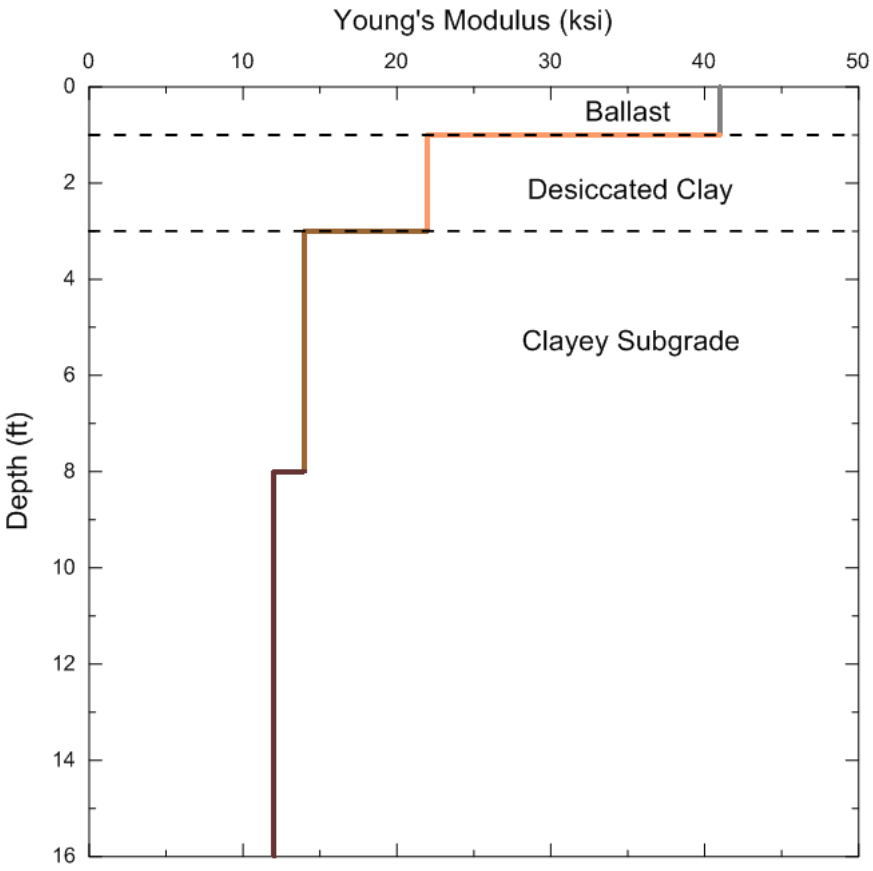

Figure 8. Profile of Young's Modulus, E, Obtained from Shear-Wave Velocity Profile for Ballast, Desiccated Clayey Subgrade, and Typical Clayey Subgrade Material at Jobe Materials Track Test Site

2.3 Effect of Crossties on Surface Waves

Another important result from the numerical modeling is understanding the behavior of the surface waves due to the presence of crossties. This was investigated with crossties and without on a base model. Without crossties, the waves radiate outward from the energy source much like when a rock is thrown into a quiet pond. The rock enters the water and concentric circles of waves radiate from the entry point of the rock. Figure 9 shows the LS-DYNA finite element mesh without crossties and before the energy source is excited in the model. Figure 10 shows the waves radiating from the energy source (time=0.003 sec), in the LS-DYNA model like a rock entering quiet water. The concentric contours of velocity are radiating from the energy source in Figure 10. Due to the plotting of these contours shortly after the excitation of the energy source, the contours are still close together and moving as concentric rings. Figure 11 shows the velocity contours well after excitation (time=0.01 sec) of the energy source and the waves dispersing through the medium and look more dispersed than in Figure 10.

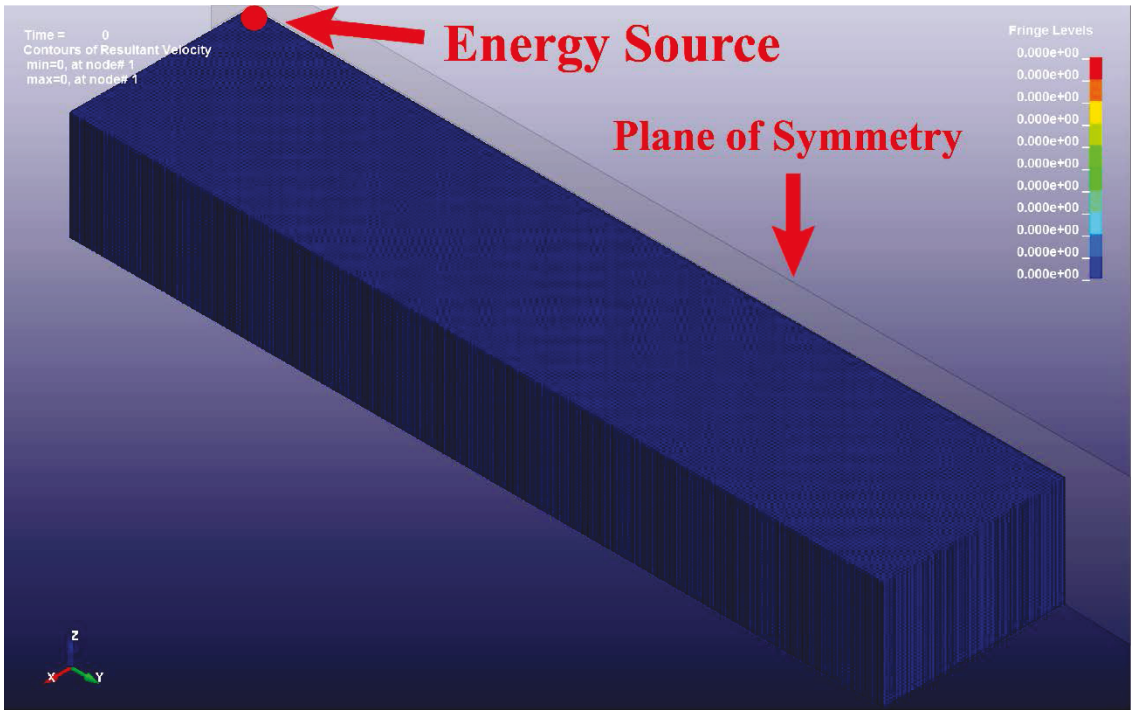

Figure 9. LS-DYNA Base Model Without Crossties

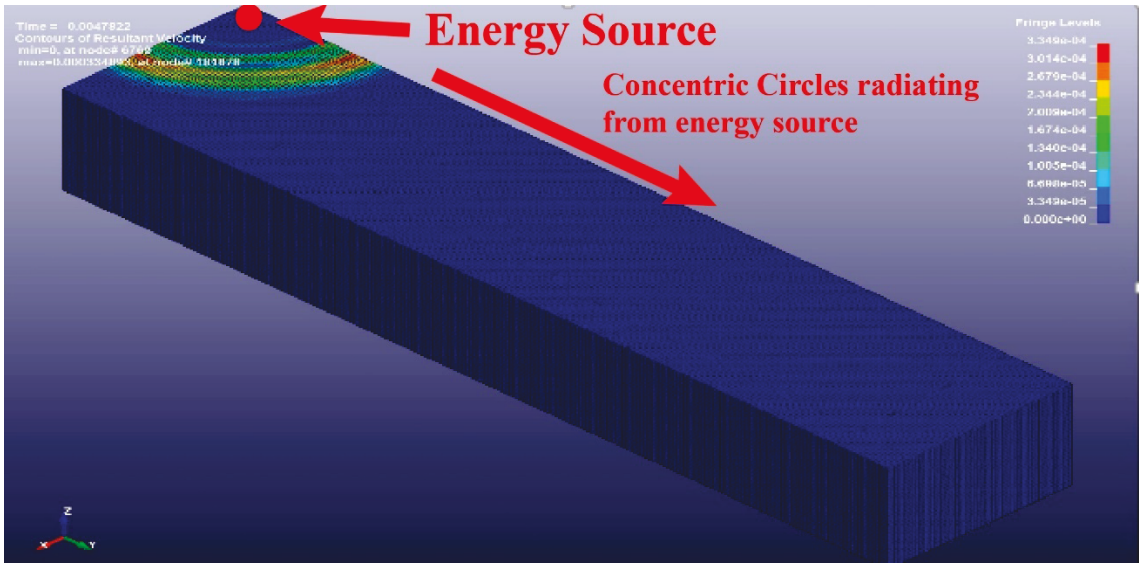

Figure 10. LS-DYNA Base Model Without Crossties and Contours of Resultant Velocity After Energy Source Excitation (Time=0.003 sec)

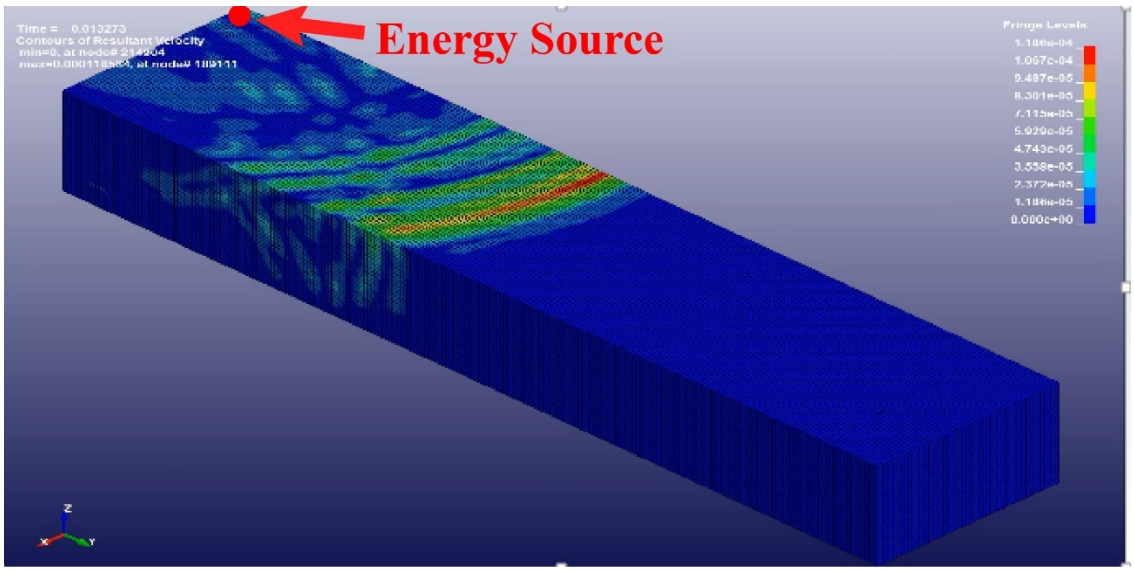

Figure 11. LS-DYNA Base Model Without Crossties and Contours of Resultant Well After Energy Source Excitation (Time=0.01 sec)

After confirming the response of the model without crossties, crossties were added to the base model by assigning the appropriate elements to the crosstie properties as shown in Table 2. Figure 12 shows the LS-DYNA finite element mesh with crossties outlined with white lines and before the energy source is excited in the model. Figure 13 shows contours of resultant velocity at 0.003 seconds with a crosstie outlined in white. This diagram is important because it shows the majority of the velocity contours moving outwards from the center of the tie and some of the velocity contours passing under the tie and appearing in the next crib. Figure 14 shows contours of resultant velocity at 0.01 seconds with crossties shown in white along the track. This diagram is important because it shows velocity contours appearing in subsequent cribs down the track. This lead to the conclusion that seismic surface waves could be used to measure the modulus of the ballast directly below a crosstie, which is important to assessing track support. In particular, the ballast modulus below a tie is important for assessing support of applied loads because of the usual presence of a tie-ballast gap, "space void," as described by Stark et al. (2015) and discussed in the next section.

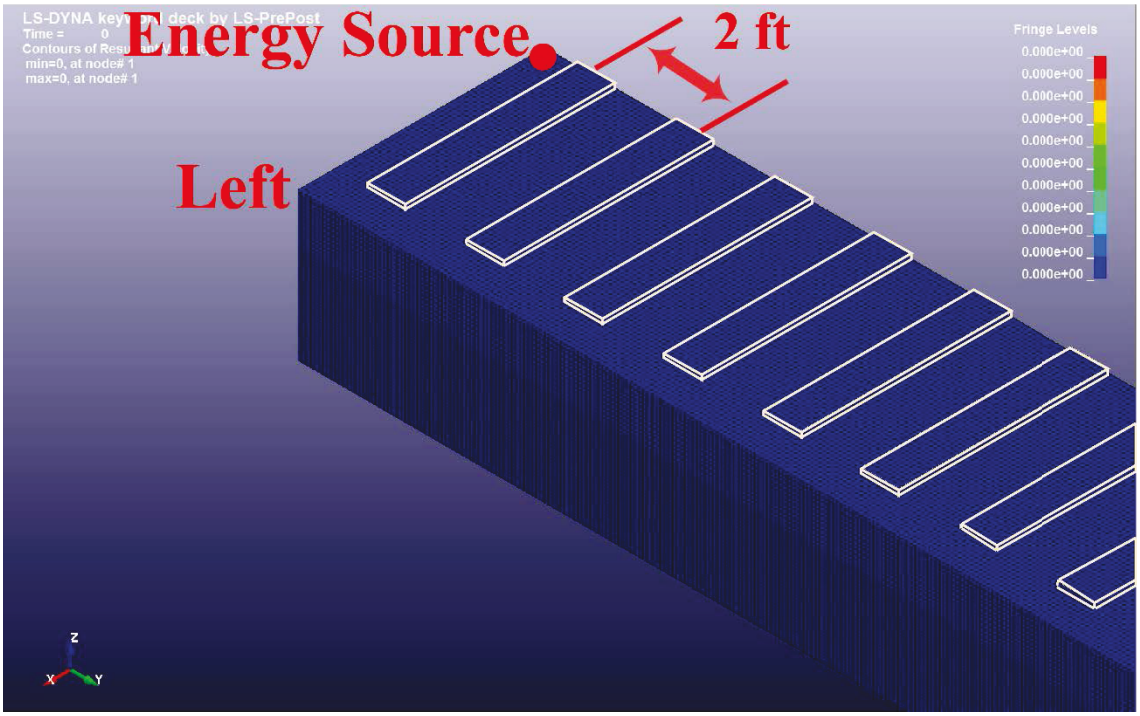

Figure 12. LS-DYNA Base Model with Crossties Outlined in White

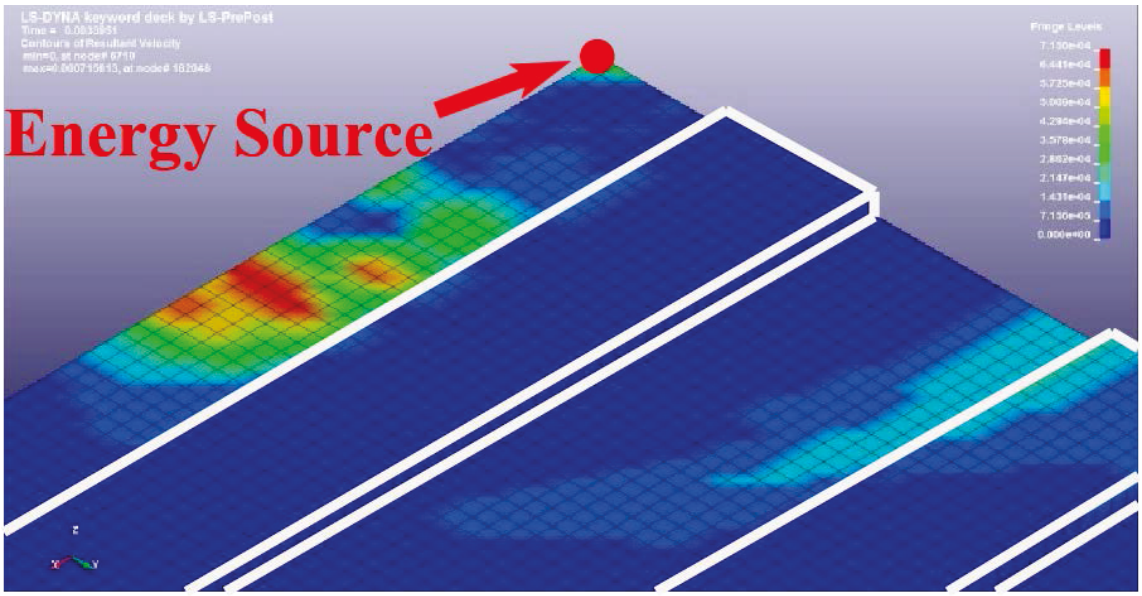

Figure 13. Close-Up of Contours of Resultant Velocity at 0.03 Seconds (Crosstie Outlined in White)

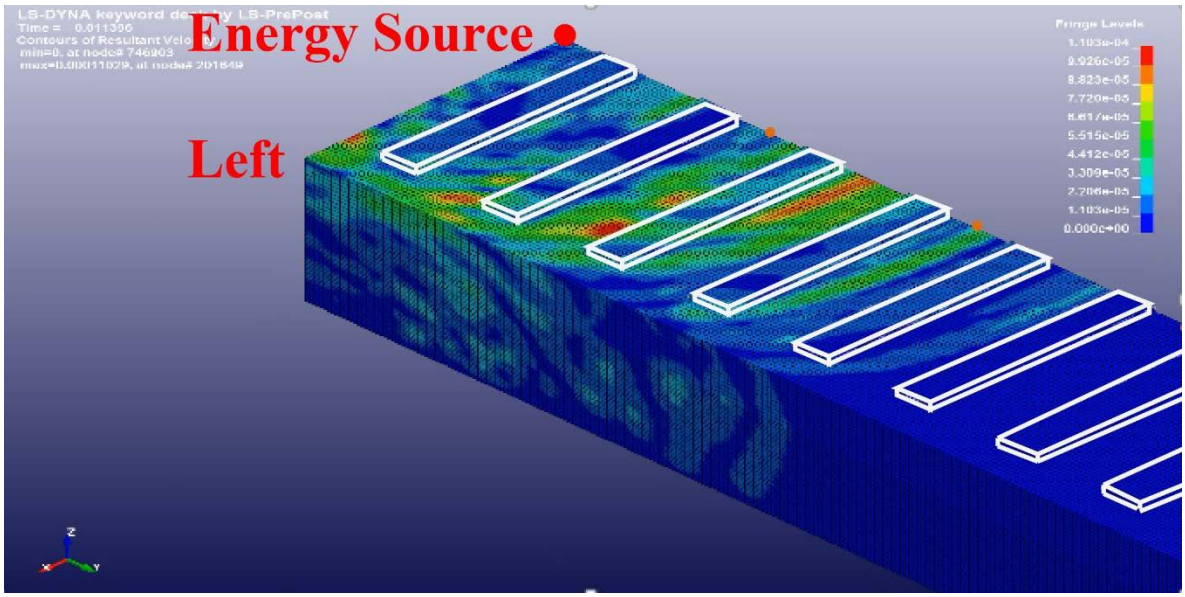

Figure 14. Contours of Resultant Velocity at 0.01 Seconds with Crossties Shown in White

2.4 Importance of Modulus Under Crossties

Field measurements of various track systems in a companion research effort show most transient tie vertical displacements consist of the following three components of movement [33]: (1) closure of a gap between the tie bottom and ballast surface (δgap), (2) initial non-linear load-displacement behavior of the ballast (δseat), and (3) displacement of ballast layer to resist the applied loads (δmob). These three main components of transient tie vertical displacement are shown in Figure 15.

The contribution of each displacement component to the total transient displacement was determined by the plotting measured peak wheel load and corresponding transient tie displacements in a load-displacement diagram similar to the diagram in Figure 15 for an instrumented site.

Based on these field measurements, Figure 15 presents a conceptual model of the tie load-vertical displacement response under either high-speed passenger or freight traffic. Formation of a gap between the bottom of the tie and ballast is the key feature of the conceptual model and while a gap may not be detrimental or significant, it is usually present under most, if not all, ties after passage of a single train due to the initial loose nature of the ballast. For example, newly laid or recently tamped track has loose ballast that is in intimate contact with the overlying tie as shown in the left schematic in Figure 15 for no wheel passes. As the first train loads the track structure, the ballast particles rearrange into a more compacted state (δseat) and displace under the applied load (δmobilized). Since the ballast behavior is inelastic and stress dependent, the particles rearrange into a denser stack and do not return to their initial state after the first train passage resulting in a gap below the tie as shown in the right schematic. After the train passes, the track is supported by ties that experienced less compaction and the rail uplift between the wheel then pulls the tie back up creating a gap between the tie and ballast for greater than or equal to one wheel pass.

The solid line in Figure 15 represents the theoretical tie load-displacement behavior with a gap between the tie bottom and ballast (δgap). As the tie is loaded, the gap closes and the ballast starts resisting the applied load by mobilizing shear resistance from ballast particle friction and interlocking. Tie displacement during the shear mobilization of the ballast is represented by δseat and the load to fully mobilize the ballast is defined as the tie seating load. Any tie displacement after seating (δmobilized) is due to displacement of the ballast and underlying soils to resist the applied wheel load and has shown to displace linearly or close to linear based on field measurements to date. As the ballast stiffness is mobilized the corresponding tie displacement is referred to as the mobilized displacement or δmobilized.

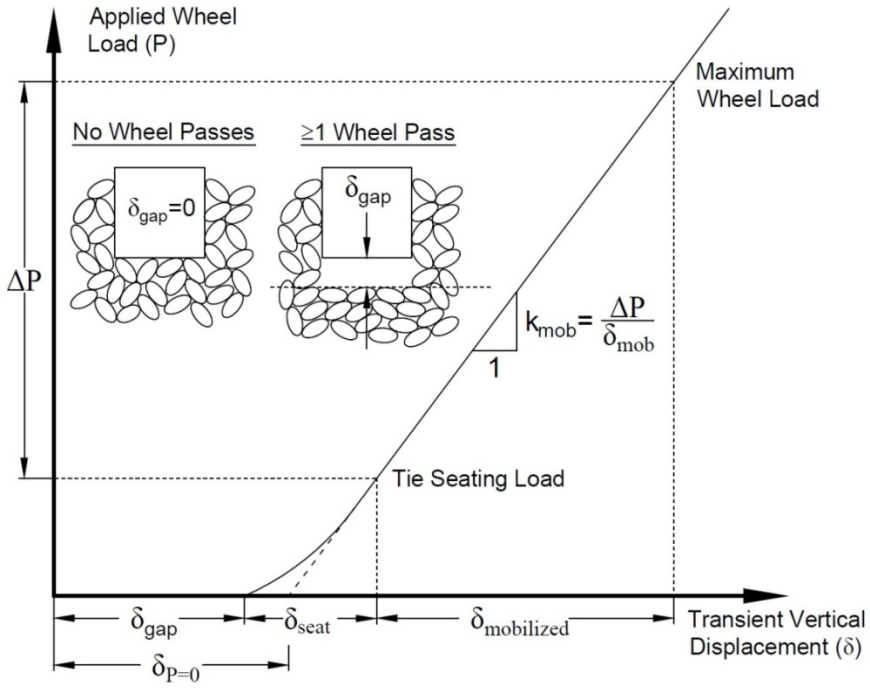

Figure 15. Transient Vertical Displacement Behavior of a Tie with a Gap Under Applied Wheel Load

Similar tack models using rail displacement instead of tie displacement have been presented [13] [39]. The rail based displacement models show similar behavior, i.e., an initial non-linear region (δseat in Figure 15) followed by a linear region representing full mobilization of ballast stiffness. The main difference is the models by Lu et al. (2008) and Sussmann et al. (2001) that focus on rail displacement for estimation track modulus instead of tie displacement. Tie displacement is used instead because the field measurements focus on tie displacements and the desire to develop tie-ballast remedial measures. This means additional vertical displacements could be occurring between the rail and tie, but are not included because the goal of the model in Figure 15 is to isolate the tie-ballast interaction, which is used for numerical modeling of new track transition designs and remedial measures.

The complexity and multiple components of track displacement suggest that a method to directly measure ballast modulus would be helpful. As a result, it is recommended that the hand-held Ballast Seismic Property Analyzer (BSPA) seismic wave device described below be modified to extend across two ties. This will allow an estimation of ballast modulus below two adjacent ties to evaluate tie support and load distribution among adjacent ties. It is suspected that optimal

track performance will correlate to a dense ballast state so the BSPA can determine if the ballast is already in this dense state or needs further compaction to provide optimal track support.

2.5 UTEP Review of Numerical Modeling

To ensure quality control of the project results, UTEP completed the task of reviewing the numerical modeling performed at UIUC and provided feedback. The main reasons for conducting the numerical analyses were to understand the interaction of seismic surface waves with concrete and wood ties, and to optimize the test set up accordingly.

The selection of the LS-DYNA as a reliable tool for numerical modeling of wave propagation is appropriate because many researchers used it to model single and multi-layer elastic layer systems. The UIUC team modeling resulted in a good representation of the interaction of the ties and ballast.

One of the limitations of the use of LS-DYNA is that it is a continuum model that represents the various layers as a continuum or solid. Due to the extremely coarse nature of clean ballast, the ballast layer may be approximated better using particulate mechanics or a discrete element model. The use of wave propagation in continuum media causes some complications in the analysis of the waveforms from receivers close to the source. These complications need to be addressed to maximize the robustness of the wave propagation model. As a result, any future study should include numerical modeling of the ballast, and should include a discrete element model, the results of which are outputted to a continuum model that is used to model underlying layers. This can be accomplished using commercially available software, e.g., Fast Lagrangian Analysis of Continuum (FLAC) and Particle Flow Code (PFC) are distributed by the Itasca Consulting Group in Minneapolis, MN. FLAC is capable of simulating static, dynamic, and hydro-mechanical behavior. PFC is a two- or three-dimensional discrete element (particle) code that is incorporated directly in FLAC2D and FLAC3D. PFC uses spherical particles or elements to represent granular particles, but can also model angular particles using the "clumping" option. By specifying the "clump logic" option, PFC allows modeling of angular granular materials, such as ballast, by building different particle shapes with multiple spherical particles. Lastly, a major benefit of PFC is the ability to couple the code directly with the continuum codes of FLAC2D and FLAC3D. Other research uses only a discrete element model to represent the ballast, but does not include it in a continuum model [15] [43].

Finally, it is recommended to use time records for future studies that are generated by the LS-DYNA as input for the surface wave reduction algorithms to quantify the impact of the ties on the outcome of the surface wave testing. In the absence of such analyses, it is recommended that the data for short spacing be collected parallel to the ties instead of perpendicular to the ties.

3. Development of Seismic Techniques for Railroads

This section describes the development of a seismic surface wave system for testing railroad track substructure systems. The best approaches for adapting existing pavement testing equipment for track substructure assessments are discussed in this section, including optimal configuration of system components and interpretation of surface wave test results to capture meaningful shear-wave velocity profiles in a short period of time. In addition, this section presents:

- The best seismic approach (SASW or MASW) and test setup for railroad testing
- The device size, location, type, and coupling of excitation with different types of crossties and spacing
- The orientation (parallel or perpendicular to rails), optimal spacing, quantity, and coupling of the receivers, e.g., geophones, in the ballast
- The testing protocol for using a surface wave method for track substructure assessment, e.g., number of excitations per tests, number of tests, receiver locations, data recorded and displayed, etc.
- Documentation on the necessary interpretation techniques and software that can be used to evaluate the recorded field data, e.g., acceleration time histories
- A list of practical and technical difficulties encountered during testing and the best alternatives to overcome them
- The specifications to acquire the desired system components to perform seismic surface wave testing for assessing track substructure

3.1 Background

When an energy source is coupled to the ground surface, three types of seismic waves are generated, i.e., compression (P-), shear (S-) and surface Rayleigh (R-) waves (Figure 16). The traveling speed of a surface wave is less than those of either P-wave or S-wave. The depth of penetration of surface wave energy decreases exponentially with depth from the free surface, and a surface wave exhibits meaningful motion energy only to a depth of approximately one wavelength.

Seismic surface waves propagating in a vertically heterogeneous (typically, layered) medium, bounded by a free surface, are dispersive; that is, waves of different wavelengths (frequencies) travel at different speeds. The dispersion of surface Rayleigh waves is much more sensitive to the variation in shear-wave velocity of the medium than Poisson's ratio or mass density of the medium. Therefore, behavior and velocity of surface Rayleigh waves is better suited for estimating the shear wave velocity and Young's modulus of the medium than compression wave velocity. Distinguished by wave type (such as Rayleigh and Love), velocity type (phase and group), and mode (fundamental and higher), dispersion data make up a large family of data. Various dispersion data have been used to quantitatively study the shear-wave velocity structure of the Earth's crust and upper mantle for more than five decades. Currently, Rayleigh wave phase velocity data are used primarily in engineering applications.

In general, a complete procedure using surface Rayleigh waves to estimate shear wave velocity and Young's modulus consists of the following three steps: (1) conducting field measurements to obtain time domain signals, (2) reducing the time signals to construct dispersion curve(s), and (3) analyzing of the dispersion data to derive a representative shear-wave velocity profile, which usually requires a back-calculation or inverse analysis process.

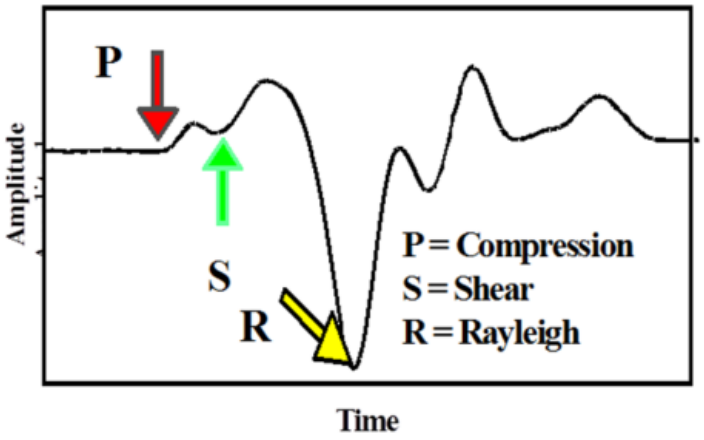

Figure 16. Three Types of Seismic Waves in a Time Record (Waveform)

The introduction of surface wave method in engineering applications has resulted in an increasing use of this method in geotechnical site investigations and flexible pavement evaluations [20] [24] [26] [37] [46]. Currently, engineering applications primarily use Rayleigh wave phase velocity data to estimate shear wave velocity as shown in Equation (3). During the last two to three decades, this method was implemented in different approaches, such as the SASW and MASW, in engineering applications [20] [27]. Major differences among different surface wave approaches (SASW, MASW, etc.) stem from field measurement requirements and dispersion curve construction. Irrespective of the approach considered, there are common best practices that should be used to obtain the dispersion curve, which are discussed below and were implemented in this study. Due to ease of laboratory and field testing, as well as the complexity of ballast material in terms of receiver installation and impact source application, the SASW approach was primarily used for the measurements and interpretations.

3.2 SASW Approach and Measurements

In the SASW approach, the field equipment required for surface wave testing consists of an impact energy source, e.g., a sledgehammer, two or more receivers (geophones or accelerometers) placed along a line on the ground surface, and a computer-based data acquisition system (Figure 17). The use of different energy sources (in terms of intensity and contact area with the ground surface) is to generate surface wave energy over a range of frequencies, depending on the detection depth of interest. Figure 18(a) presents a schematic diagram of the common configuration for surface wave testing.

The main output of the field surface wave testing is measurement of a series of time records from different receivers. In the SASW approach, each pair of time records is processed in the frequency domain to develop a dispersion curve and then the dispersion curve from different receiver spacings are combined to form a representative dispersion curve. This representative dispersion curve for all accelerometers (phase velocity vs frequency) is used to derive a

representative shear-wave velocity profile. The advantage of the SASW approach is that the data processing is straightforward, understandable, and readily apparent so the reliability of the data can be judged in real time as was done in the Seismic Pavement Analyzer. The Seismic Pavement Analyzer is an automatic device developed under the first Strategic Highway Research Program (SHRP I) for conducting SASW tests on pavements [18].

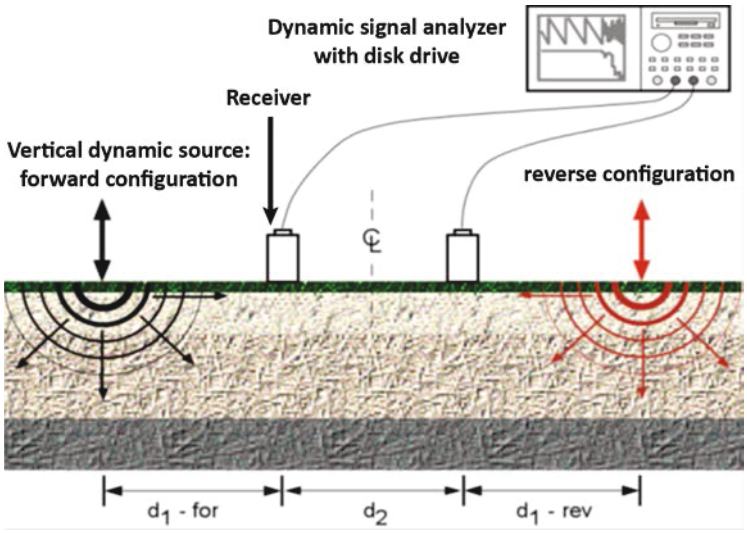

(Source: www.GeoVision.com)

Figure 17. Setup of SASW Test

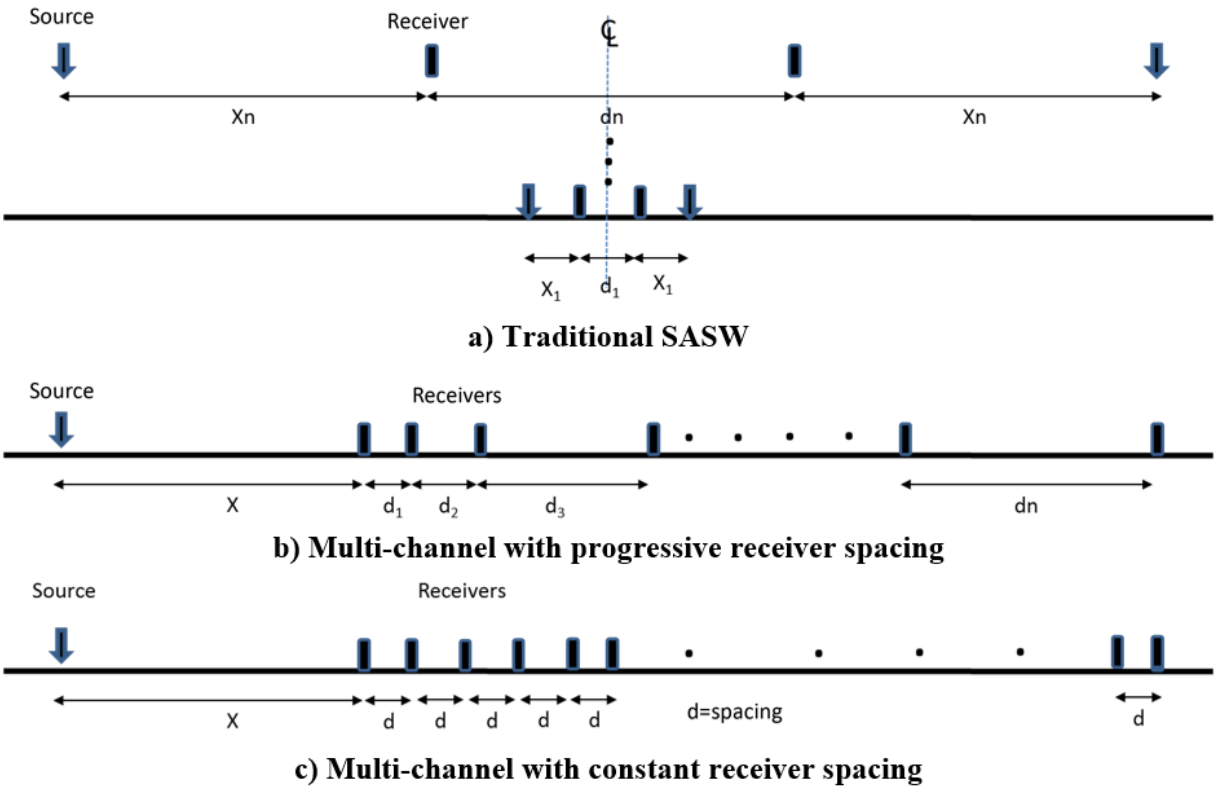

Figure 18. Common Configurations for Surface Wave Testing: (a) Traditional SASW, (b) Multi-Channel with Progressive Receiver Spacings, and (c) Multi-Channel with Constant Receiver Spacing

3.3 MASW Approach

Both MASW and SASW techniques were reviewed during this study to investigate whether MASW performs better than SASW. MASW data collection is based on multiple wave signals being collected on the ground surface along an array of receivers from the wave source (such as an impact event) as shown in Figure 18(b) and (c). The set of signals can be obtained using several receivers and a single wave source, or a single receiver and multiple wave sources. The configuration used for the MASW approach is shown in Figure 18(c). A series of usually equally spaced receivers (typically 12 to 24 inches) is placed on the surface and all receivers record the seismic energy simultaneously [27]. The multi-channel data acquisition processes have permitted the use of more advanced signal processing algorithms to obtain the dispersion curve. The common features of these methods are that (1) they can be readily automated, (2) the results are less sensitive to the environmental noise due to the redundancy in the measurements, and (3) it is not required to assume the surface energy is focused in the fundamental mode of the Rayleigh wave. One can take advantage of the density of the measurement points with the multi-channel measurements to transform the time records not only temporally but spatially as well. Several multi-array approaches are in use at this time. The most common process is the Full-Offset Dispersion Imagining (FODI) advocated by Park (2011).

A type of 2-D Fourier transform procedure is applied to transform the data set from the spatial offset-time domain to the frequency-phase velocity domain. This type of data presentation

allows the dispersive nature of the fundamental and higher order wave modes, contained in the same signal, to be distinguished. The two main advantages of MASW over SASW interpretation techniques are: (1) results are less sensitive to environmental noise because of the redundancy in the time records, and (2) it is not required to assume that the surface energy is focused in the fundamental mode of the Rayleigh wave. However, the two main practical limitations of MASW are: (1) a dozen or more time records are necessary which increases set up time and system cost and (2) additional consideration of the source-receiver array is required to obtain reliable data for both shallow and deep strata.

MASW was also used during this study as it may overcome some of the limitations of the two-channel SASW method for railroad applications. Based on the results of this study, it is recommended that multi-channel data collection be used with the SASW method. This reduces the timing and number of receiver spacings because it does not require the 12 or more receivers typically needed for MASW. As a result, the SASW configuration shown in Figure 18(a) was used with the SASW method and is recommended for future studies.

3.4 USW Approach

If only the properties of the topmost layer of a structure (such as pavement, bridge deck, tunnel liner, and railroad ballast) are of interest, the SASW approach can be further simplified. For these applications, at wavelengths less than or equal to the thickness of the uppermost layer or its top portion, the phase velocity of propagation of surface waves is more or less independent of wavelength and function of layer uniformity (Figure 19) depending on how uniform the layer is. In this case, the average shear-wave velocity, V_s, can be easily calculated (without involving an inversion process) from the average phase velocity of the fundamental mode Rayleigh waves, Vr, measured by a two-channel system as shown above:

$$V_s = V_r * (1.13 - 0.16 * \nu) \sim 1.09 * \mathrm{Vr} \quad (5)$$

Where ν is Poisson's ratio with a value of about 0.25. This simplified SASW approach is also called the USW (ultrasonic surface wave) approach and has been implemented in several hand-held devices such as the portable seismic pavement/property analyzer (PSPA) [13].

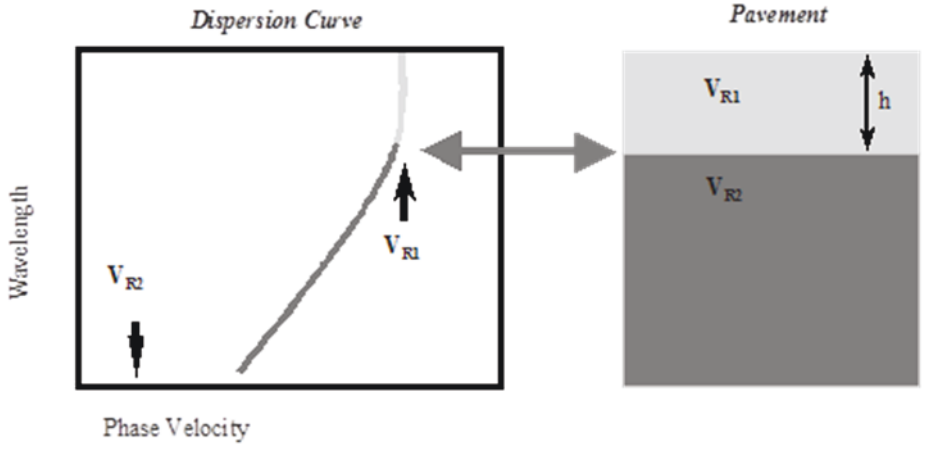

Figure 19. Illustration of USW Approach

The PSPA, as shown in Figure 20, consists of two receivers (accelerometers) and a solenoid source packaged into a hand-portable system, which can perform high-frequency seismic tests. The source package is also equipped with a transducer for consistency in triggering. The device is operable from a computer tethered to the hand-carried transducer unit through a cable that carries operational commands and returns the measured signals to the computer.

The existing PSPA devices were designed to measure the modulus of concrete and asphalt pavements as well as other paved layers with smooth surfaces. To utilize a PSPA on ballast, besides the high frequency limit as discussed later in this section, its current version needs considerable modifications and customization, particularly, in coupling of receiver unit to ballast and lengthening to be placed across one or two crossties.

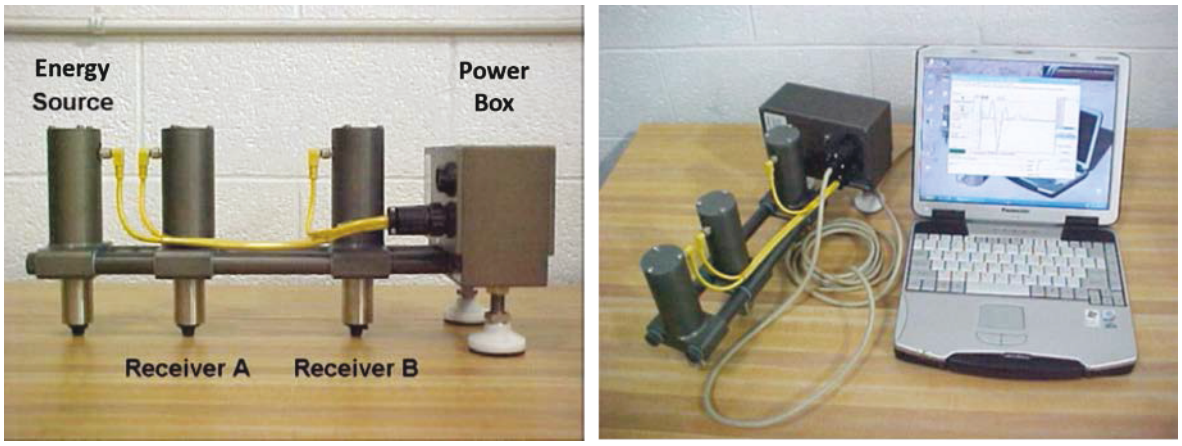

Figure 20. Portable Seismic Pavement/Property Analyzer

3.5 Best Approach (SASW or MASW) and Test Setup

Hebeler (2001), Li (2008), and Cox and Wood (2011) give practical examples of the benefits and uncertainties associated with the SASW and MASW approaches. The advantage of the SASW approach is that the data processing is straightforward understandable and readily apparent so the reliability of the data can be judged in real time. Also, a representative dispersion curve for detection depth to 100 feet (30 m) or greater can be obtained by simply changing the receiver spacing and energy source. The major disadvantage with the SASW method is the surface wave energy belongs to the fundamental mode of propagation.

The MASW method provides the dispersion curve in an automated fashion and in most instances can differentiate among different modes of propagation. The main disadvantage with the MASW method is the relatively large number of receivers necessary to manage the uncertainty in the development of the dispersion curve.

The selection of the appropriate approach was driven by the requirements of the project, while the operational constraints of the projects were as follows:

- Field test protocol should be reasonably fast and scalable
- Method should characterize the track substructure down to a depth of 15 feet (4.5 m)

Nazarian (2012) demonstrated that the different approaches to surface wave testing are equally valid as long as the data collection and analysis are compatible with the known theoretical and

experimental limitations of each approach. Based on the operational constraints and the perceived complications discussed above, the research team decided to focus on implementing the SASW approach. The main reasons for using the SASW approach are as follows:

- Tests can be performed with a 2- to 4-channel system (as opposed to the 12- to 24-channel system required for MASW) that results in significant savings in the initial costs of receivers and data acquisition system
- Test set up is much faster because only two to four receivers must be coupled to the ballast
- Easy system configuration to the depth of interest by changing the source and receiver configurations
- Automation is easier with the SASW method and can be implemented in future development

In May 2013, the FRA representatives met during a project meeting and concurred with the recommendation of pursuing the SASW approach. In the same meeting, the FRA representatives expressed their preference towards the implementation of the USW type tests with a device similar to the PSPA with the understanding that the current PSPA required significant modifications.

3.6 Testing Protocol for Track Substructure Assessments

Based on the SASW approach selected, the best practices from seismic surface wave testing of pavements were considered for implementation for the multi-layered nature of the railroad trackbed. The main components of the field SASW setup consists of a source, two or more receivers, and a data acquisition device. These components should be selected carefully to ensure the desired results are provided to the end user.

Source (Energy)

The main requirement of the source is to couple surface wave energy over a range of frequencies so that a complete and continuous dispersion curve is obtained. The energy sources considered are hammers and drop weights for portability. A large-size sledgehammer typically couples adequate energy to pavements and soil sites to effective depth of profiling of about 30 ft. (9.1 m). For depths of investigation of up to 60 ft. (18 m), drop weights have been used. Due to these energy sources lacking high-frequency energy, they should be used in conjunction with a high-frequency source to characterize the ballast properly. Several small ball-peen hammers were selected for this purpose. Given the open structure and looseness of ballast, the effectiveness of these traditional sources on coupling energy to ballast was of concern and had to be evaluated.

Receivers

Geophones and accelerometers are the most common receivers used in seismic testing. The characteristics of all receivers used in the array should be as identical as possible, and the coupling of the receivers to the medium (in this case ballast) should be uniform and in place. Important characteristics of a geophone for a proper field measurement are its natural frequency and its sensitivity. Based on the authors seismic wave testing experience, 4.5 Hz geophones

were selected as one alternative. Their concerns with using geophones were the difficulty in coupling them with ballast and the lack of sensitivity to high frequency energy necessary for characterizing the ballast. As such, a set of accelerometers was also selected for initial evaluation with the SASW approach. The concern with the accelerometers was their ability to monitor low-frequency energy for characterizing the deeper strata.

Data Acquisition System

With advances in software and hardware, most commercial data acquisition systems are appropriate for surface wave measurements as long as the acquisition parameters are selected correctly. A four-channel dynamic signal analyzer and a four-channel data acquisition board from National Instrument (NI) were used in this study.

Source-Receiver Configuration

In the traditional SASW approach, two receivers are used at a time as shown in Figure 18(a) [21]. Several pairs of time records are collected by progressively doubling the distance between the receivers. The shortest spacing between the receivers is typically equal to the shallowest depth of investigation and the longest spacing is roughly equal to the maximum depth of interest for subsurface profiling (15 ft. or 4.5 m). A source offset equal to the distance between the two receivers is suggested. The common receiver mid-point array, where the two receivers are moved symmetrically between measurements against a center point and two sets of data are collected using the source on both sides of the array, is recommended (Figure 18(a)). This is done as a measure to account for the dipping layers and to decrease the uncertainty in the final dispersion curve. The source is changed as the distance between the receivers increases to ensure the energy in the appropriate range of frequencies is generated and detected for all receivers. By today's standards, this process is tedious and time consuming because it was developed when even a two-channel data acquisition system was prohibitively expensive. With currently available data acquisition systems, the configuration can be modified so many time records can be collected simultaneously based on the receiver configuration. Zywicki and Rix (2005) describe how to optimize the receiver spacings. Typical source-receiver configurations used to acquire time records with the two four-channel data acquisition systems are shown in Figure 18(b) and 18(c). The parameters of interest are the source-to-first-receiver spacing, i.e., source offset, X, and receiver spacings, d1 through d4. These parameters should be carefully selected to obtain the dispersion curve in the range of interest to ensure the fidelity of the signal in the receivers [49]. Almost uniquely applicable to railroad track, the orientation of the receiver array (parallel or perpendicular to rails) had to be considered as well as the optimal spacing, quantity, and coupling of the geophones to the ballast. As discussed later, several alternatives were considered and tested experimentally to optimize the source-receiver array and orientation.

3.7 Interpretation Techniques and Software Used

The end result of the field-testing is a series of time records that are manipulated to obtain a shear-wave velocity profile. The two interpretation tools needed for this purpose are an algorithm to construct a dispersion curve and an inversion process to obtain the shear-wave velocity profile that fits the average dispersion curve

Constructing Dispersion Curve

In the traditional SASW approach, this step consists of analyzing each pair of time records collected individually to develop several individual dispersion curves and combining them to a representative dispersion curve [21]. Nazarian and Desai (1993) propose an algorithm to automate this process. This algorithm was used to obtain a representative dispersion curve in this study.

To obtain the dispersion curve for each receiver pair, the two-time records are transformed into the frequency domain, and subjected to spectral analysis to obtain the so-called wrapped phase spectrum. The wrapped phase spectrum is then unwrapped. Knowing the unwrapped phase, ϕ_u, at a given frequency, f, for a pair of receivers that are spaced at a distance d_i, the phase velocity, V_{ph}, and wavelength, λ, can be estimated from:

$$V_{ph}(f) = \frac{2\pi f d_i}{\phi_u}; \qquad \lambda = \frac{V_{ph}}{f} \tag{6}$$

Coherence function, an outcome of spectral analysis when data are collected repeatedly with the same configuration, is usually used as a quality control tool. A low coherence value (typically less than 0.9 compared to the ideal 1.0) is an indication of the lack of seismic energy or the contamination of energy with higher-mode surface waves or body waves in one or both receivers. Phase data in the regions with low coherence are removed from the construction of the dispersion curve. To ensure the near-field energy contamination is minimized, the frequencies where the unwrapped phase is greater than 180 degrees, i.e., the wavelength is less than twice the distance between the receivers, should be used. To minimize the energy associated with the higher modes of propagation, phase velocities associated with phases greater than 720 degrees are not used.

The most uncertain and tedious portion of this activity is the phase unwrapping. This process relies also on the consistency between the dispersion curves from different receiver spacings. Aside from the limitations discussed above, the dispersion curves may not be consistent because of the strong lateral heterogeneity of the site. Abdallah et al. (2005) propose a process to minimize these problems by using a non-parametric fitting algorithm that utilizes a numerical fundamental mode dispersion curve as a constraint.

Inversion Process

The final step in the surface wave method includes estimating the variation in shear-wave velocity (V_s) with depth from the average or representative dispersion curve. As a closed-form solution is not available for this task, the so-called inversion process is usually considered. The inversion process consists of estimating an initial V_s profile, developing a numerical dispersion curve from the assumed V_s profile, e.g., estimated from the soil profile or engineering judgement, comparing the experimental and theoretical dispersion curves, and adjusting the V_s profile iteratively until the difference between the experimental and numerical dispersion curve is below an acceptable threshold.

The inversion process consists of the following two components: (1) an algorithm to estimate the dispersion curve numerically, i.e., a forward-model, and (2) an algorithm to adjust the assumed V_s profile to minimize the differences between the experimental and numerical dispersion curves, i.e., optimization algorithm.

Forward Modeling

Ideally the numerical dispersion curve should be as representative of the field testing as possible. The first numerical formulation of the propagation of surface waves in a multi-layered medium is attributed to Thomson (1950) and Haskell (1953). For a horizontally layered, vertically heterogeneous, isotropic, elastic medium over a half-space, they provided the differential equations for motion-stress vectors of surface waves that can be solved via a transfer matrix. This pioneering work has been studied by numerous researchers to improve its computational efficiency and to adopt it for the near surface applications as summarized by Pei et al. (2008). Nazarian and Stokoe (1985) adapted this formulation for the original SASW method with some adjustments to minimize its numerical instabilities associated with short wavelengths. Despite its simplified assumptions, the Haskell-Thomson type solutions are the most widely used algorithms in surface wave profiling due to their time-efficiency. Yuan and Nazarian (1993) present a detailed explanation of the algorithm used in this study.

Optimization Algorithm

The optimization algorithm is the process of iteratively comparing the experimental and numerical dispersion curves and minimizing the differences between them. The number of dispersion points (N) are chosen from the experimental dispersion curve for comparison with corresponding numerical values. An M-layer profile is specified by the layers' shear-wave velocities (with assumed constant Poisson's ratios and densities). In the simplest form, the optimization is carried out by an experienced analyst that manually changes the assumed V_s profile and visually or with simple statistics judges when the two dispersion curves are close enough [21]. As this is a subjective and time-consuming process, it allows the analyst to use their experience and any other information about the site. For very complex sites, an experienced analyst is preferred for this trial and error process.

The basis of surface wave testing is the use of an optimization or error minimization algorithm. These algorithms automatically and rapidly provide a V_s profile that statistically describes the measured dispersion curve. Most minimization techniques are based on the generalized inversion technique as explained in many textbooks such as Santamarina and Fratta (2005). One such approach as discussed in detail in Yuan and Nazarian (1993) is used in this study. The generalized inversion technique assumes a linear relationship between perturbation in the V_s of the layers and the resulting change in phase velocities. The partial derivative with respect to each parameter to be determined is carried out to estimate the change in that parameter for the next iteration. Also, the percent change in layer shear-wave velocities between iterations is typically constrained for stability [48].

3.8 Technical Difficulties and Best Alternatives

Seismic testing on a rail track system is much more complicated than that on soil sites or pavements due to the presence of ballast, rails, crossties and other track components as well as the complexity of ballast-subgrade structure in terms of the variation of shear-wave velocity with depth. The following sections explore concerns regarding testing of railroad substructure assessment.

3.8.1 Coupling Between Receiver and Ballast Material

Railroad ballast, especially its top portion, consists of loose rock of size up to 2.5 in. (7 mm), which makes it difficult to directly place geophones or accelerometers on the "surface" of ballast with stable coupling for high-fidelity signals (containing noises caused by other factors). Each receiver should be affixed to a spike with a flat head that would be driven into the ballast with a sledgehammer prior to testing. To overcome the coupling problem, the accelerometers are fixed to the top of a 4 in. (100 mm) long metal spike that is driven into the ballast using the hammer Figure 21. After driving the spike into the ballast the accelerometers are connected to the top of the spike with a high-strength magnet, as seen in Figure 22, to ensure coupling with the ballast and accurate readings. A hammer was then used to impact the strike plate, inducing seismic surface waves through the track structure. For larger accelerometer spacing, i.e., out to 16 ft. (4.9 m), a 30 lbs. kettlebell (not shown) was used to impact the ballast instead of a hammer (see Figure 21).

Figure 21. Metal Spike and Installation of Metal Spike for Coupling Accelerometers to Ballast

Figure 22. Accelerometer Attached to Top of Metal Spike Using a High Strength Magnet

3.8.2 Effect of Receiver Mounting Resonant Frequency

Seismic testing with any surface-wave testing approach for railroad substructure (ballast and subgrade) assessment in full depth requires the receivers to have a broad frequency response range (from several Hz to 2 kHz or higher). For testing over such a frequency range, accelerometers are more suitable than geophones. The high frequency usable limit is a function of the natural resonance of an accelerometer. The mounting method of an accelerometer will significantly impact its "mounted" resonance. Under ideal circumstances, the accelerometer mounting should provide total use of the transmission region. If the mounting resonance is significantly less than the accelerometer's resonance, the high frequency limit of the receiver will be compromised. Each mounting method has an associated resonance which deceases as the mounting mass increases. When mounting with a metal spike, as described above, the expected useable frequency ranges for the transmission of vibrations (signals) to the accelerometer can be lower than 500 Hz [29]. Such a frequency would have a significant impact on the quality of high frequency signals from surface wave testing on ballast. These signals are mainly related to the ballast layer(s) and the top portion of the subgrade.

3.8.3 High Frequency Scattering and Attenuation of Ballast Material

At least in the small scale, railroad ballast is a highly heterogeneous and loose material. The speed of surface waves propagating in ballast can be as low as 500 ft/sec as shown in Section 4 and reported in other studies, e.g., Bei (2005). To detect the property of the top portion of a ballast layer by the surface wave method, surface waves having a frequency of 1,000 Hz or higher is necessary, which means that the wavelength would be 0.5 ft. or less. Tee aggregate size (2 inches (50 mm) or greater) of ballast causes high frequency scattering, apparent attenuation, and phase conversion (from body waves to surface waves and vice versa) and create difficulties in surface wave testing. These difficulties may result in lack of repeatability and large errors in measurement. The random spatial variation of heterogeneity and the temporal change in scattering characteristics may also result in low signal-to-noise ratio in data collection.

3.8.4 Influence of Crosstie

When an impact force is applied to ballast, crossties may become additional sources of scattering or the secondary sources, thus lowering the signal-to-noise ratio, in particular, for high-frequency waves. This influence varies, depending on the orientation of receiver array (perpendicular or parallel to crossties) and the location of impact source relative to crossties.

3.8.5 Analysis of Dispersion Data

Qualitative analysis of surface dispersion data through either forward modeling or inversion is successful for soil foundations and pavement structures. Dispersion curves obtained from the two types of structures are named the normal dispersion (where the velocity of shear-wave propagation generally increases with depth) and the inverse dispersion (where the velocity of shear-wave propagation generally decreases at least to certain depth), respectively. For structures, like a road, where shear-wave velocities may vary irregularly with depth, (typically, low-high-low) the surface wave method (either SASW or MASW with fewer channels) analysis of dispersion data may face the following difficulties:

1. Dispersive trend may dominate high frequency ranges, thus, the experimental dispersion curve should be considered as an effective or apparent due to the contributions of higher modes [7]. In addition to inverse dispersion, the fundamental mode dispersion curve (phase velocity vs. frequency or wavelength) is discontinued or branched [11] [44]. During testing, this would cause additional inconsistency in the experimental data.
2. Measurement errors critically impact the analysis of surface wave dispersion data in terms of resolution and uncertainty in the resulting model. The estimate of these errors becomes more difficult for the reasons stated above.
3. The basis of any forward modeling or inversion process is the availability of a reliable and fast algorithm for solving the forward problem (calculation of theoretical dispersion data at any specified frequency for a given shear-wave velocity model). Such a tool is not currently available for models of irregular shear-wave distribution with depth.

3.8.6 Calculation of Modulus

As mentioned above, for a homogeneous, isotropic, and linear elastic solid medium, Young's modulus or elastic modulus (E) from point-receiver land/surface-seismic data (e.g., reflection or refraction or surface wave data) can be calculated from the following formula:

$$E = 2 * G(1 + \nu) \quad (7)$$

Where G is the shear modulus and

$$G = \rho * V_s^2 \quad (8)$$

Where ρ is the mass density. If the seismic data is the phase velocity of the fundamental mode Rayleigh wave, shear-wave velocity, V_s, can be calculated from Equation (3) or derived through an inversion process.

The modulus calculated from point-receiver surface-seismic data is a low strain modulus ($<10^{-4}$) and its value is, in general, significantly larger than that measured under high strain condition. Some quantitative relationships between this modulus and the moduli measured with other types of tests have been well or fairly defined for different pavement materials, such as, hot mixed asphalt, granular base and subgrade [3] [22].

On the other hand, railroad ballast is a highly heterogeneous and loose material with air voids (non-solid) as high as 37 percent when it is clean [43]. For such a material, the issues are how effectively the modulus of the ballast can be calculated using the above formula and how to relate the modulus to other engineering parameters used for track design and evaluation.

3.9 Specifications for Purchase on Seismic Testing Equipment

The alternative components needed to conduct surface wave testing are explained above in this section. Based on this initial assessment and research activities discussed in the next sections, the specifications for acquiring a seismic system and the alternative vendors are provided in Section 6.

3.10 Best Alternatives for Seismic Testing

The alternative test configurations and algorithms needed to conduct surface wave testing are also explained above in this section. Based on this initial assessment and research activities discussed in the next sections, a systematic protocol for performing the field surface wave tests is also provided in Section 6.

4. Improving Seismic Techniques for Track Assessments

This section presents the results from the initial laboratory and field testing used to adjust and improve existing pavement related to seismic testing equipment, which aided in performing cost-effective and rapid track substructure assessments. In addition, this section presents:

- How railroad personnel can acquire their own system based on the following specifications: customized surface wave test setup for assessing railroad track substructures, which consists of detailed information on the components of the system, e.g., receivers, excitation systems, computer, data acquisition software, AD converter, etc..
- How technical information provides meaningful data to operate the system.
- How to interpret the data with extensive information to obtain profiles of shear-wave velocity and shear modulus vs. depth.

4.1 Initial Experimental Efforts and Results

Due to the complexity of seismic tests on a railroad, certain technical knowledge and experience will be part of the basis for developing a surface-wave testing system by improving the existing hardware and customizing the current software for use in the railroad environment. The initial work plan required limited experimental work under actual track conditions using the low-density ballasted track at Monticello Railway Museum and an abandoned rail bed in El Paso, TX. The research team noticed from the onset that a more rigorous and extensive experimental plan was needed because of the many variables involved. As such, the experimental efforts were broken down into the following three steps: (1) small-scale laboratory testing to develop a system, (2) large-scale field-testing to refine the system, and (3) a revenue railroad to actually test the system. The small-scale testing was performed on the UTEP campus to primarily study the coupling of seismic energy and receivers to the ballast. The large-scale field-testing was performed on an 11 ft. by 20 ft. (3.3 by 6.1 m) ballast bed with a thickness of 1 ft. (0.3 m) without ties specifically constructed for this project to refine/optimize sensor spacings and the excitation source. Finally, a revenue railroad outside of El Paso, TX, was used for testing and verification purposes. More than a dozen trips to the large-scale field-testing facility and the revenue railroad were necessary to refine the equipment.

To simplify the discussion in this section, only phase velocity and shear-wave velocity are used to explain the test results. Conversion of the shear wave velocity to shear and Young's modulus is explained in Section 2.1 and can be performed using Equations (1) and (2).

4.2 Initial Equipment Used

The initial candidate equipment and major accessories used in these tests included:

- A four-channel signal analyzer (Tektronix 2630) and a National Instrument DAQ model 6062E (see Figure 23)
- Several sets of accelerometers (including PCB 308B02 with frequency range of 3 to 3,000 Hz) and Mark Products 4.5 Hz geophones (see Figure 24)

- A metal spike with removable magnetic seat for receiver mounting (Figure 25)
- Impact energy sources (sledgehammers and kettlebell weight see Figure 27)

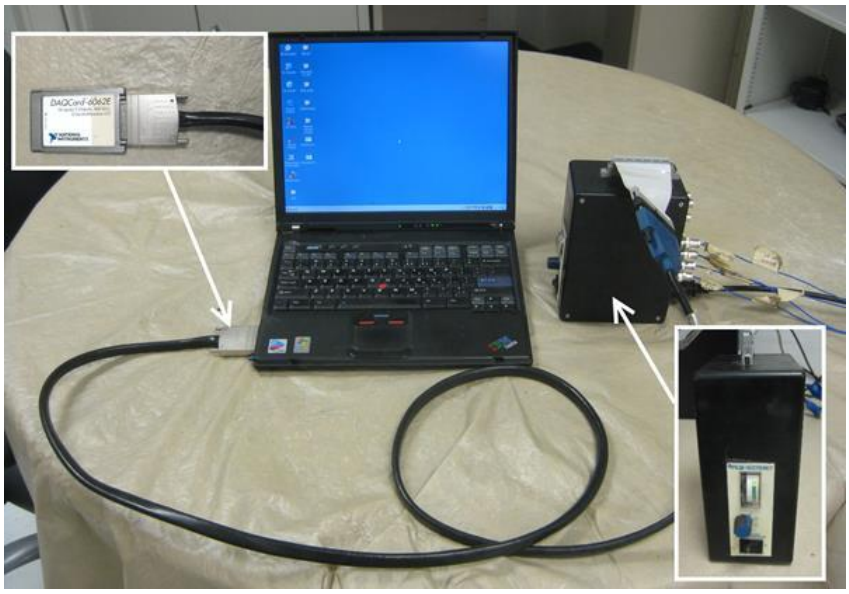

Figure 23. Data Acquisition Hardware: A National Instrument DAQ Model 6062E (Top Inset) and an Interconnection Box with PCB Signal Conditioner (Bottom Inset)

Figure 24. Geophone and Accelerometer

Figure 25. Accelerometer, Magnetic Seat, and Metal Spike

Figure 26. Impact Energy Sources (2-oz Ball-Peen Hammer, 3 lb. Sledgehammer, 10 lb. Sledgehammer and 30 lb. Kettlebell Weight)

4.3 Laboratory Small Scale Testing

During testing, a 1-ft (0.3 m) thick ballast layer was used with an open drum as the foundation that had a 3-ft (1 m) diameter filled with compacted soil, as seen in Figure 27, while ballast particles range from 0.5 to 1.5 inches. The objectives of the small-scale testing were:

- To determine a practical means for coupling the receivers to the ballast and determining the optimal impact energy source
- To observe the quality of signals at high frequencies (500 Hz to 3,000 Hz) while concentrating on ballast properties only
- To obtain knowledge about the phase velocity values of Rayleigh waves propagating in ballast material

Figure 27. Setup of Small Scale Laboratory Ballast Testing Setup at UTEP

Figure 28 shows average-quality records from tests with 0.5-ft (0.15 m) and 1.0-ft (1.0 m) receiver spacings. In each image in Figure 28, phase spectrum of transfer function, coherence function, waveforms from near and far receivers are located at the upper left, upper right, lower left, and lower right, respectively. Each transfer function or coherence function represents the average generated by five energy impacts. Some portions of the transfer functions, which are used for deriving dispersion curves, are contaminated particularly for the test with the small receiver spacing (0.5 feet). As discussed above, several factors such as high-frequency scattering and attenuation, as well as mounting coupling frequency may cause the noisy waveforms and the transfer functions. The effects of these factors are also partially reflected in the coherence function. In addition, the reflections from the inner wall of the drum could be another factor.

Figure 29 represents the dispersion curves derived from the transfer functions shown in Figure 28 through a smoothing procedure [19]. The weighted average phase velocity of 660 ft/sec is obtained when wavelengths of up to 1-ft (thickness of the ballast layer) are considered (USW approach). This average phase velocity is equivalent to an average shear-wave velocity of about 710 ft/sec with an assumed Poisson's ratio of 0.3 for the ballast layer. The dispersion curves are plotted in two manners, phase velocity vs. wavelength and phase velocity vs. frequency, to illustrate that surface wave testing can characterize the wavelength or frequency range of a ballast layer.

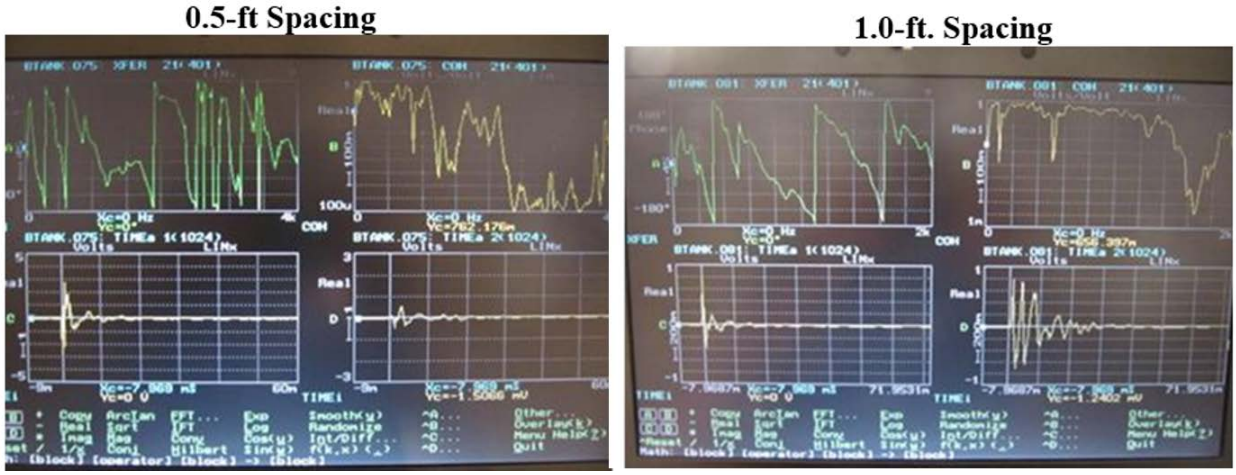

Figure 28. Photo Images of Measurement Records from Small-Scale Laboratory Testing at UTEP (Left: 0.5-ft Accelerometer Spacing, Right: 1.0-ft Accelerometer Spacing)

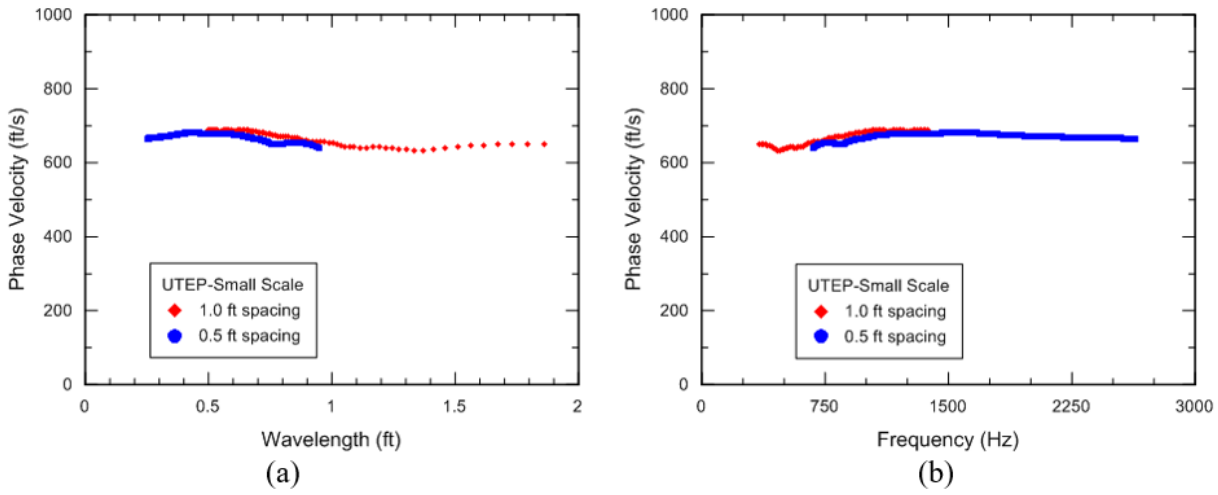

Figure 29. Typical Results of: (a) Phase Velocity vs. Wavelength and (b) Phase Velocity vs. Frequency from Small-Scale Testing at UTEP

The observations and experience from the small-scale testing can be summarized as follows:

1. Accelerometers, instead of geophones, are necessary for receiving high-frequency signals with short receiver spacings.
2. To generate a stable impact, a small metal strike plate should be embedded into the ballast to receive the impact prior to testing.
3. Receivers should be affixed with a magnetic seat attached to the top of a spike driven into the ballast. The use of a magnetic seat instead of plastic or similar soft materials is required to minimize the attenuation of high frequency signals.
4. The spikes should have enough strength and a minimum length (2 times of the largest aggregate size in ballast) to be driven firmly into the ballast.

5. The interference and noise mentioned above can have significant negative impacts on the quality of high frequency data (from short receiver spacings).

4.4 Large Scale Field Test Pad

As shown in Figure 30, a ballast bed was built on an old and well compacted soil foundation for the large-scale testing. The ballast bed is 22 ft. (6.6 m) long and 11 ft. (3.3 m) wide and has a thickness of 1 ft. (0.3 m), as ballast particles range from 1.0 to 3.0 inches. The effects of lateral reflections were eliminated when tests were conducted along the central portion of the ballast bed. This is a big improvement over the laboratory testing. The ballast material (crushed limestone) is similar to that used in small scale testing. The top portion of the foundation soil (containing small gravel and crushed rock) was quite stiff characterized by an average California Bearing Ratio (CBR) of 95 from Dynamic Cone Penetrometer (DCP) tests.

Figure 30. Ballast Test Pad for Large Scale Seismic Testing Near UTEP

The objectives of the large-scale testing were to:

- Investigate the consistency and variation of high frequency data collected at different locations on the ballast due to differences in receiver coupling and wave path (scattering pattern)
- Study the feasibility of whether the average shear-wave velocity can be reasonably estimated in a statistical manner through simple USW approach
- Confirm the accelerometers used in the small-scale testing can be also effectively used in data collection at low frequencies (20 Hz or less) so that a shear-wave velocity profile can be defined up to a depth of 15 ft. (4.5 m)
- Determine the optimal impact sources, e.g., hammer, that can be used to effectively generate surface wave signals at different frequency ranges (receiver spacings) in ballast
- Obtain a dispersion curve that contains the phase velocity data up to wavelengths of 30 ft. (9 m) or greater

In the first step of this testing, two short receiver spacings (0.5 and 1 ft.) were used. Phase velocity dispersion curves obtained from acceptable measurements at different locations on the

ballast bed are shown in Figure 31. Due to the smaller size of the variation of dispersion curves up to the wavelength of the thickness of the ballast bed (1 ft. or 0.3 m), the USW approach was used to analyze that data. The statistics of phase velocities at wavelengths up to 1 ft. (0.3 m) are summarized in Table 4. Due to the velocities in a dispersion curve not evenly distributed with wavelength, the average phase velocity from each test is reached through a moving average.

Statistically, the phase velocities at wavelengths up to 1 ft. (0.3 m) from multiple tests at both 0.5 ft. and 1.0 ft. receiver spacings are consistent. The data shown in Table 4 provides experimental criterion, i.e., what level of variation in terms of ballast shear-wave velocity caused by fouling, particle size distribution, density, etc., can be identified by surface wave testing. The variation of ballast shear-wave velocity should be around 5 percent for the small differences in phase velocity shown in Table 4. The statistics of phase velocities from the ballast test bed using closely spaced accelerometers are also shown in Table 4.

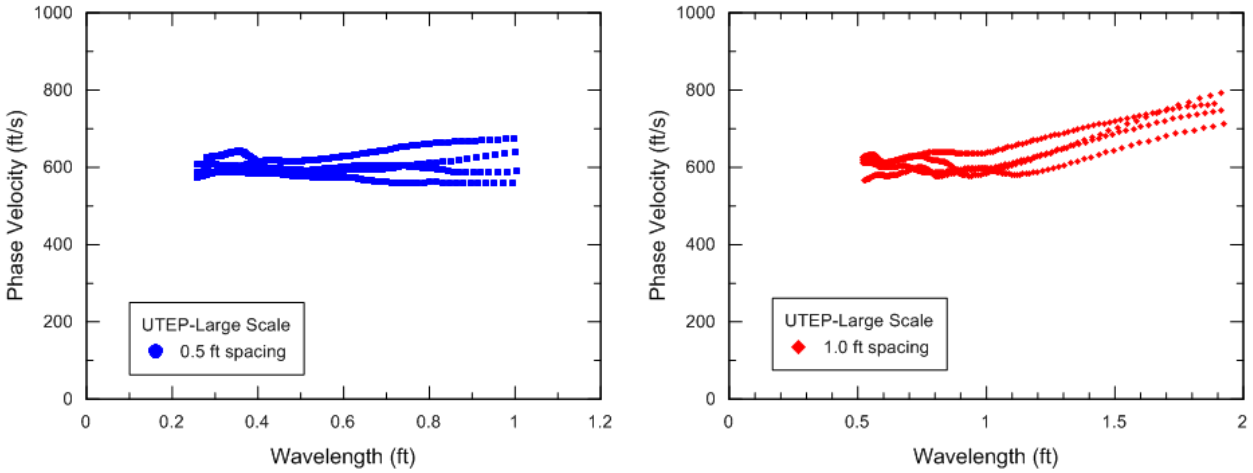

Figure 31. Dispersion Curves Obtained from Closely Spaced Accelerometers on Ballast Test Bed Near UTEP with Receiver Spacings of 0.5 and 1.0 Feet

Tests with a PSPA were also conducted on this ballast bed at the same locations where SASW tests were performed. The average phase velocity from the PSPA tests is about 730 ft/sec (223 m/sec) for the ballast, which is greater than the values shown in Table 4. These differences, which are related to the differences in receiver coupling and impact source mechanism as well as scattering pattern, need further studies.

Table 4. Statistics of Phase Velocities from Ballast Test Bed Using Closely Spaced Accelerometers

	Average Phase Velocity (ft/second & m/second)		
Test	**0.5 ft. (0.15 m) Receiver Spacing**	**1.0 ft. (0.30 m) receiver spacing**	**Difference in Phase Velocity**
1	582	599	-17
2	631	630	1
3	590	585	5
4	605	610	-5
Average	602	606	7
Standard Deviation	22	19	6
Coefficient of Variation (%)	3.6	3.1	0.9

In addition, the average phase velocity obtained from tests on this ballast bed is about 10 percent less than that from tests on the ballast in the laboratory drum. These differences are attributed to the differences in particle size distributions in the two cases with the ballast test bed having significantly larger size ballast particles (1.0 to 3.0 inches).

In the second step of the large-scale testing, tests with receiver spacings of 0.5, 1, 2, 4, 8, 12 and 16 ft. (0.15, 0.3, 0.6, 1.2, 2.4, 3.7, and 4.9 m) from the energy source were conducted to generate a broad-band dispersion curve. Such a broad dispersion curve can be used to derive a shear-wave velocity profile from the ballast layer down to a depth of 10 ft. or more in the soil foundation. Before reaching that point, it is important to first understand the characteristics of a dispersion curve obtained from tests on this ballast-soil foundation structure. The phase velocity from the first four receiver spacings (0.5, 1.0, 2.0, and 4.0 ft.) vs. wavelength and frequency are shown in Figure 32. Phase velocities at wavelengths between 0.5 and 2 times of spacing lengths were adopted from each receiver pair.

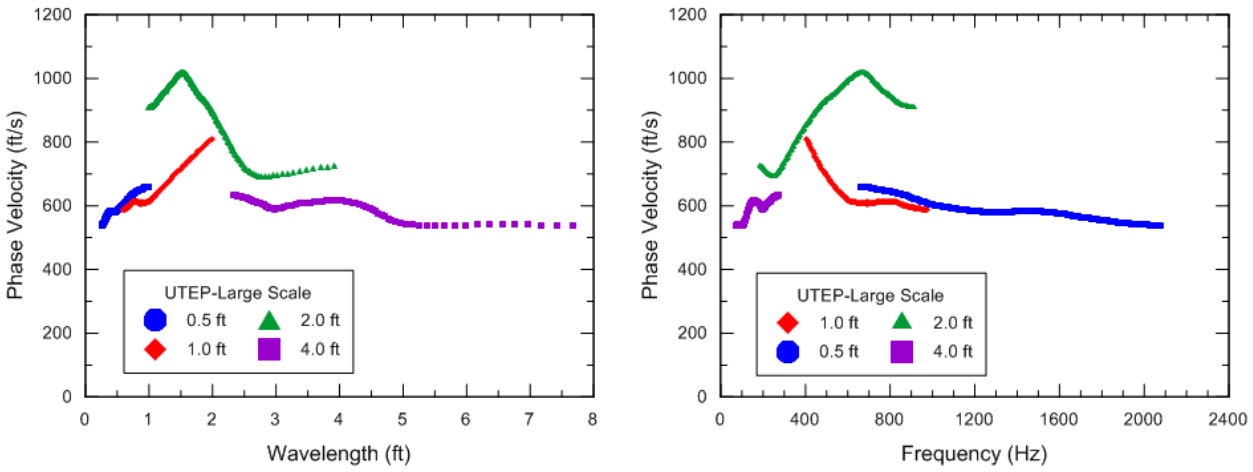

Figure 32. Typical Results of: (a) Phase Velocity vs. Wavelength and (b) Phase Velocity vs. Frequency from Ballast Test Bed Near UTEP with Receiver Spacings of 0.5, 1.0, 2.0, and 4.0 Feet

The dispersion curves shown in Figure 32 represent a typical composite dispersion pattern characterized by the following features (there are more features and issues on composite dispersion that could be addressed and discussed than those covered in this report):

1. Phase velocities from receiver spacings of 0.5 and 1.0 ft. (0.15 to 0.30 m) at wavelengths less than 2 ft. (0.6 m) or at frequencies greater than 400 Hz represent a normal dispersion pattern (velocity increases with wavelength increases or frequency decreases). As expected, the dispersion curves from these two receiver spacings are smoothly and closely connected.
2. There is a big gap between dispersion curves from receiver spacings of 0.5 and 1.0 ft. and receiver spacing of 2 ft. and 4 feet. The later may contain the higher-mode component as earlier mentioned. With the waveform imaging technique used in MASW approach, such a gap may be represented by a broad contour.
3. Starting at a wavelength of about 2 ft. (see Figure 32(a) and receiver spacings of 2.0 and 4.0 ft.), phase velocities represent an inverse dispersion pattern (velocity decreases with wavelength increases or frequency decreases) and are accompanied by a gap or discontinuity (branching).

Obviously with any curve fitting or handpicked approach, a final dispersion curve (for inversion use) constructed from the data provided in Figure 32 only represents the mixed or average dispersion curve, which means the dispersion data are combined or approximated. This feature of a composite dispersion curve is essential and important for understanding the result derived from a set of composite dispersion data.

Figure 33 shows the dispersion data obtained from all receiver spacings (0.5 ft. to 16 ft.) and a representative or "measured" dispersion curve that is used for the inversion process (Section 3.2). The representative or "measured" dispersion curve is developed by combining all the raw data into one dispersion curve. Based on the representative or "measured" dispersion curve shown in Figure 33, a shear-wave velocity profile for the ballast bed site was derived. Figure 34

shows the derived shear-wave velocity profile and the comparison of matched and measured dispersion curves in which the match dispersion curves are calculated from the inversion process.

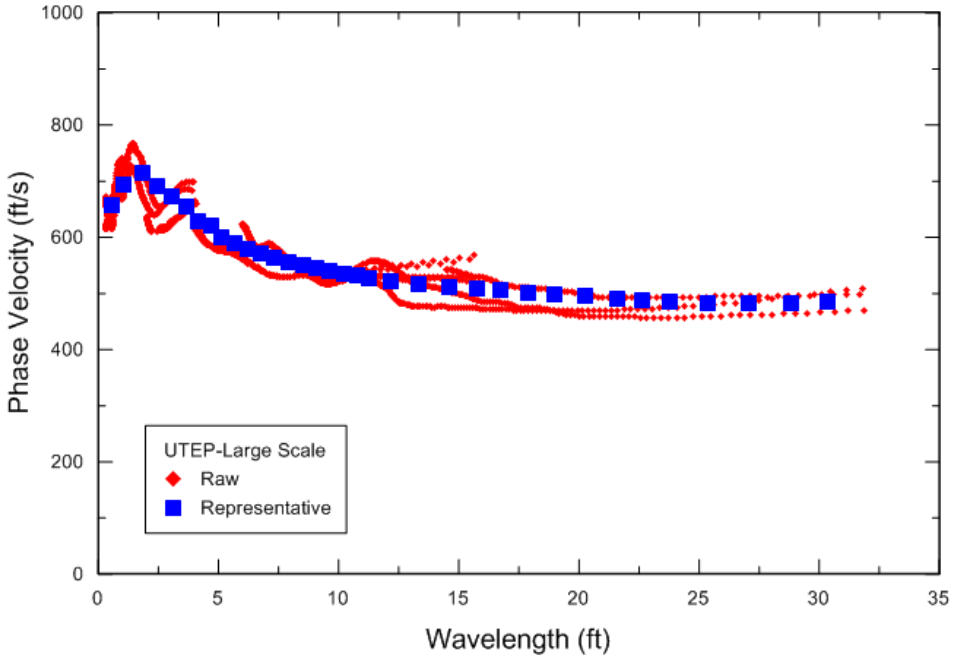

Figure 33. Raw and Representative Dispersion Curves for All the Measured Dispersion Curves from Ballast Test Pad Near UTEP

While conducting a data analysis and an inversion process, the ballast bed was divided into two layers: the upper and lower ballast. This treatment was also applied to all cases in this study where the inversion process was involved. The upper ballast layer consists of more coarse aggregates with more air voids, and thus has a lower density and unit weight, typically, 1,700 kg/m3 to 1,800 kg/m3 (106 pcf to 112 pcf) for clean ballast, depending on the rock type and ballast borrow source. Normally, the propagation speeds of all seismic waves in the upper ballast are lower than those in the lower ballast because of the greater void space.

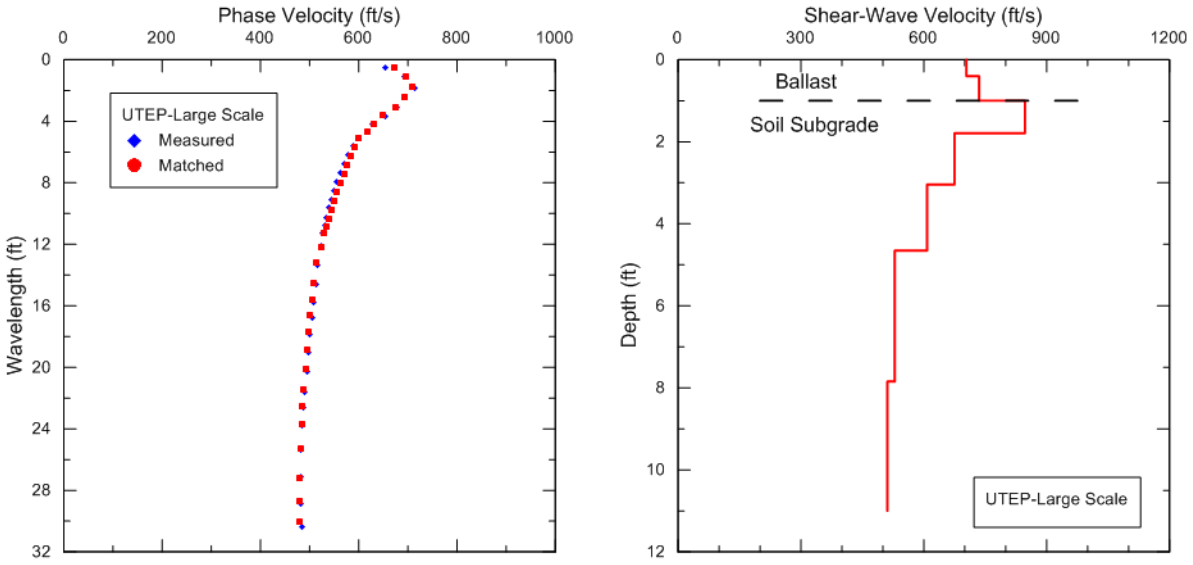

Figure 34. Plots of: (a) Comparison of Measured and Matched Dispersion Curves and (b) Derived Shear-Wave Velocity Profile from Ballast Test Bed Testing Near UTEP

The experience from the large scale test bed testing can be summarized as follows:

1. The accelerometers and impact sources used are suitable for receiving low-frequency (20 Hz or less) signals with a receiver spacing up to 20 feet (6 m).
2. In most cases, a small hammer (1 to 2 lbs.), a large hammer (8 to 10 lbs.), and a weight drop (30 to 40 lbs.) provide sufficient energy and can be used as impact sources successfully for surface wave measurements for receiver spacing less than 4 ft. (1.2 m), 4 to 12 ft. (1.2 to 3.6 m), and greater than 12 ft. (3.6 m), respectively.
3. To generate a stable impact, a metal strike plate should be used and embedded into the ballast prior to testing when a sledgehammer is used as impact source.
4. The effects of receiver mounting resonance, high frequency scattering, and high frequency attenuation decrease with increasing receiver spacing (deceasing frequency) and can be ignored for receiver spacing of 4 ft. and greater.

4.5 Field Testing on El Paso, TX, Revenue Railroad

This field testing was performed on a section of railroad located inside the northwest yard of Jobe Materials, Inc. in El Paso, TX (Figure 35). The site consists of timber ties with spacings of 2-ft. (0.6 m), which is larger than the typical 19.5 inches (0.5 m). The track in that section consists of a 10-inch (250 mm) thick ballast bed and subgrade that contains two caliche layers: one immediately under the ballast and another at a depth of about 10 feet (3 m). The ballast was slightly fouled along this track section. In comparison with the ballast materials used for small-scale testing and large-scale testing, the ballast in this track was considerably larger/coarser.

Figure 35. Photos showing: (a) Location Map of Jobe Materials Field Test Site North of El Paso International Airport and (b) Overview of Test Area with Portable Surface Wave Test Equipment and Laptop, Timber Ties, 136 Rail, and Ballast

The objectives from testing at this revenue railroad are:

- To confirm that the accelerometers used in the small-scale and large-scale testing can also effectively be used in data collection from a revenue railroad track
- To confirm that the impact energy sources used in the large-scale testing can also effectively be used to study the effect of crossties on the resulting measurements

Initially tests were conducted at the track center with receiver spacings of 2, 4, 8, and 16 ft. (0.6, 1.2, 2.4, and 4.8 m) from the energy source. Tests were also conducted at the track center with receiver spacings of 1, 2, 4, 6, 14, and 18 feet (0.3, 0.6, 1.3, 1.9, 4.3 and 5.6 m). The final dispersion curves constructed from the data obtained from all these field tests are shown in Figure 36. The derived shear-wave velocity profile is also included in this figure.

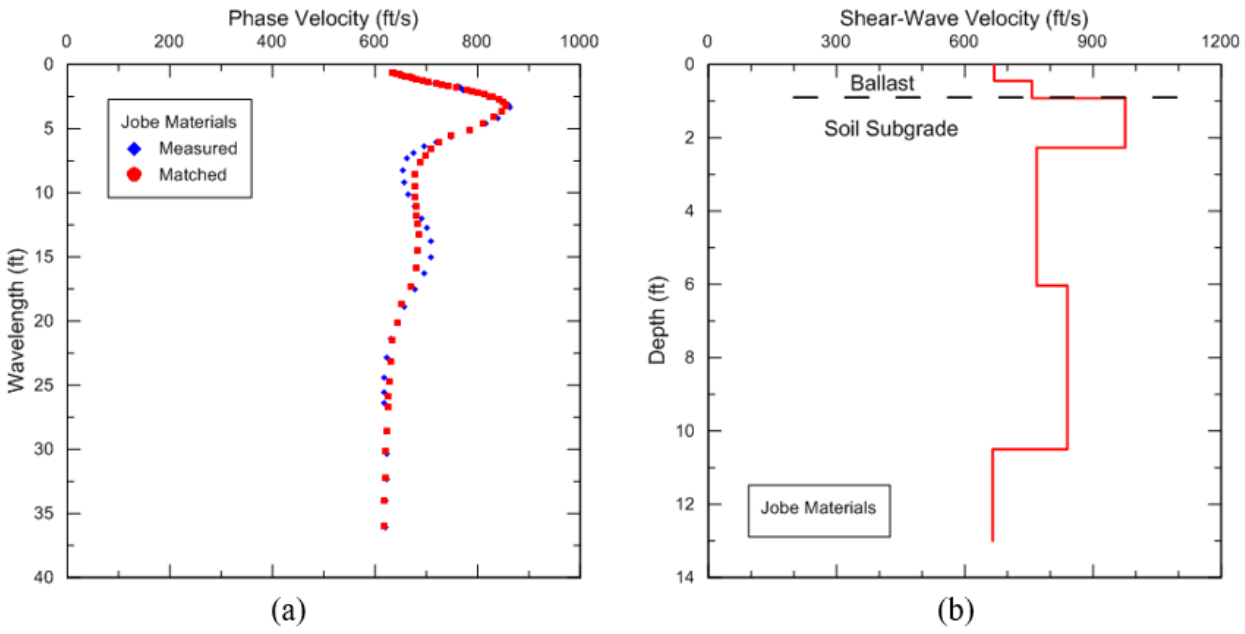

Figure 36. Plots of: (a) Comparison of Measured and Matched Dispersion Curves and (b) Derived Shear-Wave Velocity Profile from Jobe Materials Track Testing

The shear-wave velocity profile at this site was derived in an alternative manner. Due to both normal and inverse dispersion trends existing in the dispersion curve, the curve was broken into two parts: (1) one curve (wavelengths less than 4 ft. (1.2 m)) with normal dispersion trend and (2) a second curve (wavelengths equal to or greater 4 ft. (1.2 m)) with inverse dispersion. The two parts of the dispersion data/curve were inverted separately. The shear-wave velocity profile shown in Figure 36(b) is a combination of the results from these two inversion procedures. However, the shear wave velocity profile found in Figure 36(b) shows the ballast layer with a shear wave velocity of 650 to 750 ft/sec that is underlain by a much stiffer soil with a shear wave velocity of over 900 ft/sec. The upper caliche layer exhibits a decrease in shear wave velocity probably due to an increase in moisture content as the upper part of this layer was desiccated in the arid climate of El Paso. At a depth of about 10 ft. (3 m), the lower caliche layer exhibits a shear wave velocity of 600 to 700 ft/sec.

The experience from the tests on this railroad trackbed can be summarized as follows:

1. The accelerometers and impact sources used are suitable for receiving low-frequency (20 Hz or less) signals with receiver spacings up to 20 feet (6 m).
2. Due to the scattering from large size aggregates in ballast and the effects of crossties, it is difficult to obtain reliable high frequency (greater than 500 Hz) data, which corresponds with a receiver spacing 2 ft. (0.6 m) or less.
3. The effects of crossties decreases significantly as signal frequency decreases or receiver spacing increases.
4. The current automated inversion process has difficulties to deal with the dispersion data from the structure of irregular shear-wave distribution with depth.

5. Full-Scale Seismic Wave Testing

This section presents the results from full-scale testing at several railroad revenue service sites using the seismic wave system described in the previous section. In addition, this section presents:

- The data used from full-scale or revenue service testing including shear-wave velocity, shear strength, and shear modulus profiles vs. depth at the HTL sites tested at the Transportation Technology Center (TTC) in Pueblo, CO.
- A comparison was conducted of the shear-wave velocity, shear strength, and shear modulus data with the actual conditions installed at the test locations using available GPR and other data at the HTL sites.
- Documentation of a realistic evaluation of the surface wave system, which provides the opportunity to further improve the testing methodology for the surface wave techniques as well as the development of new, objective testing equipment and protocols.

Full-scale surface-wave tests were conducted at the following four revenue service sites:

1. HTL of TTCI at Pueblo, CO
2. UP near Ogallala, NE
3. PAL at Gilbertville, KY
4. Amtrak at South Kingstown, RI

This section presents the results of tests at these railroad sites, which include the estimated shear-wave velocity profiles of ballast and subgrade with the SASW approach and the average shear-wave velocities of ballast with the USW approach as described in Section 2. The USW approach was implemented using: (1) PSPA for measurement of average velocity of top 12 inches of the ballast and (2) seismic signals collected with short spacings from the SASW tests.

5.1 The HTL at TTCI in October 2013

The HTL is one of seven tracks that belong to TTCI in Pueblo, CO.[1] The HTL consists of 30 major sections, which are categorized based on the unique features of each section and are shown in Figure 37.

In HTL, seismic wave tests were performed at six sections on October 28 and 29, 2013, and two sections on April 2, 2014. A summary of these tests is presented in Table 5 for the 2013 testing and Table 5 for 2014, respectively.

[1] Association of American Railroads (subsidiary of TTCI). Test Tracks: High Tonnage Loop – HTL. http://www.aar.com/tracks.php.

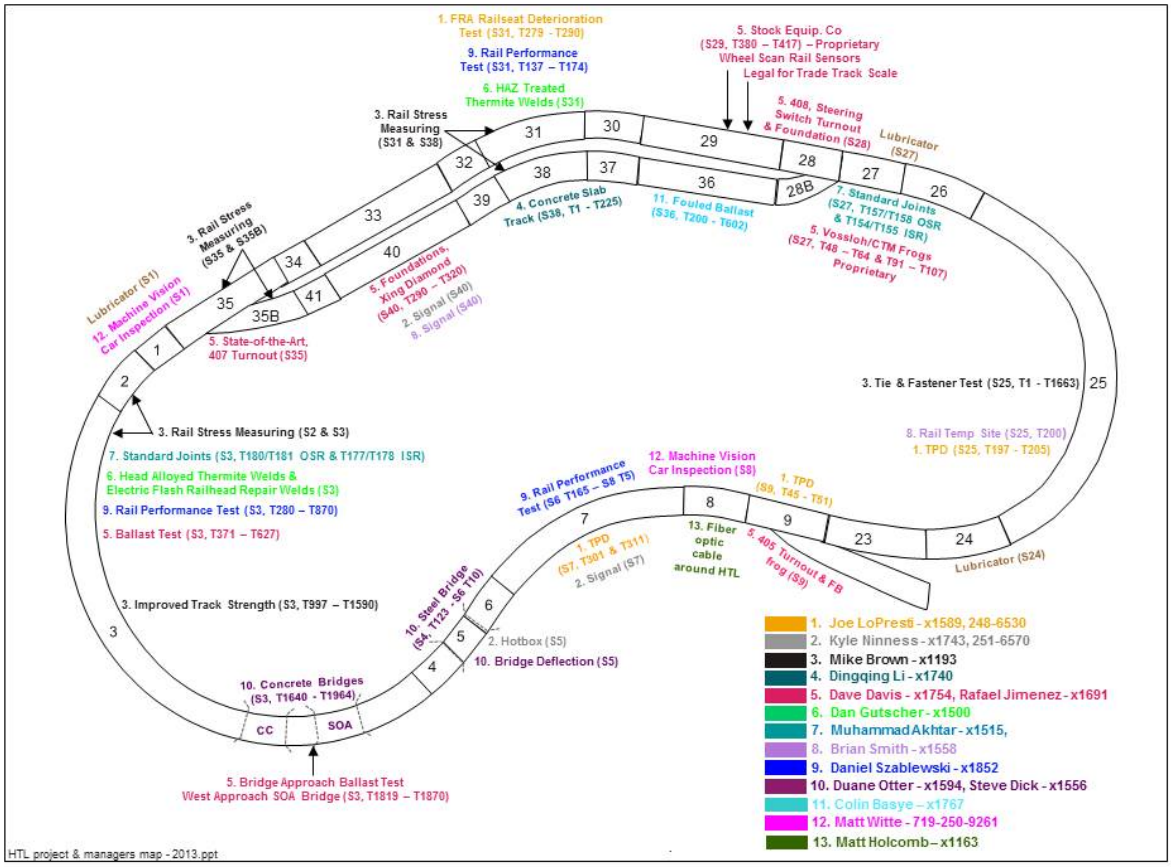

Figure 37. Diagram Showing Various Sections Around HTL at TTC in Pueblo, CO

Table 5. Test Sites at HTL (October 2013)

Section #	Tie Numbers	Section Feature	Ballast Thickness (inch/meter)	Test Remarks
9	89 to 94	Dry	16/0.41	Fouled Ballast
	89 to 94	Wet		
8	148 to 143	Dry	26/0.66	Clean Ballast
7	588 to 583	Dry	24/0.61	Clean Ballast
29	430 to 421	Concrete Tie – Failed HMA	28/0.71	Weak Subgrade
	479 to 488	Wood Tie – Intact HMA		
36	400 to 390	0% Fouling	32/0.81	Fouling at different levels
	314 to 301	10% Fouling	30/0.76	
	230 to 221	20% Fouling	32/0.81	
3	1831 to 1822	Granite	46/1.17	Ballast of different rock types
	1805 to 1796	Basalt	40/1.01	

Table 6. Test Sites at HTL (April 2014)

Section #	Tie Numbers	Section Feature	Ballast Thickness (inch/meter)	Remarks
29	430 to 421	Concrete Tie – Failed HMA	28/0.71	Weak Subgrade
	479 to 488	Wood Tie – Intact HMA		
36	10% Fouling	10% Fouling	30/0.76	Fouled ballast

5.1.1 SASW Tests on October 28 and 29, 2013

This section of the report provides a summary of the test results from the seismic surface wave testing based on the SASW approach conducted on October 28 and 29, 2013, at the HTL. The sections tested during this site visit are: HTL Sections 9, 8, 7, 29, 36, and 3. The following discusses the testing and test results for each of these track sections.

HTL Section 9

This track section is located near a dirt road crossing. The ballast at this site was significantly fouled with fine soil due to windblown dust from the dirt road and surrounding area. The average thickness of the ballast was 16 inches (0.41 m). Tests were first conducted in the natural condition of the dry fouled ballast, i.e., no additional water added. The site was then sprayed with water and tests were conducted on the wet fouled ballast. Four accelerometers were placed on the ballast at spacing of 20, 40, 60, and 80 inches (0.5, 1, 1.5, and 2 m) along the center of the track in a longitudinal direction between the rails.

The dispersion data, and the shear-wave velocity profile from the dry experiment, were not available due to an absence of high quality data and an inadequate amount of time to repeat the tests. As stated, high quality data implies that there is an availability of a phase spectrum plot to produce a reliable dispersion curve. However, dispersion data are available for analysis (inversion) from the wetted ballast tests. Figure 38 shows the dispersion curves and corresponding shear-wave velocity profile for the wetted ballast experiment. The shortest wavelength of the dispersion curve shown in Figure 38 for the wetted experiment is 2 ft. (0.6 m), which is not sufficient to characterize the top portion of the ballast. As a result, the estimate for the shear-wave velocity of the top ballast layer is not as reliable, even though the calculated dispersion data from the derived model agrees with measured values. In terms of shear-wave velocity, the average shear-wave velocity in the ballast layer (<16 inches) is 710 ft/sec as opposed to 521 ft/sec in the subgrade (>16 inches). This suggests the ballast layer is 36 percent stiffer than the subgrade from the average shear-wave velocities of 710 ft/sec and 521 ft/sec.

Due to the high level of ballast fouling and the short period of time between the application of water and testing, only the top portion of the ballast layer was moistened by the limited amount of sprayed water. Therefore, the dispersion curve at wavelengths greater than 2 ft. (0.6 m) or so and the shear-wave velocity profile (for the bottom portion of the ballast and subgrade) under the wet experiment are also representative of the shear wave velocity profile that was present under the dry experiment conditions.

HTL Section 8

This test site had a visually “clean” ballast layer as the average thickness of the ballast was 26 inches (0.66 m). Four accelerometers were placed at the center of the track at nominal spacings of 20 inches (0.51 m). Figure 39 shows the dispersion curves and corresponding shear-wave velocity profile for this section. The dispersion curve for Section 8 shows a normal dispersive trend as compared to the dispersion curve for Section 9. Thus, the derived shear-wave velocities of the ballast for Section 8 show an opposite trend to those of Section 9. The shear-wave velocity of the upper portion of the ballast (552 ft/sec) is 23 percent less than the lower portion of the ballast (716 ft/sec vs. 552 ft/sec). However, the difference between the shear-wave velocities of the ballast and the subgrade is about 3 percent (716 ft/sec vs. 696 ft/sec). This implies that the lower portions of the ballast and the subgrade have similar stiffnesses at this site, which is probably due to some migration of the ballast into the subgrade.

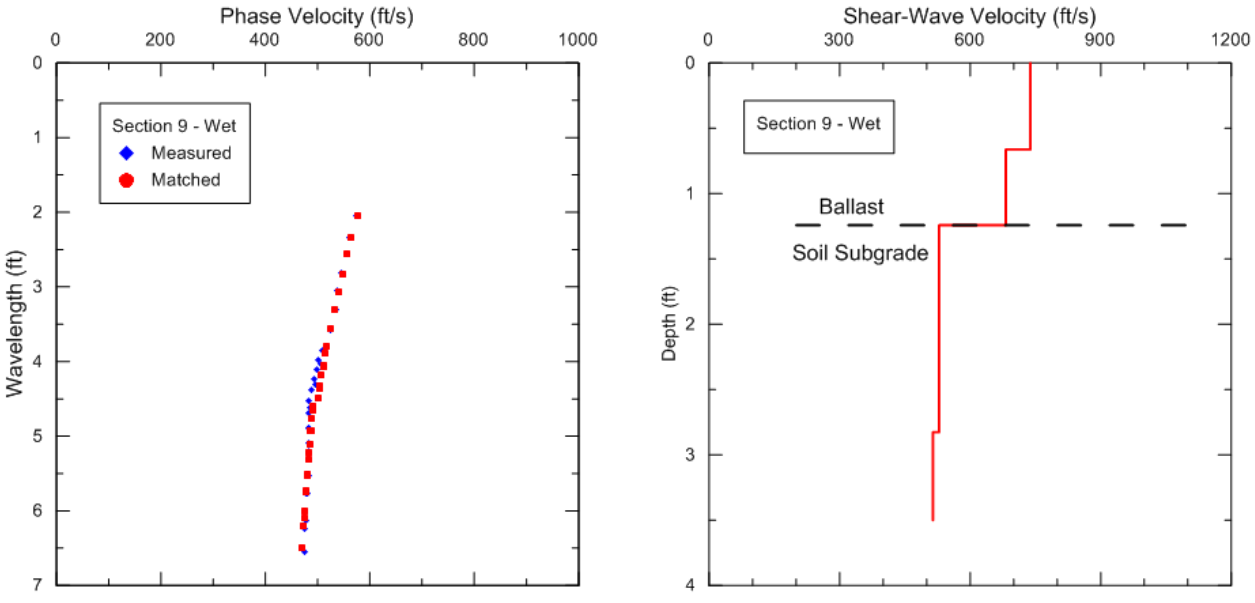

Figure 38. Plots of: (a) Comparison of Measured and Matched Dispersion Curves and (b) Derived Shear-Wave Velocity Profile from Section 9 After Wetting of the Fouled Ballast at HTL on October 29, 2013

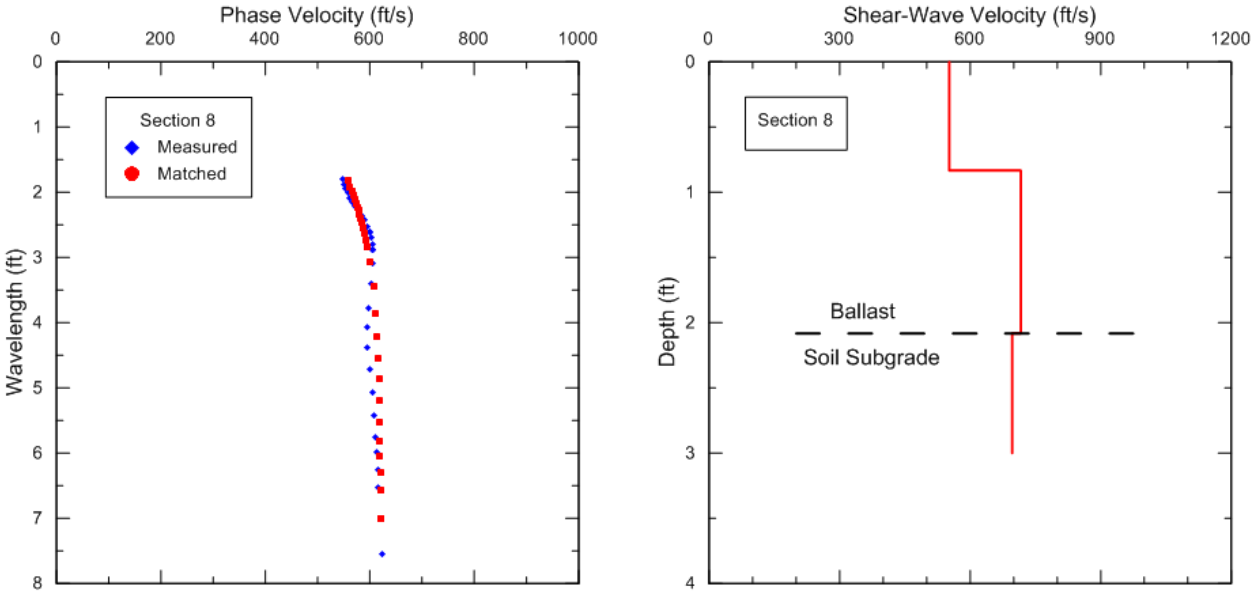

Figure 39. Plots of: (a) Comparison of Measured and Matched Dispersion Curves and (b) Derived Shear-Wave Velocity Profile from Section 8 at HTL on October 29, 2013

HTL Section 7

This section is located west of Section 8 and had a 16 inch (0.4 m) thick ballast layer. The array of accelerometers was positioned similar to Section 8 and Section 9, i.e., four accelerometers were placed at the center of the track at nominal spacings of 20 inch (0.51 m) giving distances of

20, 40, 60, and 80 inches from the energy source. The dispersion data at long wavelengths, thus, the shear-wave velocity profile for the subgrade were not available for this section because of the short-spacing setup of the accelerometers limiting the collection of long wavelength data. To obtain long wavelength dispersion data, the spacing of the accelerometers had to be expanded as discussed in the next sections. This is an important finding for recommendations for future testing presented below.

HTL Section 29

This section is situated along the northern portion of the HTL. The main feature of the section is that the track was constructed over a bed of Buckshot Clay. The track was originally comprised of 20 inches (0.5 m) of ballast, 4 inches (0.1 m) of hot mix asphalt (HMA), and 4 inches (0.1 m) of clean gravel and sand. Due to the presence of the Buckshot Clay layer underneath the track, the track section is also named as "historically weak subgrade" section. Section 29 was divided into two sub-sections. One of them had concrete ties and the other had wood ties. The sub-section with concrete ties had a failed HMA layer. In contrast, the HMA layer along the sub-section with wood ties was still intact. The subgrade in the concrete tie section was considered weaker than that in the wood tie section.

Seismic tests along these two sub-sections were conducted with the same test set up. The test set up consists of two "source-receiver" configurations. In the first configuration, the accelerometers were placed along the center of the track and between the ties such that their positions were approximately 2, 4, 8, and 16 ft. (0.6, 0.8, 1.6, and 4.8 m) from the location of the impact energy source. Figure 40 shows the schematic of the configuration. To increase the depth of the investigation and assess the influence of the Buckshot Clay layer, the accelerometer spacing was doubled and tests were repeated. In this second source-receiver configuration, the positions of accelerometers were 4, 8, 16, and 32 ft. (1.2, 1.6, 3.2, and 9.6 m) from the energy source. Figure 41 shows the schematic of the second configuration. The SASW results from the concrete tie section are labeled as "concrete tie – failed HMA" (CF) and "wood tie – intact HMA" (WI) in the wood tie section.

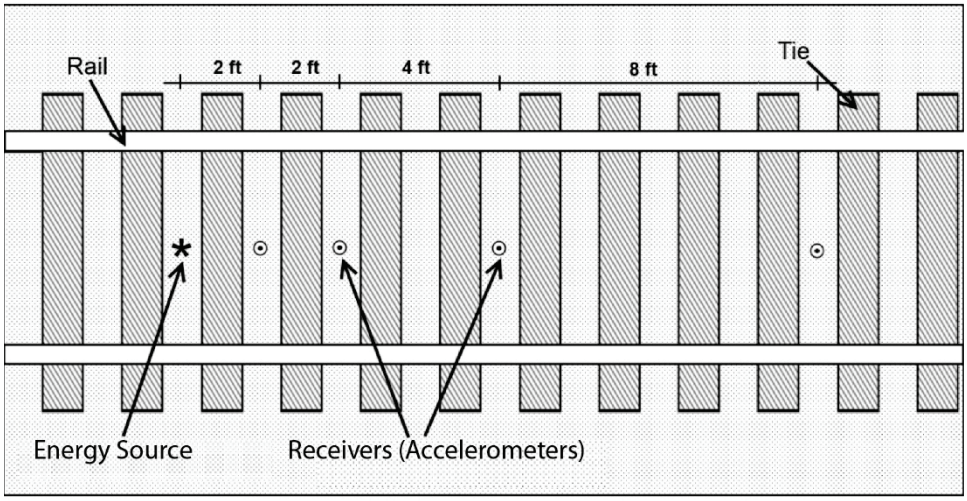

Figure 40. Data Collection Setup for Short Array (Small Spacing Between Accelerometers) SASW Tests at HTL on October 29, 2013

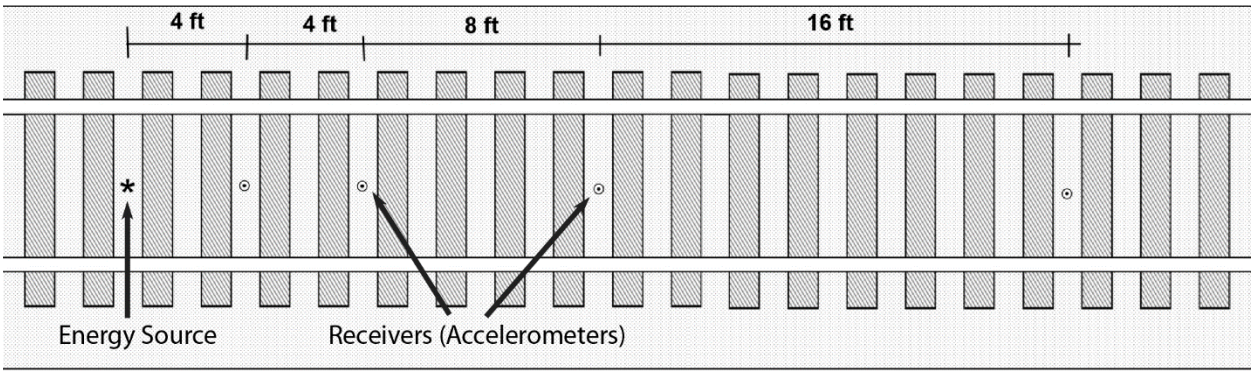

Figure 41. Data Collection Setup for Long Array SASW Tests (Large Spacing Between Accelerometers) 29 at HTL on October 29, 2013

Dispersion curves are obtained from each of the source-receiver configurations. For each sub-section, the measured dispersion curves are merged to produce a representative dispersion curve for inversion. Figure 42 shows the shear-wave velocity profiles and corresponding dispersion curves for both sub-sections. The velocity profiles show that the ballast layers of both sections almost have the same velocities. However, the velocity of subgrade for the concrete tie and failed HMA section "CF" is 17 percent less than the wood tie and intact HMA section "WI."

This 17 percent decrease in shear wave velocity for the "CF" section is in good agreement with the area recently experiencing a bearing capacity failure in the Buckshot Clay causing failure of the overlying HMA.

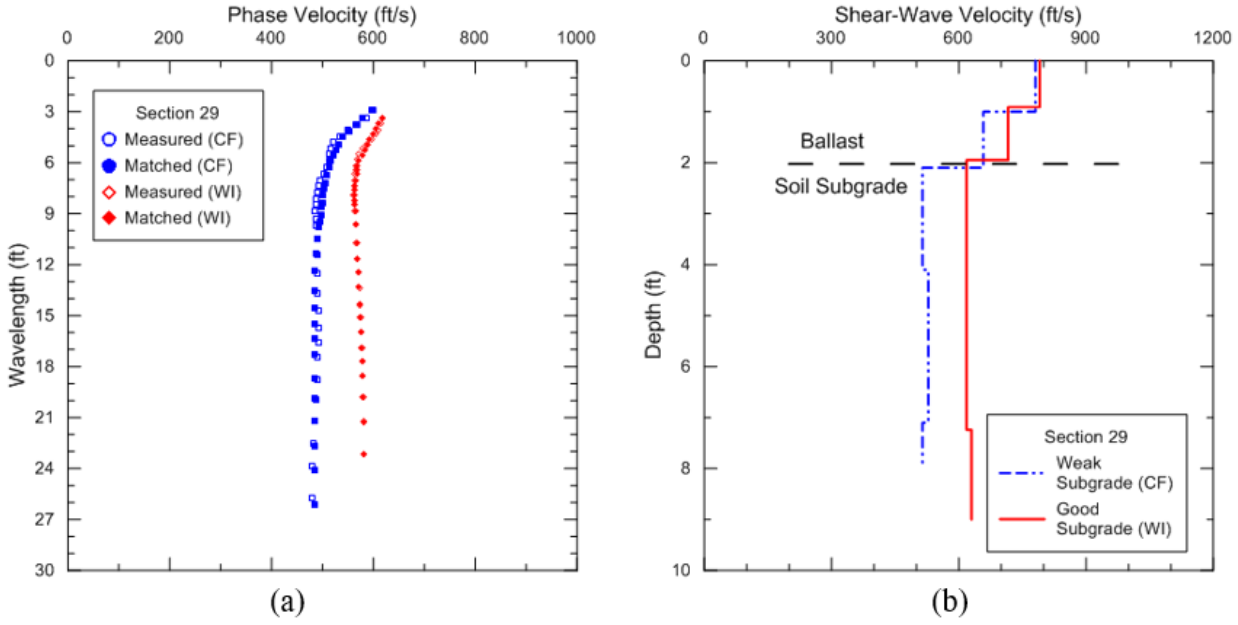

Figure 42. Plots of: (a) Comparison of Measured and Matched Dispersion Curves and (b) Derived Shear-Wave Velocity Profile from Section 29 at HTL on October 29, 2013

HTL Section 36

Section 36 is located south of the Section 29 and has a 32-inch (0.81 m) thick ballast. The entire section was separated into three sub-sections, distinguished by the level of ballast fouling. Two end sub-sections had fouling levels of 0 percent (clean ballast) and 20 percent, and the middle sub-section had a fouling level of 10 percent. However, the ballast in all sub-sections visually looked quite clean and most likely, the main reason for the similar appearance of ballast in the three sub-sections was due to the repeated percolation of rain water into the ballast washing out some of the fouling material.

The accelerometers were placed along the center of the track, between rails and ties, as shown in Figure 40. Figure 43 shows the dispersion curves and corresponding shear-wave velocity profiles for all three sub-sections in Section 36. The velocity profiles for 0 percent and 20 percent fouled sub-sections are similar. The average velocities of deeper subgrade soils (below 3.5 ft. (1.1 m)) for all sub-sections are also similar. However, there are some distinct differences in the velocity of the top and bottom portions of the ballast, which may reflect differences in fouling.

The average shear-wave velocity of ballast for the 10 percent fouled section is 24 percent less than the average shear-wave velocity for the 0 percent and 20 percent fouled sections. Differences in velocity are expected in ballast depending upon the level of fouling and ballast gradation, moisture content, and fouling material. However, the SASW results reveal a similarity in the shear-wave velocities of the ballast for clean and highly fouled ballast. This may be due to the influence of additional factors or that fouling levels on these sub-sections might had been altered due to climatic changes, cyclic train loading, or the fouling being washed away by rain and/or snow.

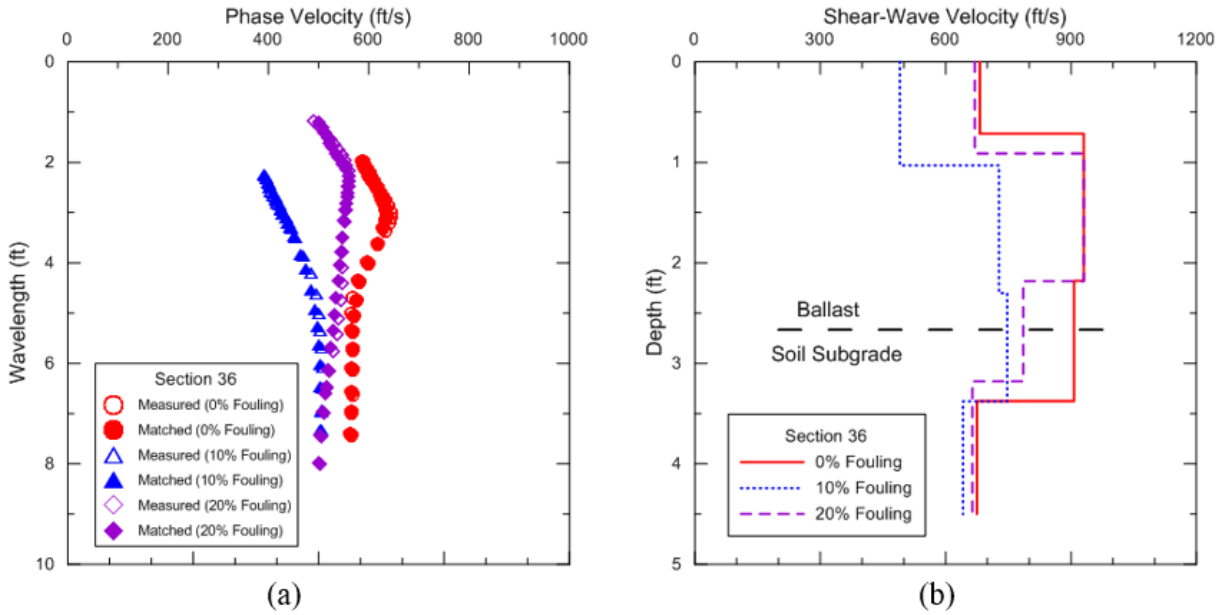

Figure 43. Plots of: (a) Comparison of Measured and Matched Dispersion Curves and (b) Derived Shear-Wave Velocity Profile from Section 36 at HTL on October 29, 2013

HTL Section 3

Section 3 is located along the western portion of the HTL. The main feature of this track section is the different rock types used for ballast. In particular, granite and basalt rock were used for ballast in two separated sub-sections of Section 3. As the focus of the experiment in Section 3 was investigating the effect(s) of ballast rock type on measured phase velocity, the dispersion curves were constructed from the short spacing array as shown in Figure 40. Figure 44 shows the resulting shear-wave velocity profile and corresponding dispersion curves for the granite ballast sub-section. The velocity profile shows an increasing trend of ballast velocity, i.e., the lower portion of the ballast exhibits a higher velocity than the upper portion. In addition, the velocity in the top portion of the subgrade (786 ft/sec) is 7 percent greater than the lower portion of the ballast (727 ft/sec), which is probably due to desiccation in the upper portion of the subgrade. However, the velocity of the subgrade at deeper depths below 7 ft. (2.1 m) (686 ft/sec) is about 12 percent lower due to less desiccation with depth. This is due to the decreasing trend of the phase velocity at deeper depths in the matched dispersion curve.

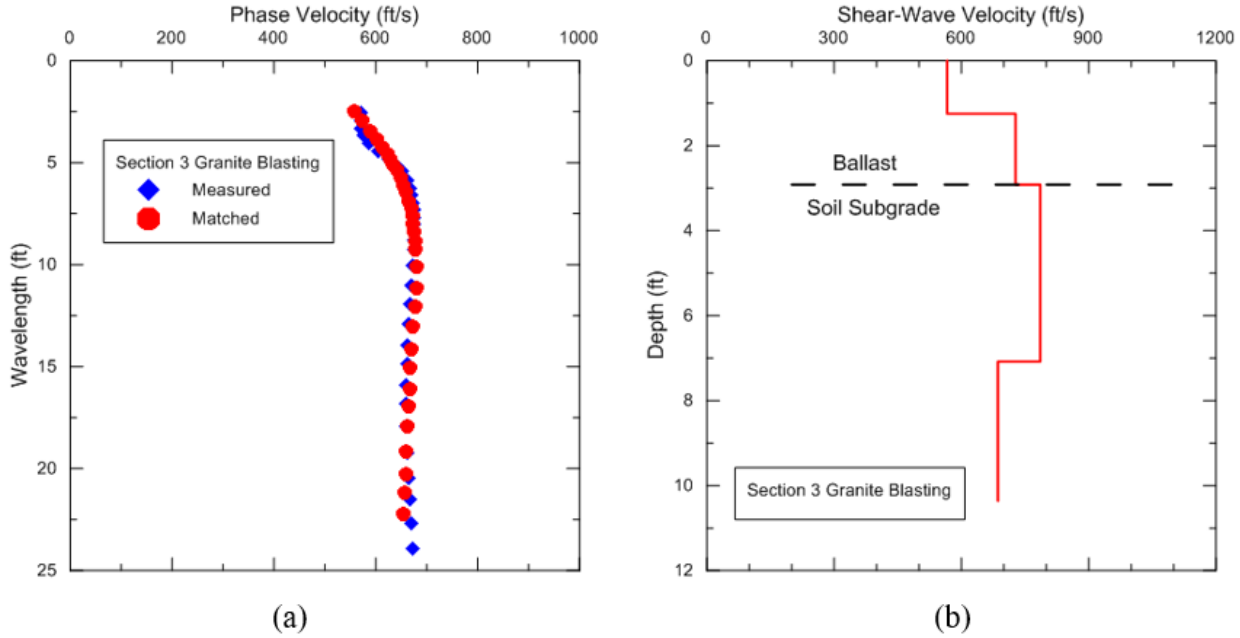

Figure 44. Plots of: (a) Comparison of Measured and Matched Dispersion Curves and (b) Derived Shear-Wave Velocity Profile from Section 3 with Granite Ballast at HTL on October 29, 2013

5.1.2 USW Tests on October 28–29. 2013

This section of the report provides the results from the Ultrasonic Surface Wave (USW) approach using the hand-held device called the PSPA and SASW interpretation techniques. One set of the results was obtained from the PSPA and the other set from the USW analysis of data collected from the short receiver spacings through the SASW tests (Figure 40) for comparison purposes. The PSPA was placed on the ballast between ties during data collection and across the ties due to a short spacing between the receivers.

Figure 45 shows the average shear-wave velocity of full thickness of the ballast using SASW techniques and top 12 inch (0.3 m) of the ballast (PSPA) with the USW approach for all six sections of HTL. The discrepancy in the average velocity obtained from "SASW" and "PSPA" ranged from 1 percent and 46 percent for Section 7 and Section 36 (10 percent fouling), respectively. One of the reasons for the difference in the PSPA and SASW results is the wavelength of the seismic waves associated with the tests. The "SASW" uses a comparatively longer wavelength than the "PSPA," and considers both the upper and lower portions of the ballast, whereas the PSPA is only considering the upper portion of the ballast.

The lower shear wave velocity in the upper portion of the ballast (PSPA results vs. SASW results in Figure 45) is probably due to less fouling material being present because it has been washed or blown from the ballast. Less fouling material means a greater void space in the upper ballast portion, which will result in lower shear wave velocities as discussed above. Therefore, the length of the PSPA device should be increase to increase the depth of influence to obtain the range of shear wave velocity through the entire ballast layer. However, the PSPA did show shear wave velocities that are in agreement with the SASW procedure, but are much easier and quicker to obtain.

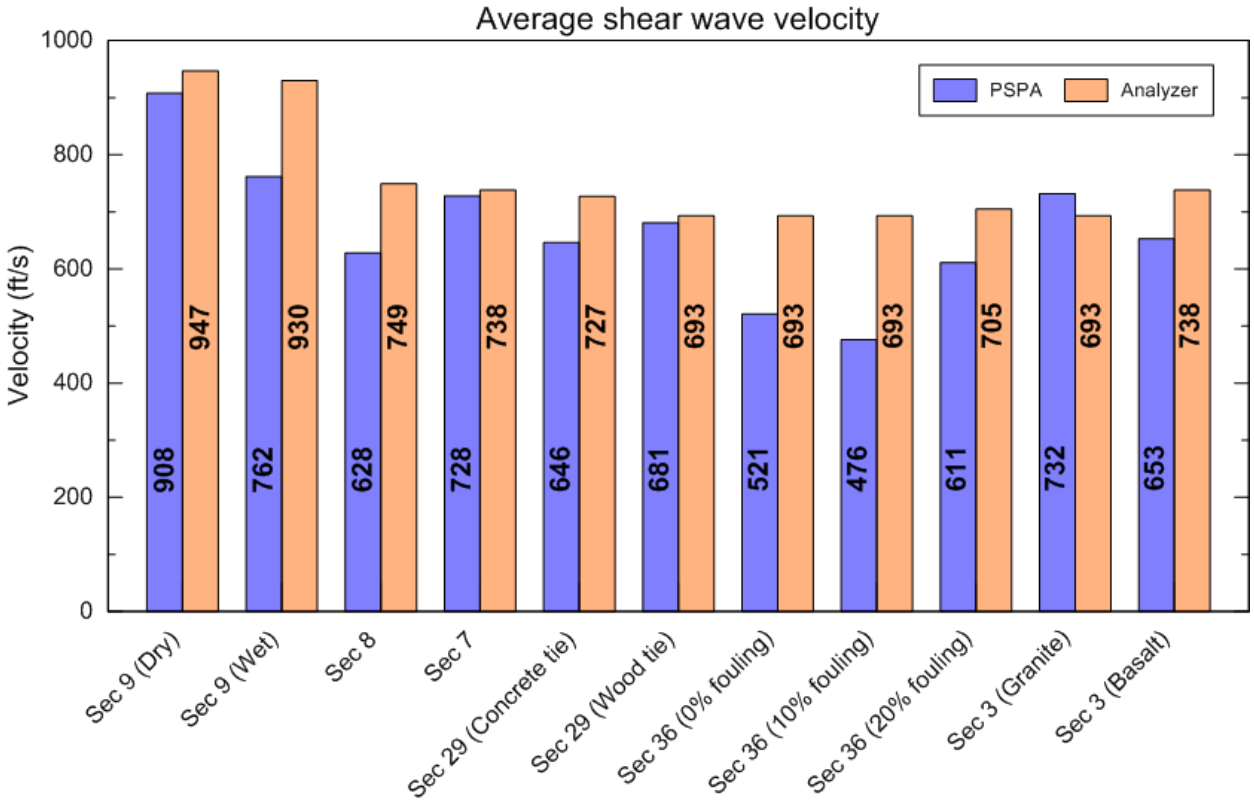

Figure 45. Average Shear-Wave Velocity of Full Thickness of the Ballast (SASW) and Top 12 Inch (0.3 m) of the Ballast Using the USW Approach (PSPA) for the HTL Sites Tested on October 29, 2013

5.1.3 Comparison with GPR and Other Data at HTL

GPR is frequently used to assess track substructure condition, e.g., types and thickness of underlying layers, changes in moisture content, etc. It is used primarily because it is a quick and nondestructive technique that has evolved over the past two decades to detect ballast contamination. GPR is usually mounted on a moving platform to inspect the substructure at commonly used track inspection speeds. GPR derived data can be displayed after processing in easy to read color-coded amplitude plots to identify anomalies or changes in the ballast and subgrade materials.

FRA and TTCI conducted the "GPR Evaluation Test Implementation Plan project at TTCI's test center near Pueblo, CO, from November 15–19, 2010 [41] [42]. The objective of the FRA and TTCI project was to advance the use of GPR on U.S. railroads by evaluating current technologies. As a result, GPR surveys were performed along the HTL by various venders and contractors, including Roadscanners Oy and HyGround Engineering LLC [10].

Several results from the GPR study were used to facilitate an interpretation of the seismic surface wave testing performed along the HTL. The GPR results were used to identify areas with uniform and well-defined layers to assess the applicability of seismic testing to railroads in general.

As a quick and non-destructive technique to detect ballast thickness and fouling, GPR is usually mounted on a moving platform to inspect the substructure at commonly used track inspection speeds, such as 40 mph (70 km/hour). As a result, GPR should be used to delineate problematic areas, and then seismic wave techniques can be used in the area to measure V_s and modulus with depth in the problematic area. Seismic wave techniques can also be used to augment GPR results. For example, seismic techniques can provide quantitative values of engineering properties for the ballast and subgrade that can assist with the interpretation of GPR results. The measured values of V_s can be also used to calibrate the GPR results to delineate areas of high and low modulus materials.

Due to GPR yielding qualitative results, the values of Young's modulus could not be compared while other parameters could be compared. For example, Figure 46 present a GIS-derived presentation of ballast depth around the HTL at TTCI. These color coded depths were compared with the depths of ballast estimated from the seismic testing at the same locations. The seismic testing in Section 36 described above shows a thickness of ballast of about 32-inch (0.81 m) thick ballast, which is in good agreement with Figure 43, which shows a ballast depth of 24 to 27 inches (0.81 m).

Another example is using GPR results to compare with the estimated level of fouling observed during the seismic testing. For example, Figure 46 present a GIS-derived presentation of relative ballast fouling around the HTL at TTCI. These color-coded category depths were compared with the observed fouling levels estimated during and from the seismic testing at the same locations. The seismic testing in Section 9 described above shows significant fouling, which is in agreement with Figure 46. These qualitative comparisons illustrate the information available from a GPR scan and their agreement with site-specific testing. For example, this section has a greater thickness of ballast or is more fouled than another section, or this subgrade is probably wetter than this section.

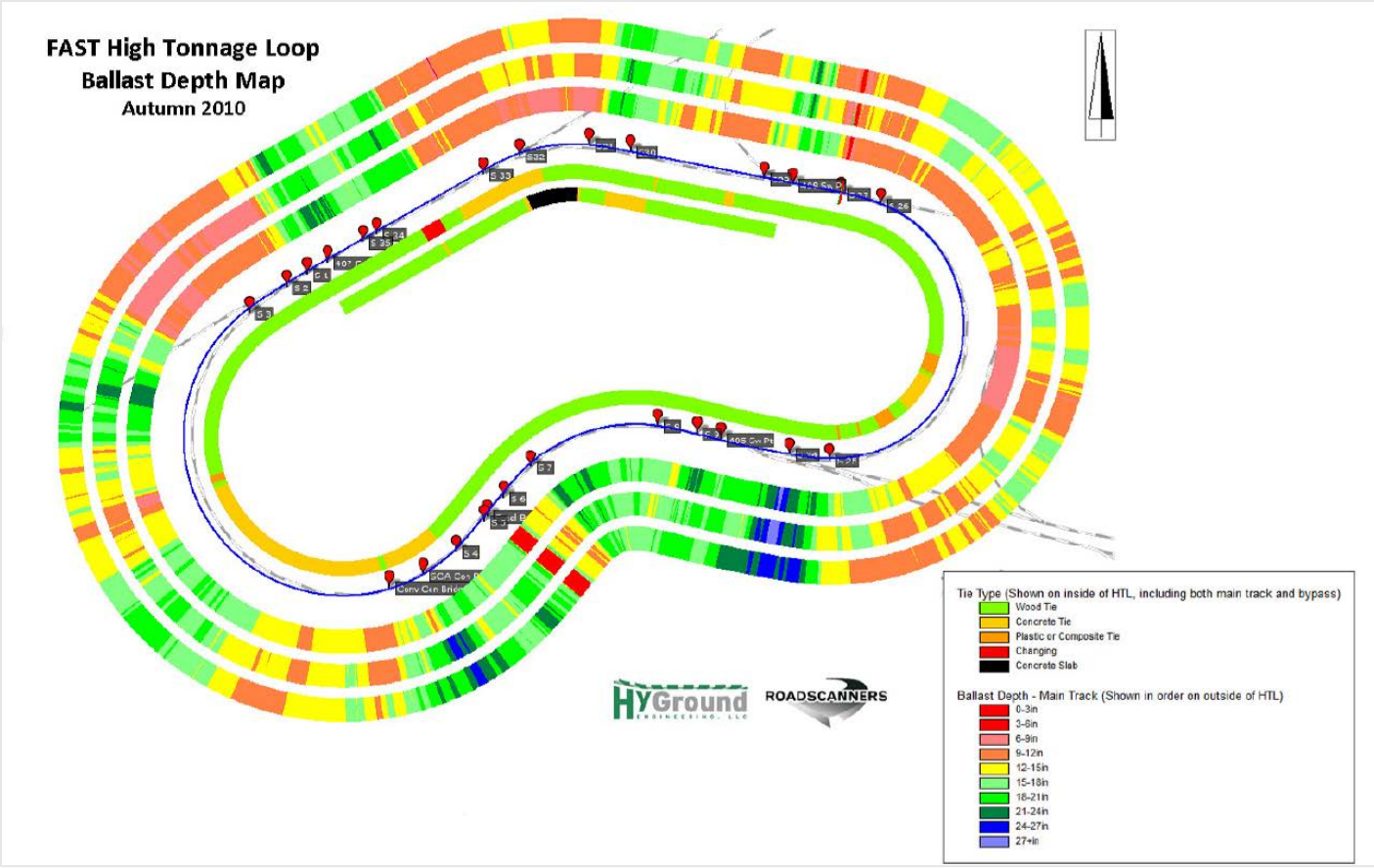

Figure 46. GIS-Map Presentation of Ballast Depth Estimated Using GPR for Left, Center, and Right at the Facility for Accelerated Service Testing (FAST) HTL Test Track [10]

5.2 HTL at TTCI on April 2, 2014

Two of the HTL track sections tested on October 28 and 29, 2013, were retested after the TTCI Track-Walk on April 2, 2014. Section 5.2 describes the testing performed on April 2, 2014, and several results. Table 6 summarizes the testing performed on April 2, 2014.

5.2.1 SASW Tests in April 2014

SASW testing was performed in Sections 36 and 29 to investigate any changes in ballast and subgrade properties since October 2013 and to confirm prior interpretations of the prior seismic data. The first sets of tests on these two track sections was in October 2013, which was early (or before) winter season while the tests in April 2014 correlate to late winter or early spring. Field measurements of crossties show climatic changes can alter some of the physical properties of a site. This section compares the results obtained in October 2013 and April 2014.

HTL Section 36, 10 Percent Fouling

The test location for this section was near (but not exactly at the same location) the October 2013 test location. However, the data collection procedure was the same as the earlier tests. Figure 47

shows the shear-wave velocity profile and corresponding dispersion curves for Section 36 (10 percent fouling). The maximum wavelength of the dispersion curve is increased from 8 ft. (2.4 m) (October 2013) to 24 ft. (7.3 m) (April 2014). The velocity profile (April 2014) shows less variation (about 3 percent) in the velocities below 2 ft. (0.6 m) at the interface of the ballast and subgrade. The primary difference is a higher ballast shear-wave velocity in April 2014 (679 ft/sec) than in October 2013 (608 ft/sec). This represents an 11 percent increase, which may be due to the clear and warm weather desiccating the upper portion of the subgrade.

HTL Section 29

During the earlier tests in October 2013, Section 29 was divided into two sub-sections: concrete tie and wood tie sections based on the type of tie laid on the track. Additionally, the HMA layer underneath the ballast layer of the concrete tie section had failed due to bearing capacity failure in the underlying Buckshot Clay, whereas the HMA layer under the wood tie section was intact. Two locations were chosen on the track in April 2014 to capture both subsurface conditions. One section had concrete ties and a failed HMA layer and the other had wood ties and an intact HMA layer. The first sub-section is labeled as "CF" and the other sub-section is labeled "WI." Seismic tests along these two sections were conducted with the test set up shown in Figure 40.

Figure 48 shows the shear-wave velocity profiles and corresponding dispersion curves for the sub-sections of Section 29 during April 2014 tests. The velocity profile for the "CF" section shows a high velocity contrast boundary at a depth of 2 ft. (0.6 m), which might be the boundary between the track (without HMA layer) and the subgrade of Buckshot Clay. Also, the velocity profile for the "WI" section shows a comparatively low velocity contrast boundary at the depth of 2.6 ft. (0.8 m), which might be the boundary between the ballast including intact HMA layer and the subgrade.

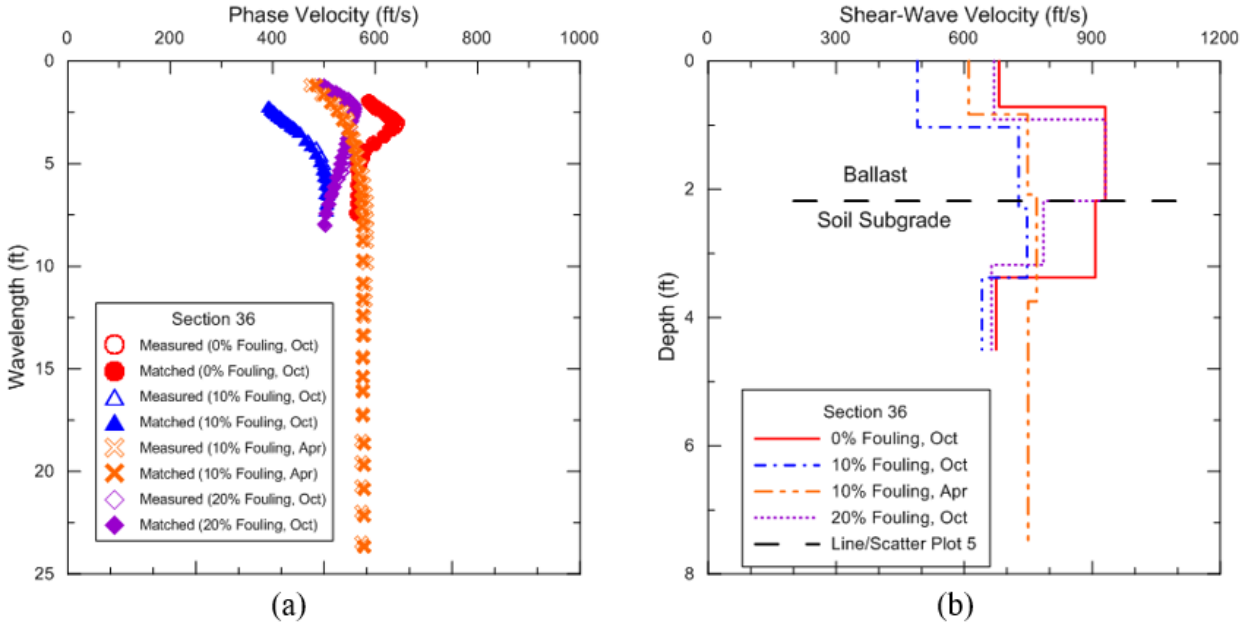

Figure 47. Plots of: (a) Comparison of Measured and Matched Dispersion Curves and (b) Derived Shear-Wave Velocity Profile from Section 36 with 10 Percent Ballast Fouling at HTL on April 2, 2014

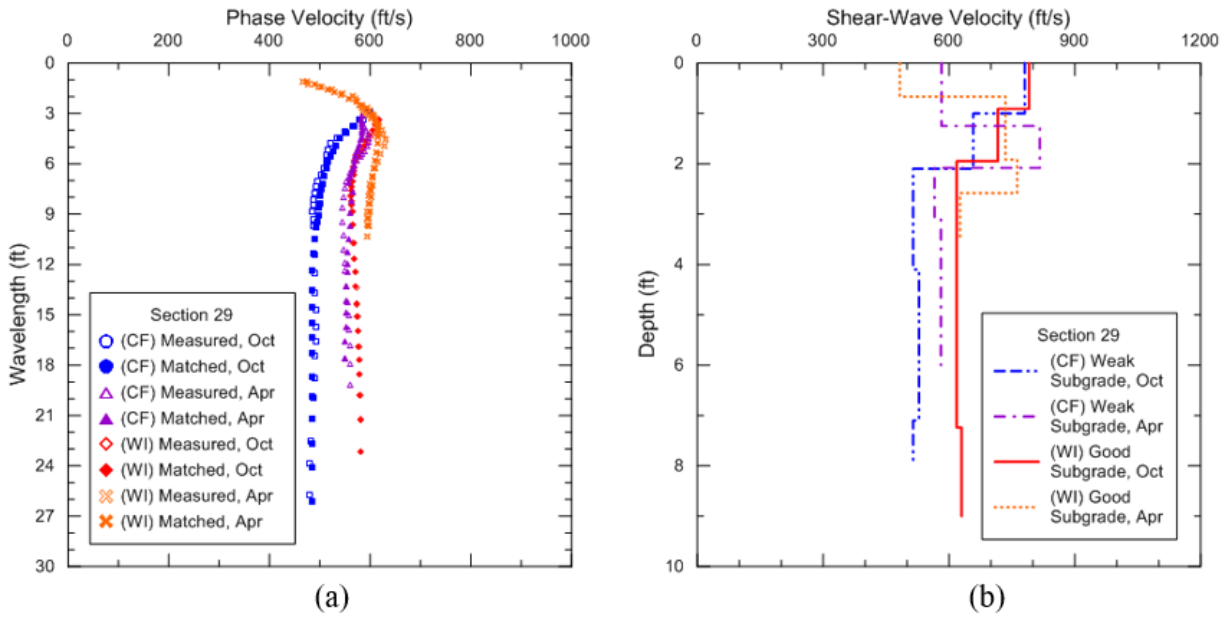

Figure 48. Plots of: (a) Comparison of Measured and Matched Dispersion Curves and (b) Derived Shear-Wave Velocity Profile from Section 29 at HTL on April 2, 2014

5.2.2 USW Tests in April 2014

This section of the report only deals with the result from the USW analysis of the data collected through the SASW approach on April 2, 2014. Figure 49 shows the average shear-wave velocity of full thickness of the ballast with the USW approach (SASW) for Section 36 (10 percent fouling) and Section 29 (CF and WI). The PSPA was not used in April 2014.

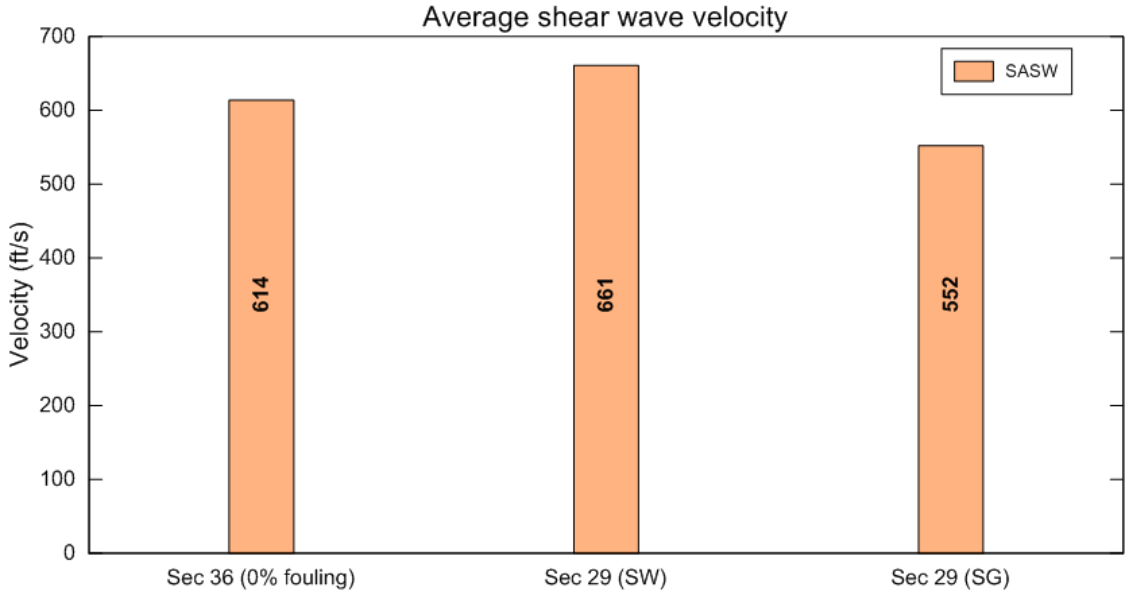

Figure 49. Average Shear-Wave Velocity of Full Thickness of the Ballast (SASW) with the USW Approach for at HTL Sites on April 2, 2014

5.3 UPR's Revenue Track near Ogallala, NE

Seismic tests were conducted on UP's revenue track near Ogallala, NE, on April 16, 2014. Three sites were selected based on the fouling level of the ballast, with reference to McConaughy Lake, are shown in Figure 50. The description of the sites is presented in Table 7. All the test sites had two tracks running parallel to each other. The tests were performed on Track 2 or the southbound track at the three sites. These three sites were selected to represent a range of ballast fouling from clean ballast to completely fouled ballast.

Figure 50. Test Sites at UP near Ogallala, NE

Table 7. Test Sites at UP near Ogallala, NE

Site	Section Feature	Ballast Thickness (inch/meter)	Test Location
1	Clean Ballast	30/0.76	Milepost 49.75
2	Completely Fouled Ballast	34/0.86	Milepost 62.90
3	Partially Fouled Ballast	28/0.71	Milepost 72.00

5.3.1 SASW Tests on April 16, 2014

During the SASW testing, the accelerometers were placed on the top of the ballast and at the center of the track as shown in Figure 40. Figure 51 shows the shear-wave velocity profiles and corresponding dispersion curves for the three sites tested.

Site 1 (Milepost 49.75)

Site 1 was located near to the western edge of McConaughy Lake. This site had a 30-inch thick clean ballast layer. The velocity of the bottom portion of ballast is 30 percent greater than the top portion of the ballast. However, the velocity of the top subgrade is only 4 percent less than the bottom portion of the ballast.

Site 2 (Milepost 62.90)

Site 2 was located east of a dirt road crossing. The site had a 34-inch (0.9 m) thick ballast layer. The ballast at this site was highly fouled with fine soil, with the major cause of fouling being dust from the dirt road. As shown in Figure 51, the velocities of all layers of Site 2 are lower than Site 1. The velocity of the top subgrade is 11 percent less than the bottom portion of the ballast.

Site 3 (Milepost 72.00)

Site 3 was located west of one of the highway bridges along Nebraska Highway 92. This site had a 28-inch (0.71 m) thick partially fouled ballast layer. The velocity profile for Site 3 is positioned between the velocity profiles of Site 1 and Site 2 (Figure 51). Upon comparing the velocities of the bottom portions of the ballast for the three sites, the velocity of ballast decreases as the fouling level increases.

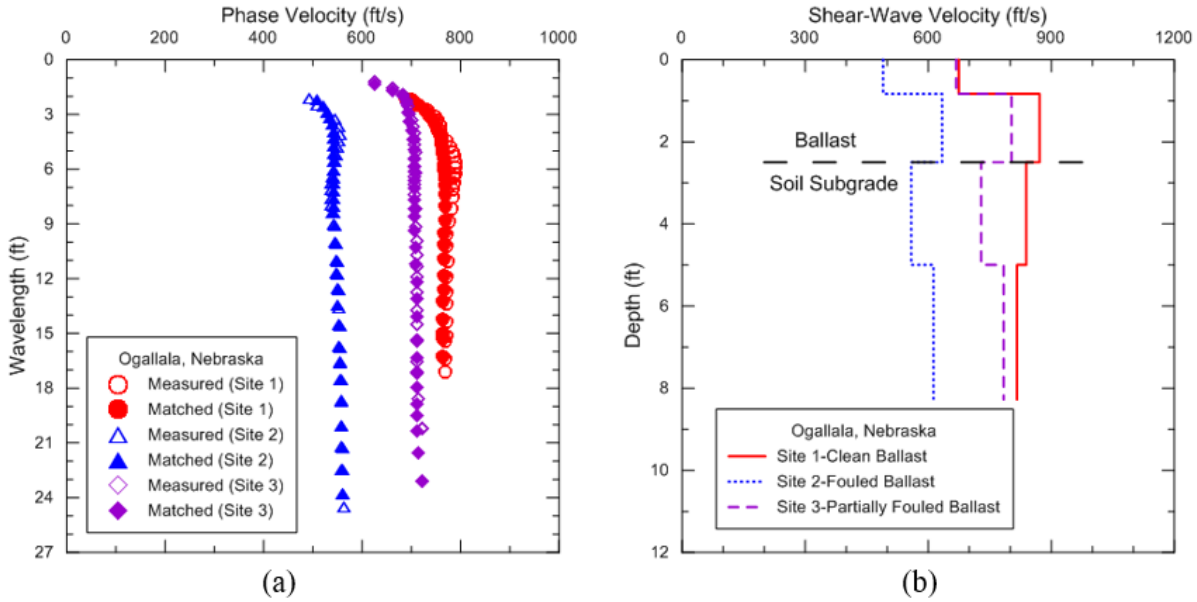

Figure 51. Comparison of: (a) Measured and Matched Dispersion Curves and (b) Derived Shear-Wave Velocity Profiles from the Test Sites at UP near Ogallala, NE

5.3.2 USW Tests on April 16, 2014

PSPA tests were also conducted at all the SASW test sites on UP's test site. Figure 52 shows the average shear-wave velocity of full thickness of the ballast (SASW) and top 12 inch (25 mm) of the ballast (PSPA) with the USW approach. The ballast shear wave velocities from "SASW" and "PSPA" for Site 1 and Site 3 are in agreement. However, at Site 2, the ballast shear velocity from "PSPA" is 53 percent greater than "SASW," which may be due to the difference in measured wavelength between the "SASW" and "PSPA" which is important because the ballast at this location was partially fouled. Therefore, the effect of greater air voids in the upper portion of the ballast may have impacted the PSPA results more than the SASW results.

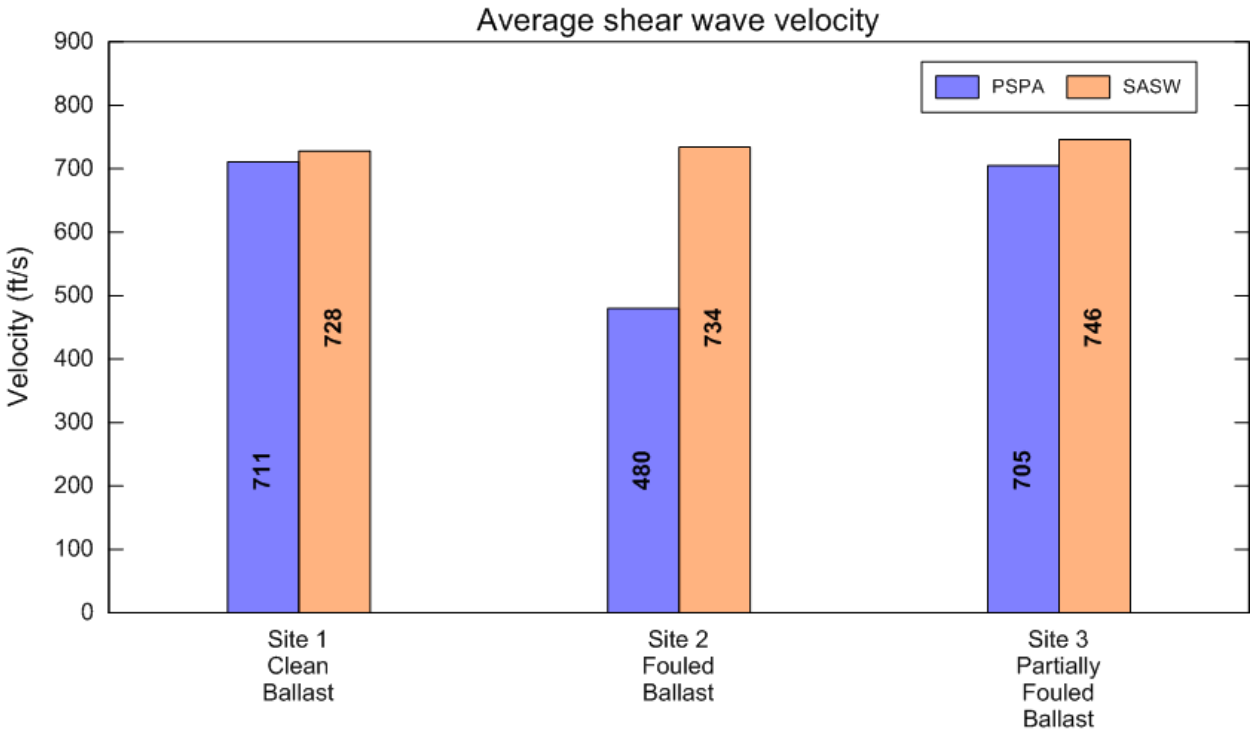

Figure 52. Average Shear-Wave Velocity of Full Thickness of Ballast (SASW) and Top 12 Inches (0.3 m) of Ballast (PSPA) with the USW Approach from all Test Sites at UP near Ogallala, NE

5.4 Kentucky Dam Bridge on Paducah & Louisville Railway, Inc.

Seismic tests were conducted on PAL at Gilbertville, KY, on June 12, 2014. The test site shown in Figure 53 is located west of the Kentucky Dam, close to US Highway 62. The track is orientated at the northeast to southwest direction with US Highway 62 running parallel to the track. The highway is located south of the track and a steep 70 ft. (21 m) thick compacted fill slope that is located north of the track.

Figure 53. Test Sites on PAL at Gilbertville, KY

The description of the site is provided in Table 8. The site was on the transition zone between the natural ground and the railway bridge. The track consisted of a 1 ft. (0.3 m) thick ballast layer overlaid on a 6 in. (150 mm) thick HMA layer. The railroad trackbed was built over an approach fill section of the railway bridge that provides support to the track. Site A is located about 50 ft. (46 m) from the west edge of the railway bridge whereas Site B is located next to the railway bridge.

Table 8. Test Sites on PAL at Gilbertville, KY

Section #	Section Feature	Ballast Thickness (inch/meter)	Remarks
Site A	6 in. thick HMA layer between ballast layer and approach fill	12/0.30	About 50 ft. west edge of the railway bridge
Site B			West of the railway bridge

5.4.1 SASW Tests

The SASW tests were performed with the "source-receivers" configurations described in Figure 40. The ballast layers of both sections looked visually clean with similar physical features. Figure 54 shows the dispersion curves and corresponding shear-wave velocity profiles for both sites. The velocities of the ballast and subgrade of Site A are slightly lower than the velocities at Site B. The velocity of the top of the subgrade for Site A is 16 percent lower than Site B. The influence of the stiffer HMA layer is more apparent in Site B, but can be observed in Site A as well.

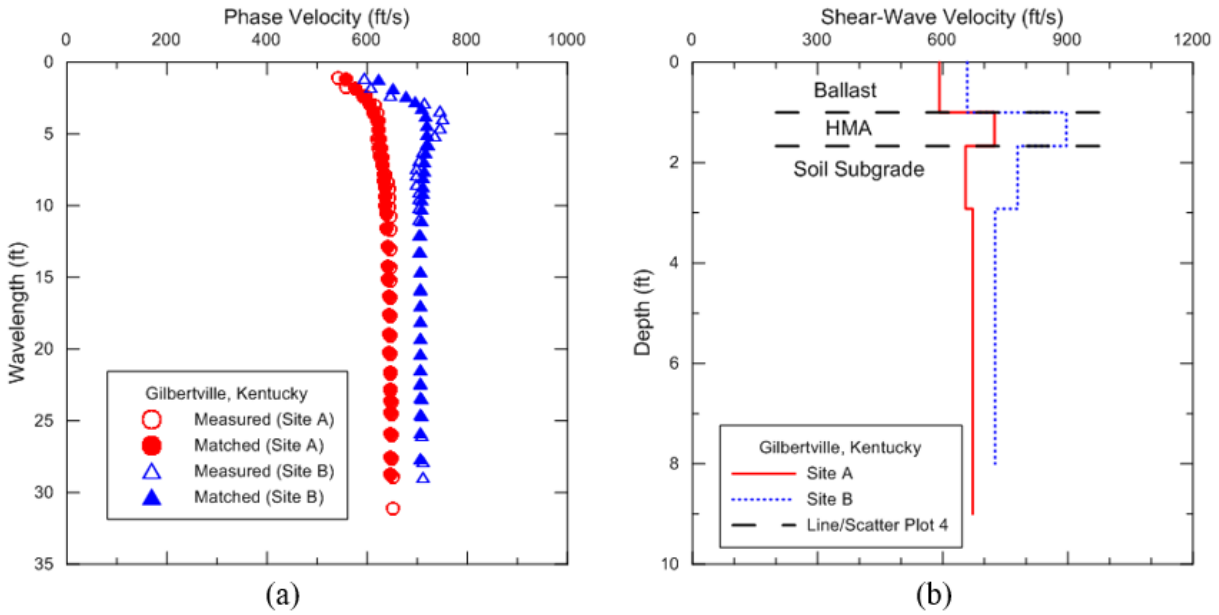

Figure 54. Comparison of: (a) Measured and Matched Dispersion Curves and (b) Derived Shear-Wave Velocity Profiles from the Test Sites on PAL at Gilbertville, KY

5.4.2 USW Tests

PSPA tests were conducted at both test locations at the PAL site. Figure 55 shows the average shear-wave velocity of full thickness of the ballast (SASW) and top 12 inches (0.3 m) of the ballast (PSPA) with the USW approach. The differences in the velocity of the "SASW" and "PSPA" for Site A and Site B are 31 percent and 23 percent, respectively. This difference is probably due to the PSPA testing only the upper 12 inch (0.3 m) of the ballast and the SASW technique of testing the entire ballast thickness.

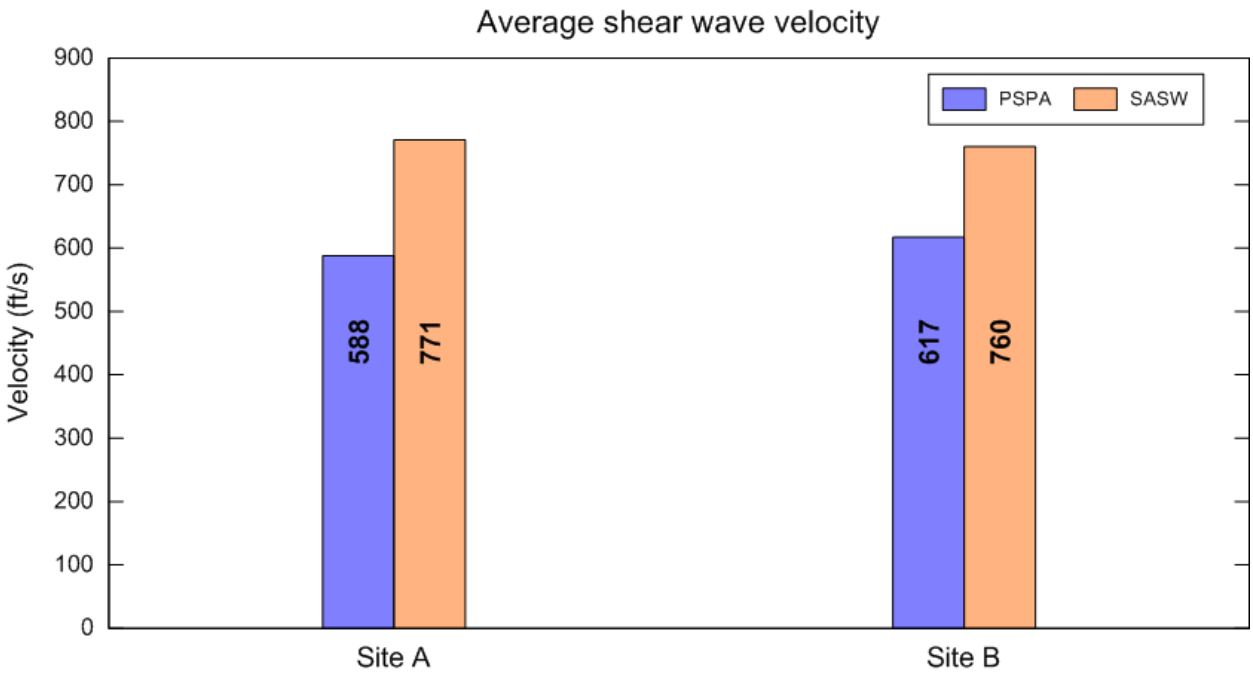

Figure 55. Average Shear-Wave Velocity of Full Thickness of the Ballast (SASW) and Top 12 Inches of the Ballast (PSPA) with the USW Approach from all Test Sites on PAL at Gilbertville, KY

5.5 Amtrak at South Kingstown, RI

A full scale seismic testing program was planned for Amtrak's Northeast Corridor near the Kingston Railroad Station in South Kingstown, RI, on February 20, 2014. The average thickness of the ballast is about 24 inch (0.6 m). The foundation of the track consists of a 5 ft. (1.5 m) high clayey embankment built over a swamp deposit. The temperature of the site during the test was below 0 °C and the track was covered with about 6 inches (150 mm) of snow. Typically, frozen track and ballast is associated with higher modulus values. The ballast was seriously "fouled" with the mix of snow and ice. Due to the malfunctioning of an SASW data acquisition system and bad weather conditions, only PSPA tests were performed at the site. The average shear-wave velocity of the top 12 inch (0.3 m) of ballast with the USW approach was estimated as 795 ft/sec (240 m/second) with a coefficient of variance (COV) of 3 percent. This average shear-wave velocity value is considerably higher than those measured for clean ballast at all other sites and probably reflects the frozen nature of the track and the voids of the ballast filled with snow, ice, and fouling material.

5.6 Realistic Evaluation of Surface Wave System and Improvements

The seismic testing conducted on revenue service and TTC track during this project shows the SASW approach can provide a realistic evaluation of the track substructure. The maximum distance of the receiver spacing should be set to encompass the desired depth of measurement. In other words, if a depth of 20 ft. is desired for the investigation, the farthest receiver should be at least 20 ft. from the energy source. The seismic testing performed here also revealed conversion of the PSPA device is viable for measuring ballast properties quickly and non-

invasively. The resulting device would be called a BSPA and the distance from the energy source to the last receiver would be 4 ft. to measure the shear wave velocity through the entire ballast layer and the upper portion of the subgrade. The BSPA device is much quicker and easier to use than the SAW equipment, but requires considerable modification because the existing PSPA devices were designed to measure the modulus of concrete and asphalt pavements as well as other paved layers with smooth surfaces.

To utilize a PSPA on ballast, besides the high frequency limit, the current version needs considerable modifications and customization to effectively couple the receivers to the ballast, lengthening the distance between the energy source and farthest receiver to span across two crossties, and developing a friendly railroad personnel software system to facilitate usage. Figure 56 shows a schematic of the tentative design for the BSPA so it can span two adjacent ties. The resulting device can be used to measure the modulus along both ties to investigate the presence of a center bounded crosstie as shown in Figure 57. Measuring the modulus along two ties is important for understanding: (1) the distribution of the applied loads along a single crosstie and between adjacent crossties, (2) rail deviations, and (3) tie bending/failure.

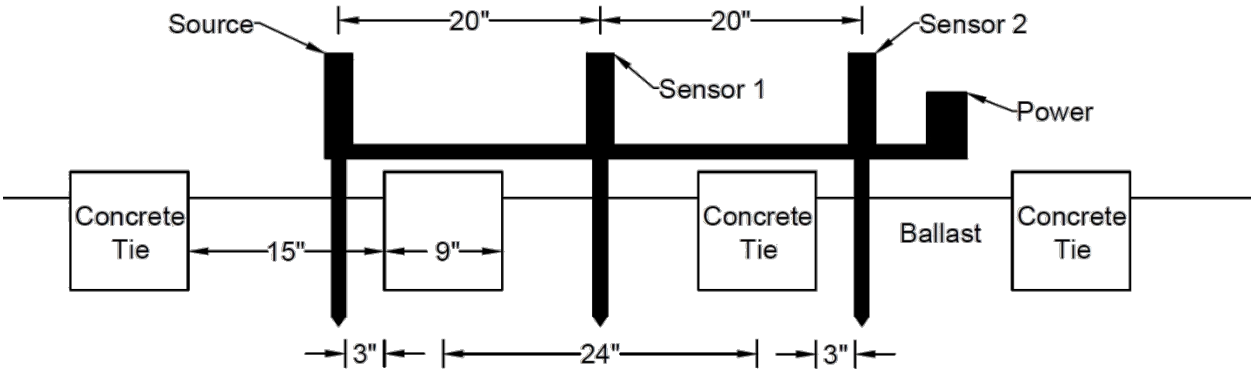

Figure 56. Proposed Configuration of BSPA

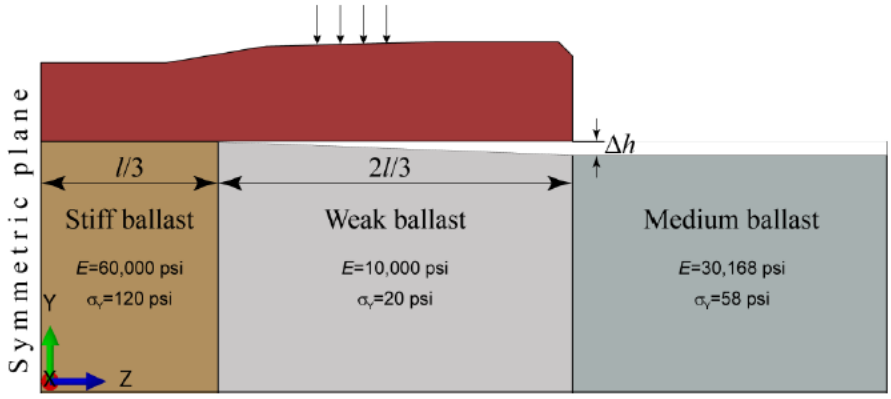

Figure 57. Cross-Section of Ballast Under a Center Bound Crosstie and the Possible Range of Young's Modulus that Could be Measured Using BSPA from Yu et al. (2015)

6. Prototype Seismic Surface Wave System

This section presents the specifications for obtaining a seismic surface wave system for FRA and railroad personnel, and the sources that can provide the necessary items to create a prototype SASW system. In addition, this section presents an Operation Manual on how to operate the SASW or MASW system for track substructure assessments and how to interpret the data to obtain profiles of shear-wave velocity and shear modulus vs. depth.

6.1 Specifications for Purchasing Surface Wave System

Specifications to create a SASW system to measure the in-place shear-wave velocity profile (shear-wave velocity vs. depth) of ballast and track substructure without requiring a borehole is presented below. The shear-wave velocity profile should be determined from an idealized experimental dispersion curve (surface wave velocity vs. wavelength or frequency) obtained from seismic surface wave measurements and SASW techniques through a process called forward modeling or an inversion process.

System Requirements:

- Data acquisition system with the following minimum requirements:
  - Air transportable
  - Minimum of four input channels
  - Capable of capturing up to 100,000 samples per channel per second
  - 16-bit resolution or equivalent
  - Adjustable pre-triggering delay
  - Adjustable number of signals to be averaged
  - Capable of accepting and rejecting the last set of time records collected
  - Capable of display of the waveforms collected in real time during testing
  - A four-channel signal analyzer (Tektronix 2630) and a National Instrument DAQ model 6062E
- Seismic receiver assembly with the following minimum requirements:
  - Minimum of four accelerometers with appropriate signal conditioning units
  - Appropriate mounting system to attach the accelerometers securely to the ballast
  - Responsive to frequencies of up to 10 kHz
  - Sensitivity of 1 volt/g or better
  - Several sets of accelerometers (including PCB 308B02 with frequency range of 3 Hz to 3 kHz) and Mark Products 4.5 Hz geophones (see Figure 24)
  - A metal spike with removable magnetic seat for receiver mounting (Figure 25)

- Assorted electromagnetic, mechanical, or drop weight energy sources to generate surface waves with a frequency from 10 Hz to 2 kHz
    - Impact energy sources (sledgehammers and kettlebell weight see Figure 26.
- Reduction software with the following minimum requirements:
    - Capable of providing the averaged phase information of the transfer functions and coherence functions of each pair of receivers in real time during testing
    - Capable of providing a dispersion curve from each set of receivers as selected by the user
    - Capable of providing an idealized dispersion curve from the individual dispersion curves selected by the user
    - Capable of providing a shear-wave velocity profile that represents the idealized dispersion curve by overlapping a theoretical dispersion curve over the idealized dispersion curve
    - Capable of estimating the shear modulus, and Young's modulus from the recorded shear-wave velocity of each layer

6.2 Initial Equipment Used

The initial candidate equipment and major accessories used in these tests included:

- A four-channel signal analyzer (Tektronix 2630) and a National Instrument DAQ model 6062E (see Figure 23)
- Several sets of accelerometers (including PCB 308B02 with frequency range of 3 to 3,000 Hz) and Mark Products 4.5 Hz geophones (see Figure 24)
- A metal spike with removable magnetic seat for receiver mounting (Figure 25)
- Impact energy sources (sledgehammers and kettlebell weight see Figure 26)

6.3 Operation Manual for Surface Wave System

This section contains the following three steps required for using the SASW system presented in Section 6.1:

1. Setting up field instruments and making measurements
2. Acquiring data to construct a dispersion curve
3. Analyzing the dispersion data to estimate the shear-wave velocity profile and to compute the substructure modulus profiles

6.3.1 Field Setup

Seismic Receiver Placement:

- Mark the locations of the receivers along a straight line (see Figure 58)

- Drive the metal spikes into the ballast at the marked locations with a hammer until the spikes are in firm and secure contact with the ballast (see Figure 59)
- Secure each accelerometer to the spike with a magnetic coupling seat or other coupling agent (see Figure 58 inset)

Energy Source Preparation:

- Mark the source location so it is in line with the seismic receiver array (see Figure 58)
- Secure a metal plate (the source for seismic signals) into the ballast with a hammer such that the plate has firm contact with the ballast to transmit the energy (see Figure 58 inset)
- Measure the actual distances of the various receivers from the energy source

Data Acquisition Hardware Setup:

- Connect the interconnection box with the computer through a cable consisting of the Data Acquisition (DAQ) card (see Figure 60)
- Power up the interconnection box and make sure the interconnection box has established communication with the computer before trying to collect data
- Assemble the data acquisition hardware as recommended by the manufacture (see Figure 60)
- Connect the seismic receivers to the data acquisition system through the interconnection box
- Ensure proper connection of the receivers to the data acquisition system as recommended by the manufacturer

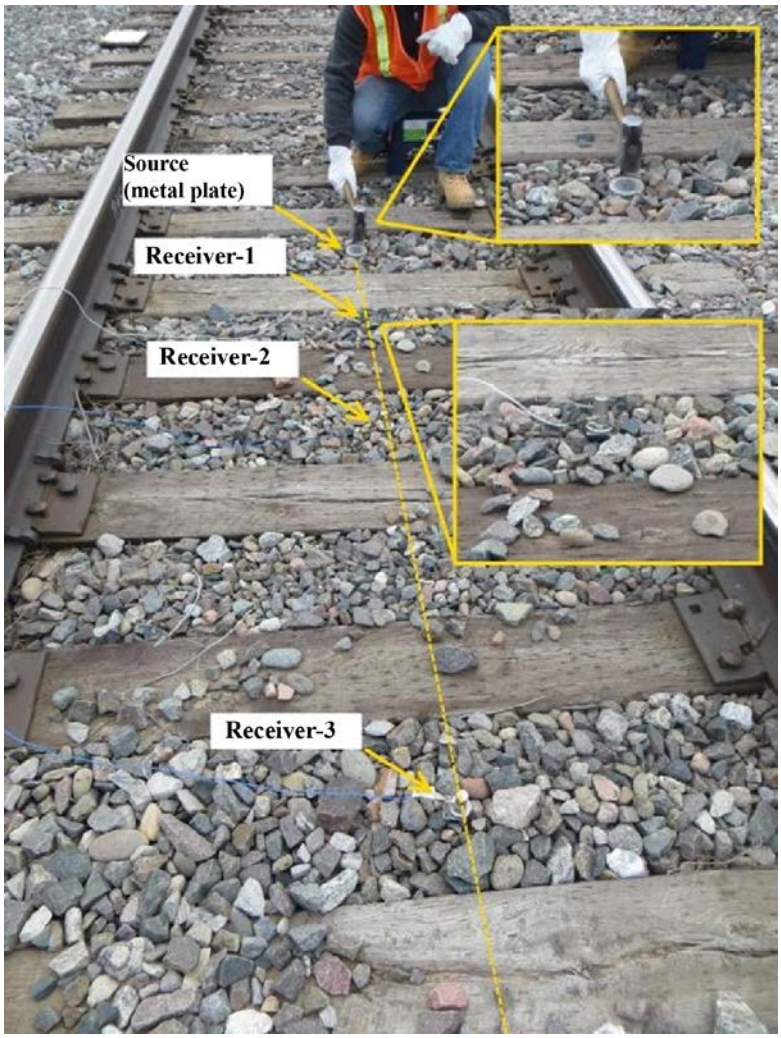

Figure 58. Source Receivers Setup for an SASW Test

Figure 59. Driving Receiver Spikes into Ballast with Small Hammer

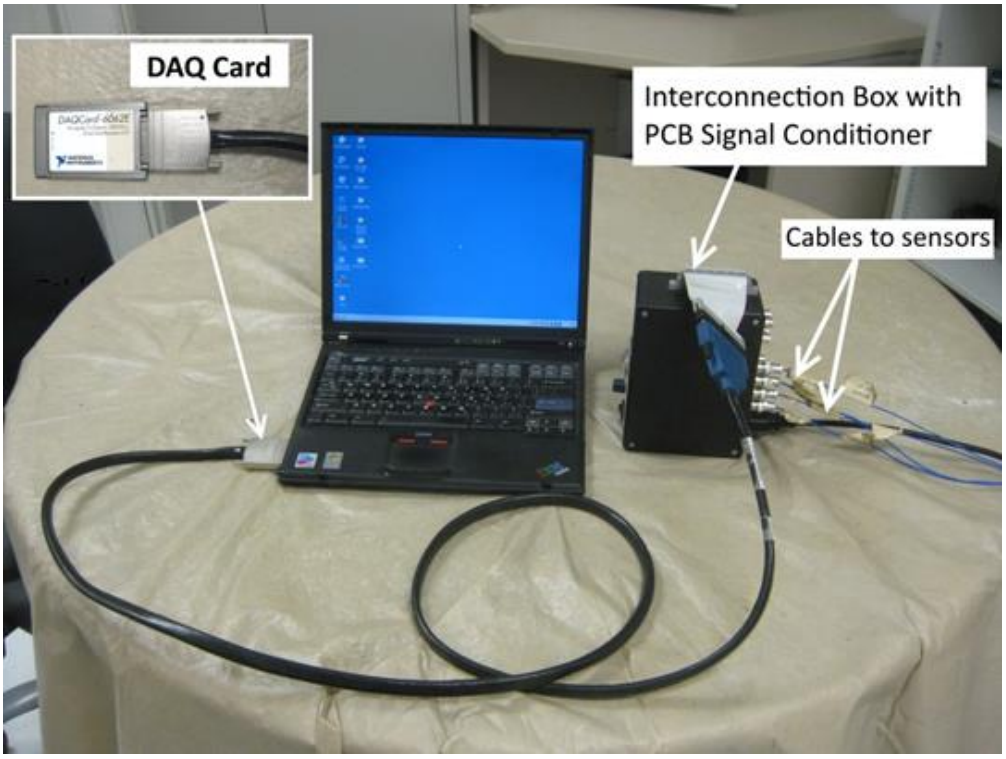

Figure 60. Data Acquisition Hardware with an Operation PC

6.3.2 Field Testing

1.1 Equipment setup and preliminary testing offers the following:

- To ensure the DAQ system sampling parameters are set properly.
  - Sampling frequency: The number of samples per unit of time (usually in Hz or sample/sec). The following sampling frequencies are recommended:
    - 2,000 Hz when the spacing of receiver pairs is less than 5 feet
    - 1,000 Hz when the spacing of receiver pairs is less than 10 feet
    - 500 Hz when the spacing of receiver pairs is greater than 10 feet
  - Pre-trigger Delay: The time lag between the initiation of recording and the arrival of seismic energy. A value of 10 percent of the record duration is recommended.
  - Number of Averages: The number of effective hammer energy hits (impacts) to generate seismic signals should be at least five effective hits to achieve representative dispersion curves (see Section 4).
  - Trigger Conditions: The conditions that must be satisfied before the DAQ system starts collecting test data. The trigger conditions should be set by trial and error but the following recommendations can be helpful:
    - Trigger amplitude: The amount of energy in volts that should be exceeded during seismic testing. A value of 15 percent of the maximum voltage received by the first accelerometer is recommended.
    - Trigger polarity: The sign associated with the trigger amplitude (i.e., positive voltage or negative voltage). Consult with the manufacturer, however, the typical recommended value is negative for plotting purposes.

1.2 Data collection and pre-reduction offers the following:

- Selection of the appropriate hammer (see Section 4)
- Strike the hammer on the metal plate (see Figure 58)
- Verification of the time domain signals are captured by the DAQ system from all receivers (see Figure 61), with Receiver 1 (R1), Receiver 2 (R2), Receiver 3 (R3), and Receiver 4 (R4)
- Review the time records for abnormal noise by discarding the records if the noise is not acceptable, i.e., the time history plots looks different than the time histories in Figure 61
- Repeat the previous three steps until the pre-specified number of effective hits is reached
- Follow the manufacturer's recommendation for generating and viewing the phase spectra and coherence functions, and review the average phase spectra and coherence functions from the collected time records. Examples of acceptable results are shown in Figure 62

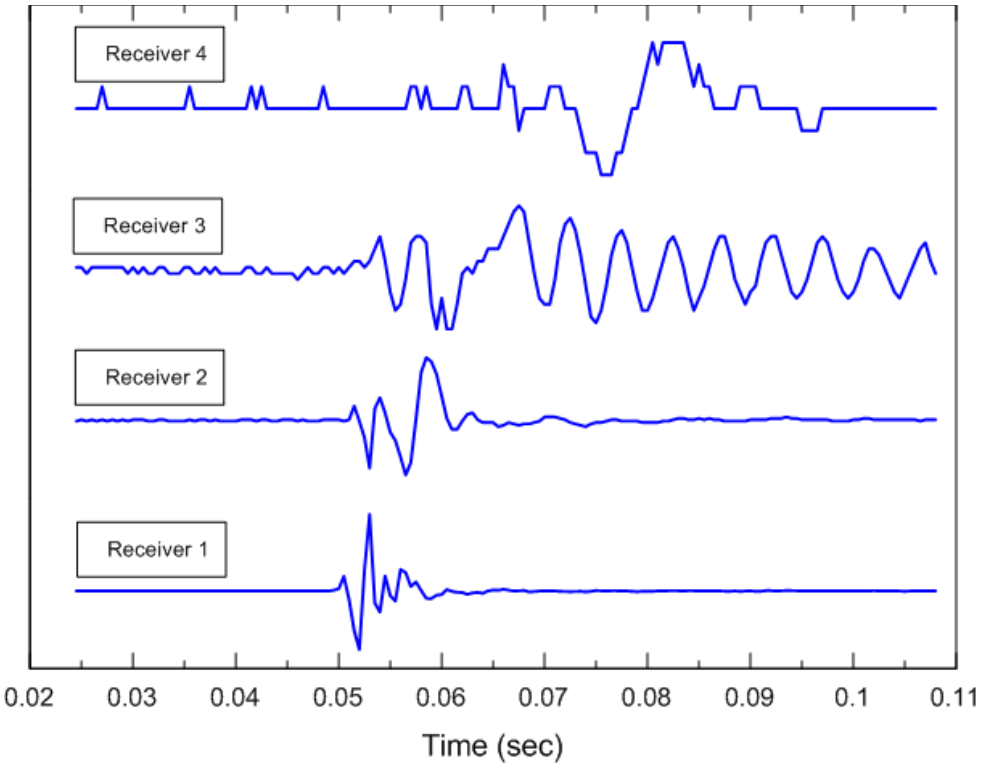

Figure 61. Time Records from a SASW Test

6.3.3 Data Reduction

Data reduction for the data obtained in Figure 61 should include the following two steps:

- Construction of dispersion curve for each individual receiver spacing
- Construction of representative dispersion curve by combining all the dispersion curves from each receiver for analysis (inversion process)

1.3 Construction of dispersion curve for an individual receiver spacing

- Unwrap the phase spectra following the manufacturer's recommendation to obtain a coherence plot (an example is shown in Figure 62)
- Review the corresponding coherence plot to select the acceptable range of frequencies that should be used in the dispersion curve (see Figure 63). The following recommendations may be helpful:
  - Use unwrapped phase angles in the range of 180 and 720 degrees
  - Avoid areas of the phase spectra with coherence values that are less than 0.95
- Convert the unwrapped phase spectrum in the range of acceptable coherence to a dispersion curve (i.e., phase velocity vs. wavelength or frequency plot) following the manufacturer's recommendation (an example is shown in Figure 64)

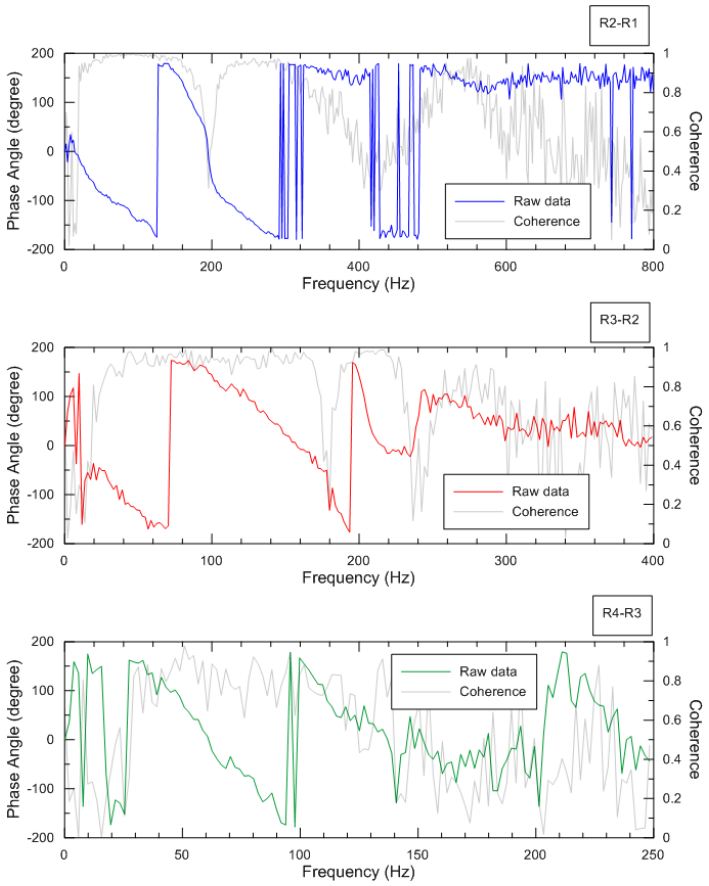

Figure 62. Average Wrapped Phase Spectra and Corresponding Coherence Functions Derived from the Time Records Shown in Figure 61. The Labels R1, R2, R3 and R4 Represent Receiver 1, 2, 3 and 4 in Figure 61

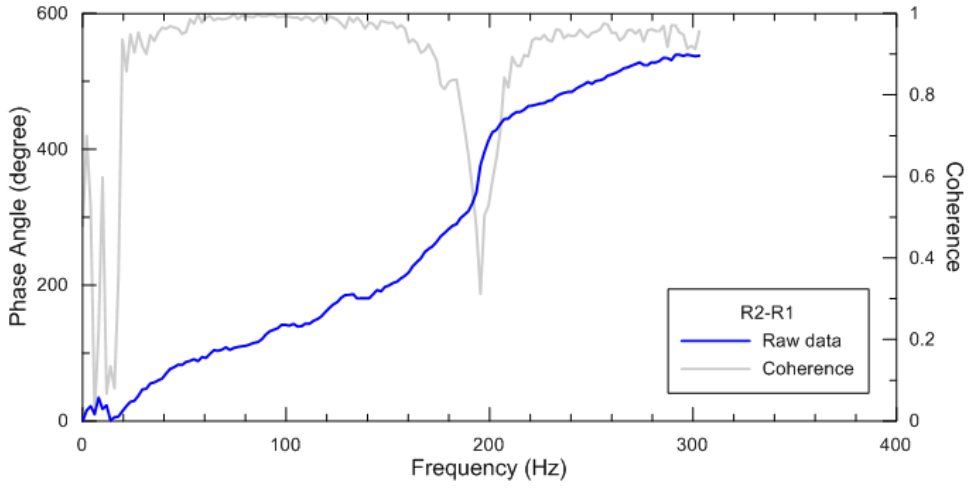

Figure 63. Average Unwrapped Phase Spectrum and Corresponding Coherence Function from Wrapped from Receiver Pair R2-R1 in Figure 61

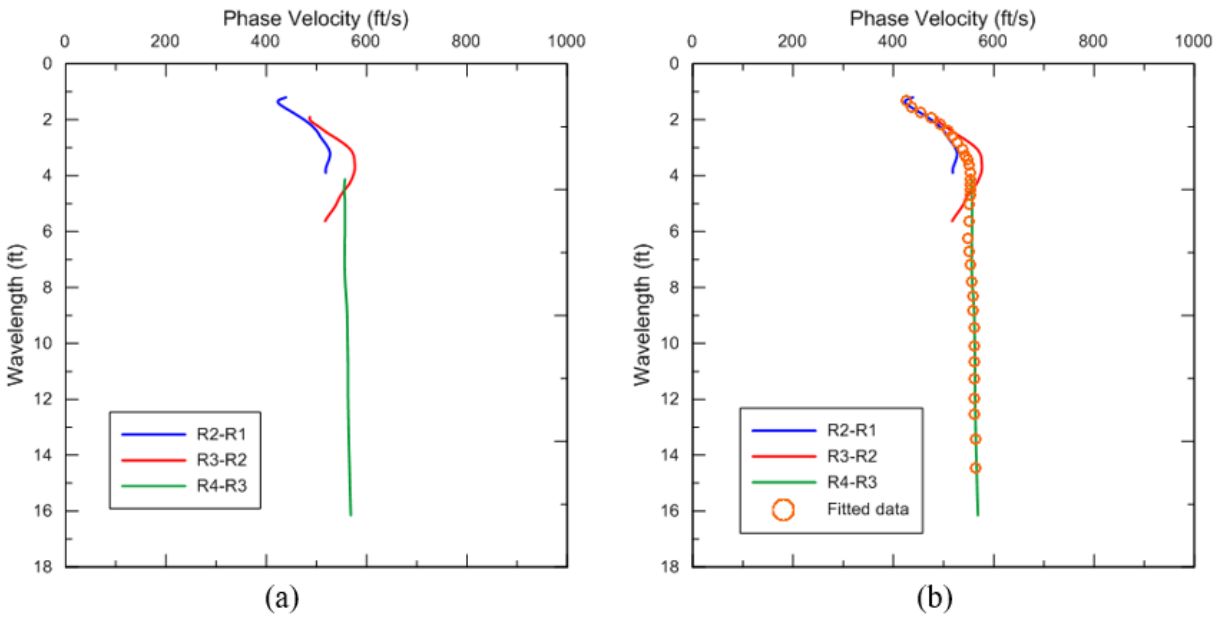

Figure 64. Data Reduction: (a) Dispersion Curves Obtained from Unwrapping Phase Spectrums Shown in Figure 60 and (b) A Representative Dispersion Curve Obtained from a Curve Fitting Process

Construction of a dispersion curve for representative dispersion curve analysis comprises:

- Fit a curve to the dispersion curves obtained from the individual receiver pairs to obtain a representative dispersion curve following the manufacturer's recommendation. The following recommendations can be helpful:
  - Use a robust curve fitting algorithm that may or may not use the coherence functions as a weighting function
  - Visually inspect the representative dispersion curve to ensure that it is a good representation of all the dispersion curves obtained from the individual receiver pairs
- Digitize the representative dispersion curve to 30 to 50 dispersion points for use in inversion following the manufacturer's recommendation. The following recommendation can be helpful:
  - Consider more data points corresponding to shorter wavelengths (higher frequencies).

6.3.4 Data Analysis (Inversion)

Utilize an inversion program to obtain the shear-wave velocity profile and other relevant stiffness parameters through the following steps.

1.4 Prepare Initial Input

- Develop an initial (a priori) subsurface model with layers representing the different soil types and assign each sublayer a shear-wave velocity, Poisson's ratio, and mass density as well as thickness to each layer. The following recommendations may be helpful:

- The number of sublayers and the thickness of each layer should be determined based on the available priori information from the site, e.g., old boring log.
- The last or deepest sublayer is typically a half-space.
- The number of sublayers should be minimized (usually not more than six).
- Thick ballast layers (greater than 12 inches) should be modeled as two layers.
- The shear-wave velocity for the top layer can be estimated based on the phase velocities of the shortest wavelengths (highest frequencies).
- Limit the total thickness of the layers to one-half to one-third of the longest wavelength.

1.5 Select Control Parameters

- Set up the control parameters for the inversion process as recommended by the developer of the algorithm, i.e., review appropriate technical paper. However, the following recommendations can be helpful for a more robust inversion:
  - Specify the type of dispersion curve from its shape
    - Normal when the phase velocity increases with wavelength
    - Inverse when phase velocity decreases with wavelength
- Maintain sublayer thickness, Poison's ratio, and density of each layer constant and only vary the shear-wave velocity assumed for each layer.
- Set the maximum number of iterations (a criterion that stops the inversion when the specified cycles of iteration are exceeded).
- Maintain a reasonable convergence criterion (when the iteration stops). A 5 percent relative standard error is recommended for this purpose. This means the estimated dispersion is within 5 percent of the representative dispersion curve that was obtained from all the measured dispersion curves.
- Set the convergence gradient (maximum percent change in the shear-wave velocity of each sublayer between iterations) to a reasonable value, a slower gradient with more number of iterations is preferred.
- Check the results for reasonableness given the non-unique nature of the inversion process.

1.6 Presentation of the Results

- At a minimum present the results in the following formats:
  - Show a graphical comparison of the measured/representative dispersion curve and matched dispersion curve (calculated from the assumed shear-wave velocity profile) to illustrate the goodness of the match (an example is shown in Figure 65(a)).
  - Show a shear-wave velocity profile with depth (an example is shown in Figure 65(b)).

- Show shear modulus and/or Young's modulus profiles, as project requires, calculated using matched dispersion curve, assumed or measured values of Poisson's ratio and mass density (see Equations 1 and 2) (an example is shown in Figure 66).
- Show a shear strength profile using an empirical relationship to be selected by the engineer based on the local experience. Several relationships have been proposed in the literature based on empirical correlations. The research team cannot endorse the empirical relationship at this time due to lack of experience with the railroad structure. No such relationship exists for ballast and sub-ballast materials.

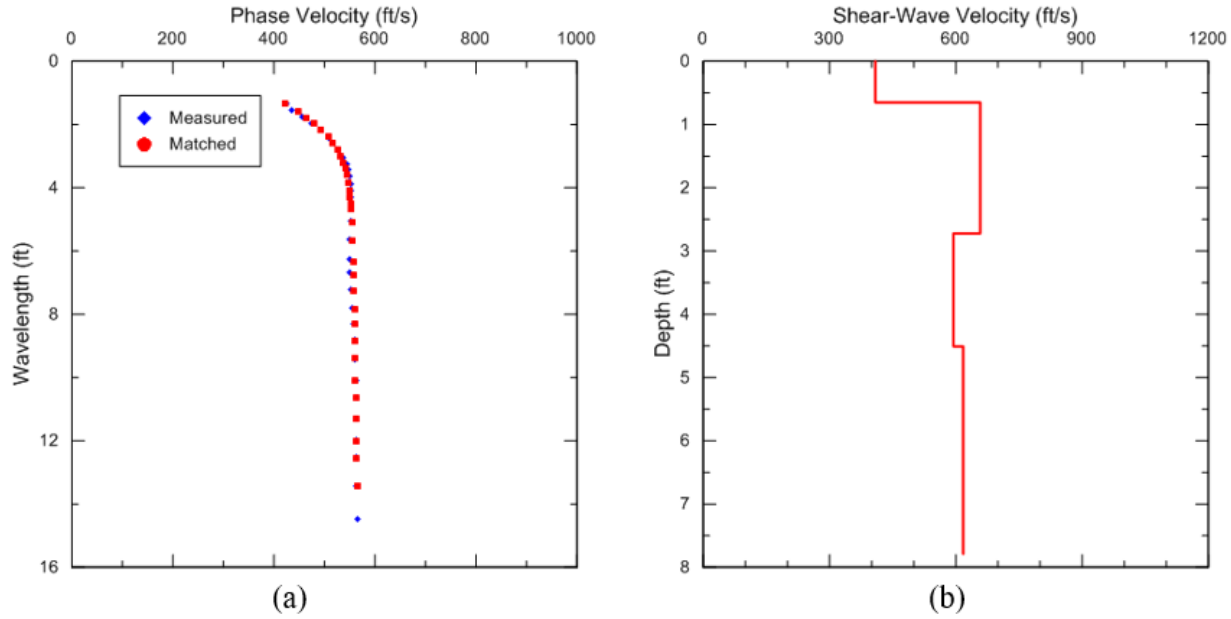

Figure 65. Diagrams Showing: (a) Comparison of Measured (See Figure 64(b)) and Matched Dispersion Curves and (b) Derived Shear-Wave Velocity Profile from Measured or Representative Dispersion Curve own in Figure 64(b)

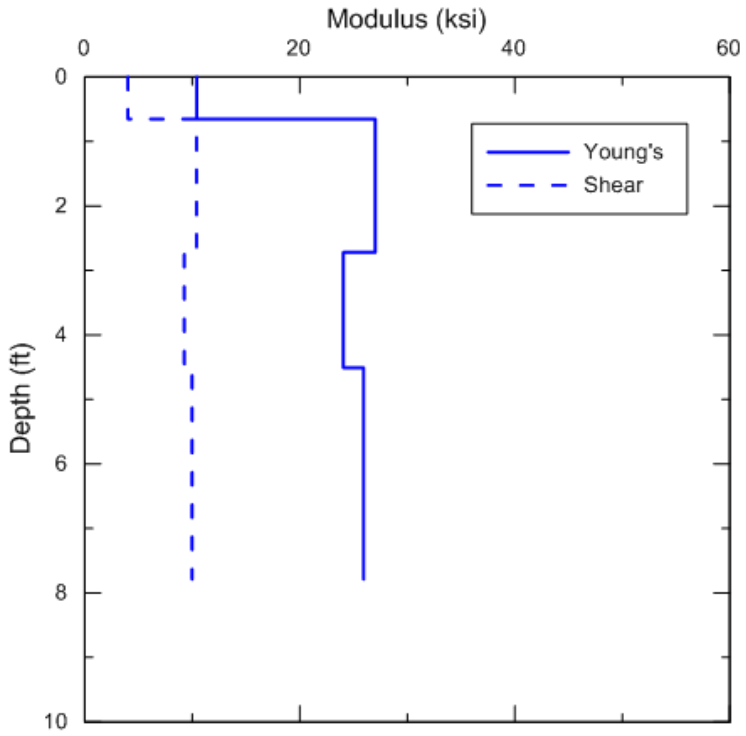

Figure 66. Shear Modulus and Young's Modulus Profiles Computed from the Shear-Wave Velocity Profile Shown in Figure 65

7. Conclusion

This report presents the results of various small-scale and large-scale experimental efforts using seismic surface-wave testing to measure the engineering properties of railroad ballast, sub-ballast, and subgrade. The advantages of seismic surface-wave testing allowed for a discussion regarding its engineering properties and ability to assess track performance. The discussion extended to theoretical and practical concerns regarding data collection, reduction, and interpretation specific to railroad substructure with possible solutions. A prototype surface-wave testing system was developed based on the Spectral Analysis of Surface Waves (SASW) approach. This system reflects hardware and software used for pavements and soils, a modification or customization of which has been applied to railroads, and consists of the following components:

- Receiver-ballast coupling (develop system for tightly coupling the seismic sensors/receivers to the ballast to measure the incoming surface waves)
- Data collection (gather a series of time history records or waveforms from various receivers/sensors)
- Data reduction (transfer time domain data to frequency domain data in the form of phase difference and coherence)
- Data analysis (derive representative dispersion curve for all time history records)
- Engineering properties (develop shear-wave velocity profile or average shear-wave velocity profile with or without inversion process)

Based on the results of this study, the following observations and recommendations can be made:

1. Surface-wave testing on a railroad track bed is more complicated than that on soils or pavements due to the presence of ballast, crossties, fastener, and rails, as well as the complexity of the ballast-foundation soil structure in terms of the variation of shear-wave velocity with depth.
2. The benefit of the SASW approach is that the data processing is straightforward and the reliability of the data collected can be judged in real time while on-site, which is particularly important for testing on a railroad application.
3. Due to the scattering from large size ballast aggregates and the effects of crossties, it is difficult to obtain reliable high frequency (greater than 500 Hz) data, which corresponds to a receiver spacing of 2 ft. (0.6 m) or less. For this reason, the property of a thin ballast layer (3 to 4 inches) or the top portion of a thick ballast layer may not be well defined with surface-wave testing using the SASW approach. However, this limitation or bottleneck may be overcome using a hand-held surface-wave testing devices like the Pavement Seismic Property Analyzer (PSPA), which should be modified to the Ballast Seismic Property Analyzer (BSPA). This high frequency problem is less of an issue as the fouling level in the ballast increases and the surface behaves more like a soil.
4. The property of the sub-ballast layers or subgrade of a railroad track bed can be well estimated with SASW testing and BSPA to a depth of about 4 to 5 feet.

5. Numerical analysis with the discrete element approach to model the ballast, e.g., using PFC in the FLAC software package, is needed to understand the pattern of scattering and its effects on seismic wave testing on railroad ballast.
6. Coupling of the receiver and ballast could be further improved to eliminate noise effects caused by the metal spike and magnetic seat, and improve the quality of the recorded time history records.
7. Due to the complexity of the subsurface profiles, the analysis software adopted is not as robust as it should be for a production-level study. An experienced analyst and manual intervention are still needed at this time. This aspect of the system should be improved for future use in the development of the BSPA for practical implementation.

8. References

1. Abdallah, I., Nazarian, S., and Yuan, D. (2005). "Production-Level SASW Reduction Algorithm." *Geo-Frontiers 2005*. Congress, GSP 133. Available at: https://ascelibrary.org/doi/pdf/10.1061/40779%28158%2912.
2. Amiri, H., Nazarian, S., and Fernando, E. (2009). "Investigation of Impact of Moisture Variation on Response of Pavements through Small-Scale Models." *Journal of Materials Civil Engineering*, *21*(10), 553–560.
3. Aouad, M. F., Stokoe, K. H., and Briggs, R. C. (1993). "Stiffness of Asphalt Concrete Surface Layer from Stress Wave Measurements." Transportation Research Record, 1384, 29–35: Washington, DC.
4. Bei, S. (2005). "Effects of Railroad Track Structural Components and Subgrade on Damping and Dissipation of Train Induced Vibration." University of Kentucky Doctoral Dissertation, 312. Available at: https://uknowledge.uky.edu/cgi/viewcontent.cgi?article=1315&context=gradschool_diss.
5. Calderón-Macías, C., and Luke, B. (2010). "Sensitivity Studies of Fundamental and Higher-Mode Rayleigh-Wave Phase Velocities in Some Specific Near-Surface Scenarios." Advances in Near-Surface Seismology and Ground-Penetrating Radar, 185–200.
6. Cox, B., and Wood, C. (2011). "Surface Wave Benchmarking Exercise: Methodologies, Results and Uncertainties." GeoRisk 2011 Conference, GSP 224, *89*(418), 845–866.
7. Foti, S., Parolai, S., Albarello, D., and Picozzi, M. (2011). "Application of Surface-Wave Methods for Seismic Site Characterization." *Surveys in Geophysics*, *32*(6), 777–825.
8. Gucunski, N., and Woods, R. D. (1992). "Numerical simulation of the SASW test." *Soil Dynamics Earthquake Engineering*, *11*(4), 213–227. Available at: https://deepblue.lib.umich.edu/bitstream/handle/2027.42/30325/0000727.pdf?sequence=1.
9. Haskell, N. A. (1953). "The Dispersion of Surface Waves on Multilayered Media." *Bulletin of the Seismological Society of America*, *43*(1), 17–34.
10. Federal Railroad Administration. (2017). "Ground Penetrating Radar Technology Evaluation on the High Tonnage Loop: Phase 1." Technical Report, DOT/FRA/ORD-17/18, p. 32, U.S. Department of Transportation: Washington, DC. Available at: https://www.fra.dot.gov/eLib/details/L19031#p1_z50_gD_y2017_m9.
11. Jones, R. (1962). "Surface wave technique for measuring the elastic properties and thickness of road: theoretical development." *British Journal of Applied Physics*, *13*(1), 21–29.
12. Li, J. (2008). "Study of Surface Wave Methods for Deep Shear-wave Velocity Profiling Applied in the Upper Mississippi Embayment." PhD dissertation: University of Missouri–Columbia.
13. Lu, S., Arnold, R., Farritor, S., Fateh, M., and Carr, G. (2008). "On the Relationship Between Load and Deflection on Railroad Track Structures." Proceedings of the AREMA 2008 Annual Conference: Salt Lake City, UT.

14. Lundqvist, A., and T. Dahlberg. (2005). Load impact on railway track due to unsupported sleepers. Proceedings of the Institution of Mechanical Engineers, Part F: Journal of Rail and Rapid Transit, Vol. 219, 67–77.

15. Mathews, G. F., IV, Mullen, R. I., and Rizos, D. C. (2014). "Studies of the Accuracy Stability and Efficiency of a New Time Integration Scheme for Ballast Modeling Using the Discrete Element Method." Proceedings of the ASME 2014 Joint Rail Conference, Paper No. JRC2014-3869: Colorado Springs, CO.

16. Nazarian, S. (2012). "Shear-wave Velocity Profiling with Surface Wave Methods." Geotechnical Special Publication, 221–240.

17. Nazarian, S., Abdallah, I., Yuan, D., and Ke, L. (1998). "Design Modulus Values Using Seismic Data Collection." Research Report 1780-1, Center for Highway Materials Research, the University of Texas at El Paso. Available at: https://library.ctr.utexas.edu/digitized/texasarchive/phase1/1780-1.pdf.

18. Nazarian, S., Baker, M. R., and Crain, K. (1993). "Development and Testing of a Seismic Pavement Analyzer." Report SHRP H-375, Strategic Highway Research Program. Available at: http://onlinepubs.trb.org/onlinepubs/shrp/SHRP-H-375.pdf.

19. Nazarian, S., and Desai, M. R. (1993). "Automated Surface Wave Method: Field Testing." *Journal of Geotechnical Engineering*, *119*(7), 1094–1111.

20. Nazarian, S., Stokoe, K. H., and Hudson, W. R. (1983). "Use of spectral analysis of surface waves method for determination of moduli and thicknesses of pavement systems." *Transportation Research Record: Journal of the Transportation Research Board*, *930*(930), 38–45.

21. Nazarian, S., and Stokoe, K. H. (1985). "In Situ Determination of Elastic Moduli of Pavement Systems by Spectral-Analysis-of-Surface-Waves Method." Report Number FHWA/TX-87/46, Federal Highway Administration. Available at: https://library.ctr.utexas.edu/digitized/texasarchive/phase2/368-1f-ctr.pdf.

22. Nazarian, S., Tandon, V., Crain, K., and Yuan, D. (1998). "Feasibility Study on Improvements to Dynamic Cone Penetrometer." Report Number TX-97 3903-2. Available at: https://library.ctr.utexas.edu/digitized/texasarchive/phase1/3903-2.pdf.

23. Nicks, J. E. 2009. "The Bump at the End of the Railway Bridge." PhD Thesis, Texas A&M University: College Station, TX.

24. Olson, L. D. (1998). "Application of the SASW Method to Pavements Structures and Geotechnical Sites." Paper P200, Olson Engineering, Inc: Wheat Ridge, CO.

25. Park, C. B. (2011). "Imaging Dispersion of MASW Data—Full vs. Selective Offset Scheme." *Journal of Environmental Engineering* Geophysics, *16*(1), 13–23.

26. Park, B., C, Ivanov, J., Miller, R. D., Xia, J., and Ryden, N. (2002). "Multichannel analysis of surface waves (MASW) for pavement: Feasibility test."

27. Park, C. B., Miller, R. D., and Xia, J. (1999). "Multichannel analysis of surface waves." *Geophysics*, *64*(3), 800–808.

28. Pei, D., Louie, J. N., and Pullammanappallil, S. K. (2008). "Improvements on Computation of Phase Velocities of Rayleigh Waves based on the Generalized R/T Coefficient Method." *Bulletin of the Seismological Society of America*, *98*(1), 280–287.

29. Peters, D. J. (2009). "Frequency Limitations Resulting from Mounted Resonance of an Accelerometer." Connection Technology Center, Inc.

30. Rix, G. J., Lai, C. G., and Foti, S. (2001). "Simultaneous Measurement of Surface Wave Dispersion and Attenuation Curves." *Geotechnical Testing Journal*, *24*(4), 350–358.

31. Ryden, N., Park, C. B., Ulriksen, P., and Miller, R. D. (2002). "Branching of dispersion curve in surface wave testing on pavements." Proceedings of the Symposium on the Application of Geophysics to Engineering and Environmental Problems, 10.4133/1.2927180: Las Vegas, NV.

32. Santamarina, J. C., and Fratta, D. (2005). Discrete Signals and Inverse Problems: An Introduction for Engineers and Scientists. John Wiley & Sons.

33. Federal Railroad Administration. (2015). "Investigation of Railroad Bridge Approach Problems along Heavy Haul Freight Lines." Research Results Report Number RR 15-10. U.S. Department of Transportation: Washington DC. Available at: https://www.fra.dot.gov/eLib/details/L16366#p1_z5_gD_kinvestigation%20of%20railroad%20bridge.

34. Stark, T. D., Wilk, S. T., Dehlin, T. J., Sussmann, T. R., Nazarian, S., and Ho, C. L. (2014, April). "Seismic Testing for Tie-Ballast Interface." Proceedings of ASME 2014 Joint Rail Conference (JRC2014), Paper No. JRC2014-: Colorado Springs, CO. Available at: http://tstark.net/wp-content/uploads/2015/08/CP0123.pdf.

35. Stark, T. D., Wilk, S. T., and Sussmann, T. R. (2015). "Evaluation of Tie Support at Transition Zones." *Transportation Research Record: Journal of the Transportation Research Board*, No.15-2902: Washington, DC.

36. Stokoe, K. H., and Santamarina, J. C. (2000). "Seismic-Wave-based Testing in Geotechnical Engineering." GeoEng 2000: international conference on geotechnical and geological engineering: Melbourne, Australia, 1490–1536.

37. Stokoe, K. H., Wright, G. W., James, A. B., and Jose, M. R. (1994). "Characterization of geotechnical sites by SASW method, Geophysical characterization of sites." ISSMFE Technical Committee #10, Oxford Publishers, New Delhi, 15–25.

38. Su, B. (2005). "Effects of Railroad Track Structural Components and Subgrade on Damping and Dissipation of Train Induced Vibration." PhD Dissertation, University of Kentucky: Lexington, KY. Available at: https://uknowledge.uky.edu/cgi/viewcontent.cgi?article=1315&context=gradschool_diss.

39. Sussmann, T. R., Ebersöhn, W., and Selig, E. T. (2001). "Fundamental Nonlinear Track Load-Deflection Behavior for Condition Evaluation." *Transportation Research Record: Journal of the Transportation Research Board*, Vol. 1742, 61–67.

40. Thomson, W. T. (1950). "Transmission of Elastic Waves through a Stratified Solid Medium." *Journal of Applied Physics*, *21*(2), 89–93.

41. Transportation Technology Corporation, Inc. (2009, August 8). "GPR Evaluation Test Implementation Plan." Test plan for project.

42. Transportation Technology Corporation, Inc. (2013, September 4). "GPR Evaluation and Implementation." *Research Digest*, TD-13-021.

43. Tutumluer, E., Qian, Y., Hashash, Y. Y., Ghaboussi, J., and Davis, D. D. (2011). "Field validated discrete element model for railroad ballast." Proceedings of Annual Conference of the American Railway Engineering and Maintenance-of-Way Association: Minneapolis, MN.

44. Vidale, R. F. (1964). "The dispersion of stress waves in layered media overlaying a half space of lesser acoustic rigidity." PhD thesis, University of Wisconsin.

45. Yu, H., Jeong, D., Marquis, B., and Coltman, M. (2015). "Railroad Concrete Tie Failure Modes and Research Needs." *Transportation Research Record: Journal of the Transportation Research Board*. Transportation Research Board of the National Academies: Washington, DC.

46. Yuan, D., and Nazarian, S. (1992). "Rapid Determination of Layer Properties of Pavements from Surface Wave Method." Transportation Research Record, 1377, 159–166.

47. Yuan, D., and Nazarian, S. (1993). "Automated Surface Wave Method: Inversion Technique." *Journal of Geotechnical Engineering*, *119*(7), 1112–1126.

48. Yuan, D., and Nazarian, S. (2003). "Variation in Moduli of Base and Subgrade with Moisture." Transportation Research Board 82nd Annual Meeting.

49. Zywicki, D. J., and Rix, G. J. (2005). "Mitigation of Near-Field Effects for Seismic Surface Wave Velocity Estimation with Cylindrical Beamformers." *Journal of Geotechnical and Geoenvironmental Engineering*, *131*(8), 970–977. Available at: https://ascelibrary.org/doi/pdf/10.1061/%28ASCE%291090-0241%282005%29131%3A8%28970%29.

Appendix A.
Specifications for Purchasing an SASW System for Track Substructure Assessments

Specifications to create a Spectral Analysis of Surface Waves (SASW) system to measure the in-place shear-wave velocity profile (shear-wave velocity vs. depth) of ballast and track substructure without requiring a borehole is presented below. The shear-wave velocity profile should be determined from an idealized experimental dispersion curve (surface wave velocity vs. wavelength or frequency) obtained from seismic surface wave measurements and SASW techniques through a process called forward modeling or an inversion process.

System Requirements:

- Data acquisition system with the following minimum requirements:
  - Airplane transportable
  - Minimum of four input channels
  - Capable of capturing up to 100,000 samples per channel per second
  - 16-bit resolution or equivalent
  - Adjustable pre-triggering delay
  - Adjustable number of signals to be averaged
  - Capable of accepting and rejecting the last set of time records collected
  - Capable of display of the waveforms collected in real time during testing
  - A four-channel signal analyzer (Tektronix 2630) and a National Instrument DAQ model 6062E (see Figure A.1)
- Seismic receiver assembly with the following minimum requirements:
  - Minimum of four accelerometers with appropriate signal conditioning units
  - Appropriate mounting system to attach the accelerometers securely to the ballast
  - Responsive to frequencies of up to 10 kHz
  - Sensitivity of 1 volt/g or better
  - Several sets of accelerometers (including PCB 308B02 with frequency range of 3 Hz to 3 kHz) and Mark Products 4.5 Hz geophones (see Figure A.2)
  - A metal spike with removable magnetic seat for receiver mounting (see Figure A.3)
- Assorted electromagnetic, mechanical, or drop weight energy sources to generate surface waves with a frequency from 10 Hz to 2 kHz
  - Impact energy sources (sledgehammers and kettlebell weight see Figure A.4.
- Reduction software with the following minimum requirements
  - Capable of providing the averaged phase information of the transfer functions and coherence functions of each pair of receivers in real time during testing

- Capable of providing a dispersion curve from each set of receivers as selected by the user
- Capable of providing an idealized dispersion curve from the individual dispersion curves selected by the user
- Capable of providing a shear-wave velocity profile that represents the idealized dispersion curve by overlapping a theoretical dispersion curve over the idealized dispersion curve.

Capable of estimating the shear modulus, and Young's modulus from the recorded shear-wave velocity of each layer.

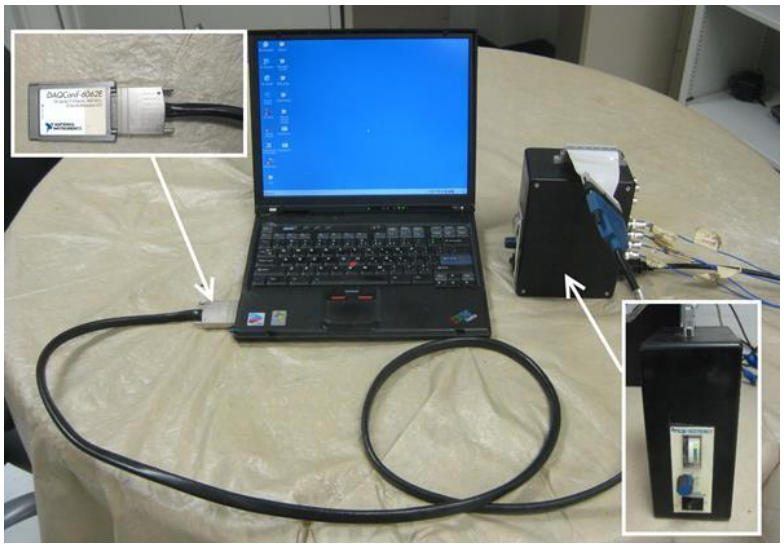

Figure A.1. Data Acquisition Hardware: A National Instrument DAQ Model 6062E (Top Inset) and an Interconnection Box with PCB Signal Conditioner (Bottom Inset)

Figure A.2. Geophone and Accelerometer

Figure A.3. Accelerometer, Magnetic Seat, and Metal Spike

Figure A.4. Impact Energy Sources (2-oz Ball-Peen Hammer, 3 lb. Sledgehammer, 10 lb. Sledgehammer and 30 lb. Kettlebell Weight)

Appendix B.
User's Guide to Operate SASW System for Track Substructure Assessments

This appendix contains the following three steps required for using the SASW system:

1. Setting up field instruments and making measurements
2. Acquiring data to construct a dispersion curve, and
3. Analyzing the dispersion data to estimate the shear-wave velocity profile and to compute the substructure modulus profiles

B.1 Field Setup

Seismic Receiver Placement:

- Mark the locations of the receivers along a straight line (see Figure B.1).
- Drive the metal spikes into the ballast at the marked locations with a hammer until the spikes are in firm and secure contact with the ballast (see Figure B.2).
- Secure each accelerometer to the spike with a magnetic coupling seat or other coupling agent (see Figure B.1 inset).

Energy Source Preparation

- Mark the source location so it is in line with the seismic receiver array (see Figure B.1).
- Secure a metal plate (the source for seismic signals) into the ballast with a hammer such that the plate has firm contact with the ballast to transmit the energy (see Figure B.1 inset).
- Measure the actual distances of the various receivers from the energy source.

Data Acquisition Hardware setup

- Connect the interconnection box with the computer through a cable consisting of the Data Acquisition (DAQ) card (see Figure B.3).
- Power up the interconnection box and make sure the interconnection box has established communication with the computer before trying to collect data.
- Assemble the data acquisition hardware as recommended by the manufacture (see Figure B.3).
- Connect the seismic receivers to the data acquisition system through the interconnection box.
- Ensure proper connection of the receivers to the data acquisition system as recommended by the manufacturer.

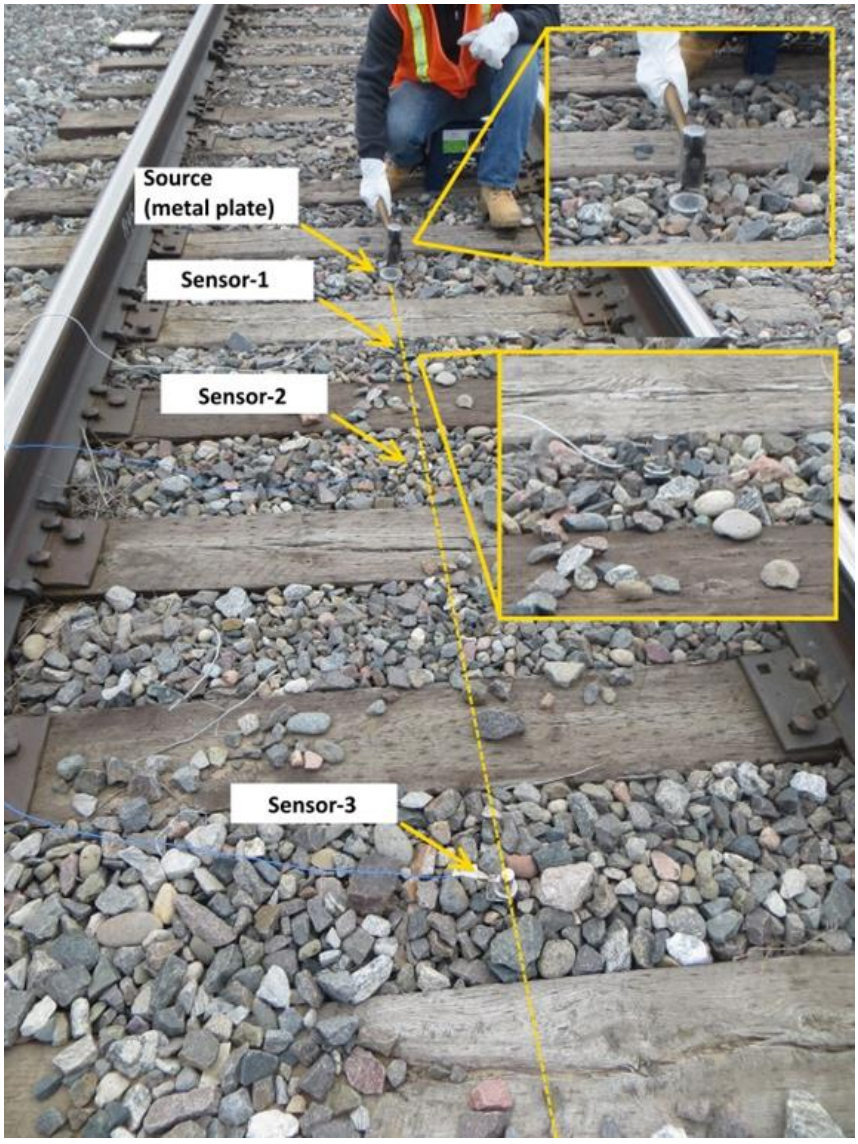

Figure B.1. Source-Receivers Setup for an SASW Test in Active Track

Figure B.2. Driving Spikes into Ballast to Couple Receivers to Ballast

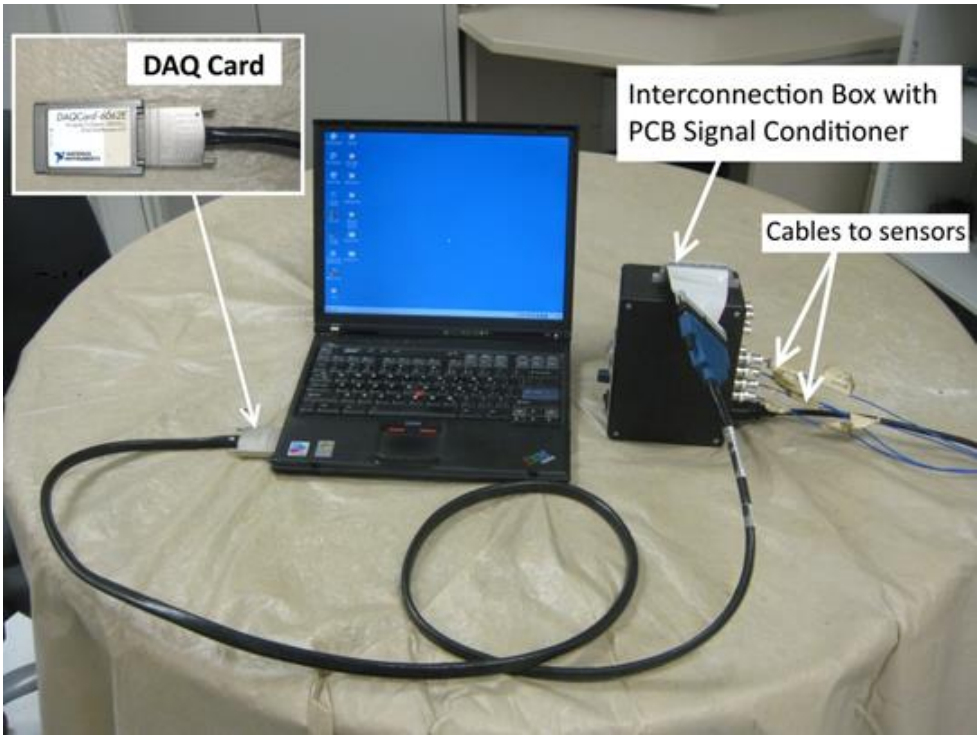

Figure B.3. Data Acquisition Hardware with an Operation PC

B2. Acquiring Data and Field Testing

1.1 Equipment setup and preliminary testing

- Ensure the DAQ system sampling parameters are set properly.
  - Sampling frequency: The number of samples per unit of time (usually in Hz or sample/sec). The following sampling frequencies are recommended:
    - 2,000 Hz when the spacing of receiver pairs is less than 5 ft
    - 1,000 Hz when the spacing of receiver pairs is less than 10 ft
    - 500 Hz when the spacing of receiver pairs is greater than 10 ft
  - Pre-trigger Delay: The time lag between the initiation of recording and the arrival of seismic energy. A value of 10% of the record duration is recommended.
  - Number of Averages: The number of effective hammer energy hits (impacts) to generate seismic signals should be at least five effective hits to achieve representative dispersion curves (see Section 4).
  - Trigger Conditions: The conditions that have to be satisfied before the DAQ system starts collecting test data. The trigger conditions should be set by trial and error but the following recommendations can be helpful:
    - Trigger amplitude: The amount of energy in volts that should be exceeded during seismic testing. A value of 15% of the maximum voltage received by the first accelerometer is recommended.
    - Trigger polarity: The sign associated with the trigger amplitude (i.e., positive voltage or negative voltage). Consult with the manufacturer; however, the typical recommended value is negative for plotting purposes.

1.2 Data collection and pre-reduction

- Select the appropriate hammer (see Section 4).
- Strike the hammer on the metal plate (see Figure B.1).
- Verify that the time domain signals are captured by the DAQ system from all receivers (see Figure B.4), with Receiver 1 (R1), Receiver 2 (R2), Receiver 3 (R3), and Receiver 4 (R4).
- Review the time records for abnormal noise. Discard the records if the noise is not acceptable, i.e., the time history plots looks different than the time histories in Figure B.4.
- Repeat the previous three steps until the pre-specified number of effective hits is reached.

Follow the manufacturer's recommendation for generating and viewing the phase spectra and coherence functions. Review the average phase spectra and coherence functions from the collected time records. Examples of acceptable results are shown in Figure B.5.

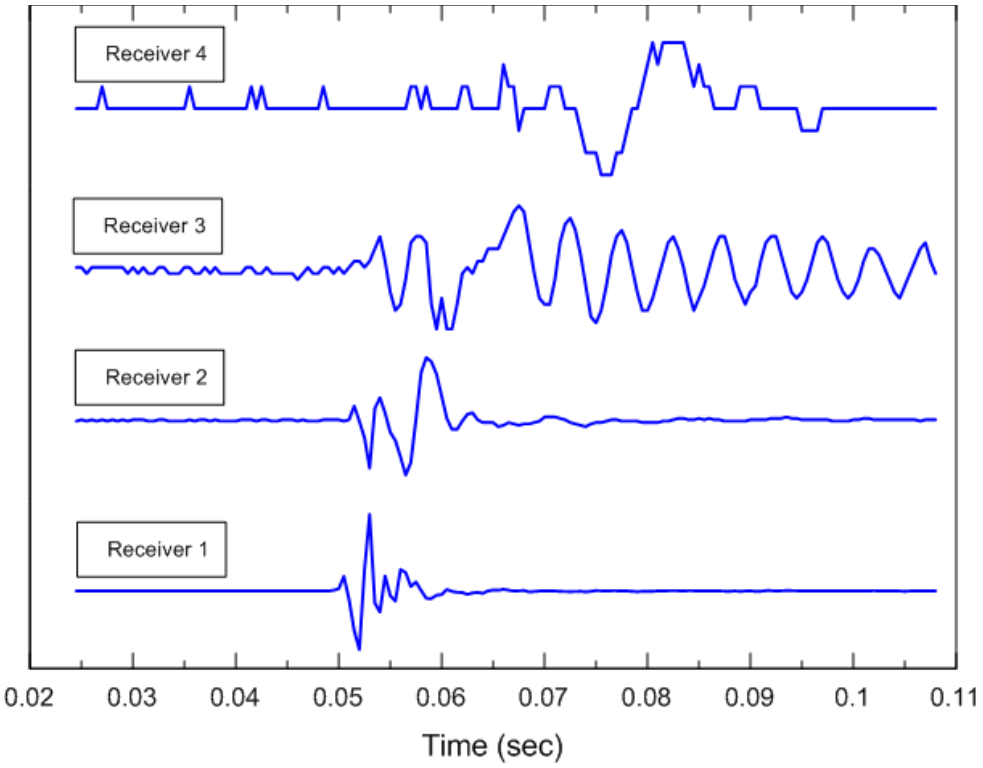

Figure B.4. Time Records from Four Receivers in an SASW Test

B.3 Data Reduction

Data reduction for the data obtained in Figure B.4 and Figure B.5 should include the following two steps:

- Construction of dispersion curve for each individual receiver spacing
- Construction of representative dispersion curve by combining all of the dispersion curves from each receiver for analysis (inversion process)

1.1 Construction of dispersion curve for an individual receiver spacing

- Unwrap the phase spectra following the manufacturer's recommendation (an example is shown in Figure B.5)
- Review the corresponding coherence plot to select the acceptable range of frequencies that should be used in the dispersion curve (see Figure B.6). The following recommendations may be helpful:
  - Use unwrapped phase angles in the range of 180 and 720 degrees
  - Avoid areas of the phase spectra with coherence values that are less than 0.95
- Convert the unwrapped phase spectrum in the range of acceptable coherence to a dispersion curve (i.e., phase velocity vs. wavelength or frequency plot) following the manufacturer's recommendation (an example is shown in Figure B.7).

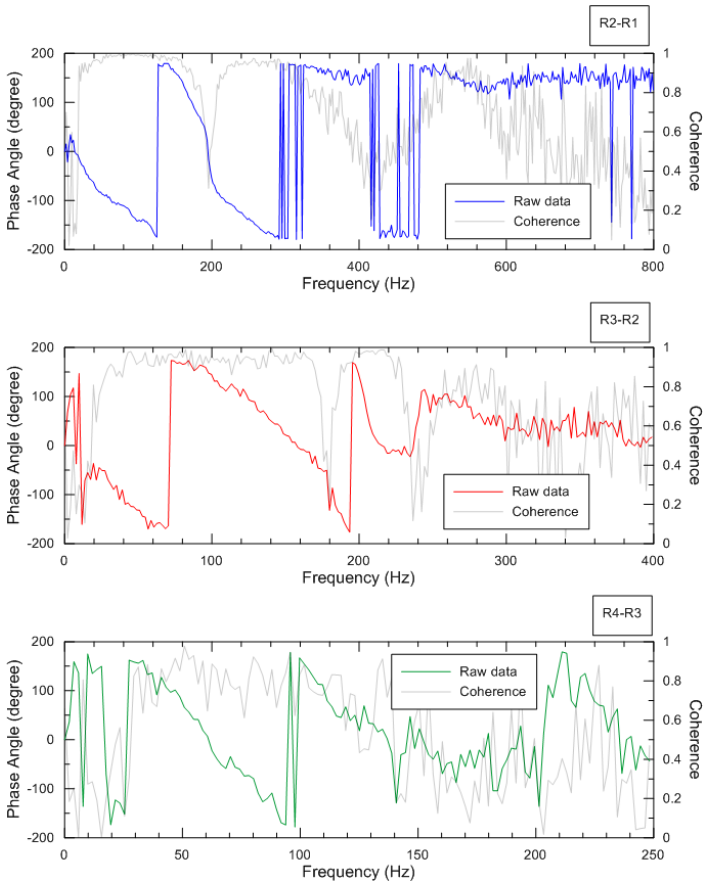

Figure B-5. Average Wrapped Phase Spectra and Corresponding Coherence Functions Derived from the Time Records Shown in Figure B.4. The Labels R1, R2, R3 and R4 Represent Receiver 1, 2, 3 and 4 in Figure B.4

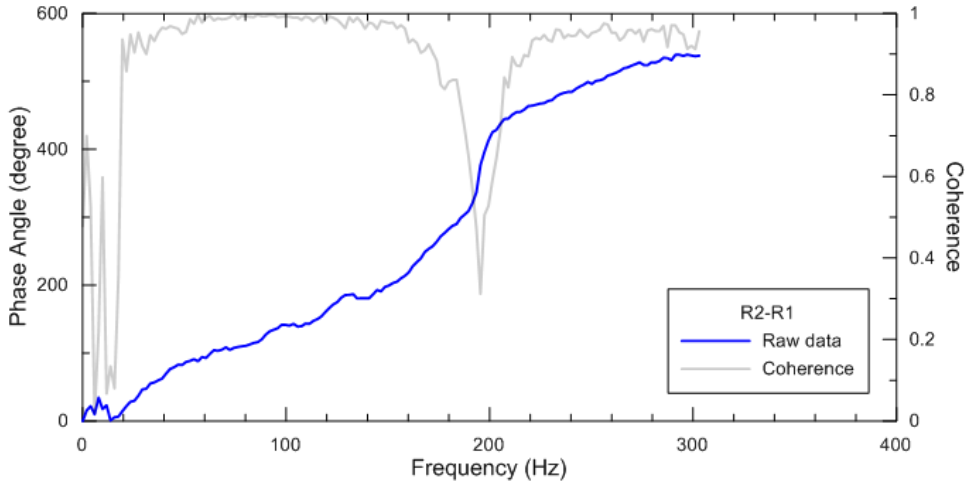

Figure B-6. Average Unwrapped Phase Spectrum and Corresponding Coherence Function from Wrapped from Receiver Pair R2-R1 in Figure B-4

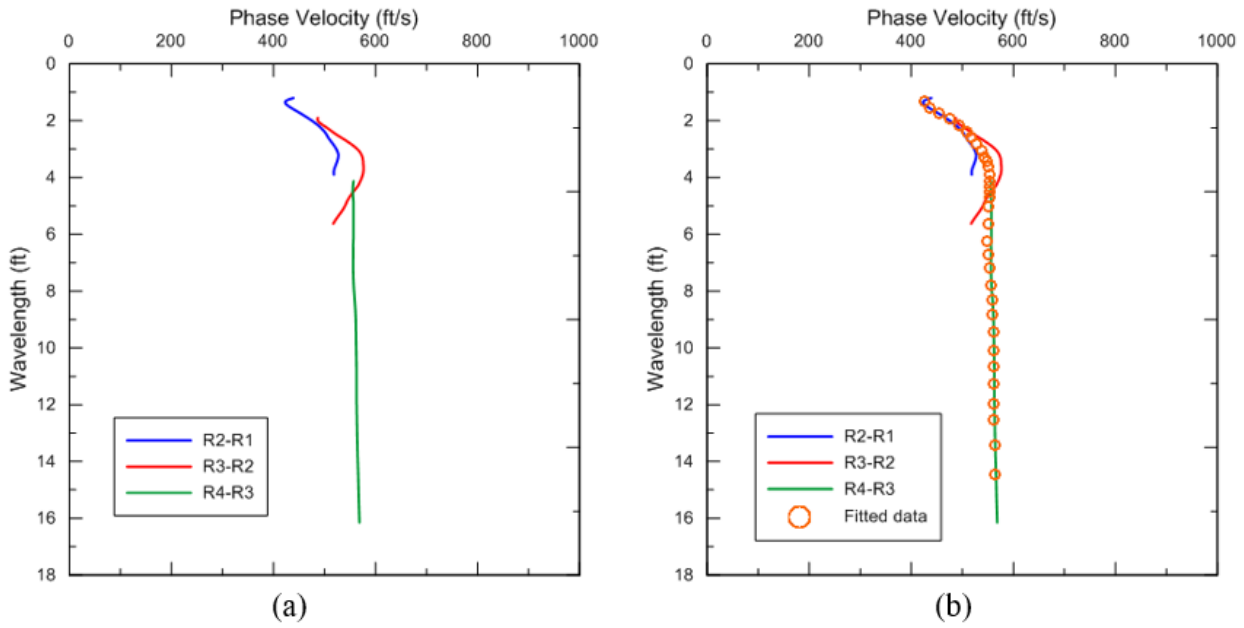

Figure B-7. Data Reduction: (a) Dispersion Curves Obtained from Unwrapping Phase Spectrums Shown in Figure B-3 and (b) a Representative Dispersion Curve Obtained from a Curve Fitting Process

Construction of dispersion curve for representative dispersion curve for analysis

- Fit a curve to the dispersion curves obtained from the individual receiver pairs to obtain a representative dispersion curve following the manufacturer's recommendation. The following recommendations can be helpful:
    - Use a robust curve fitting algorithm that may or may not use the coherence functions as a weighting function
    - Visually inspect the representative dispersion curve to ensure it is a good representation of all of the dispersion curves obtained from the individual receiver pairs
- Digitize the representative dispersion curve to 30 to 50 dispersion points for use in inversion following the manufacturer's recommendation. The following recommendation can be helpful:
    - Consider more data points corresponding to shorter wavelengths (higher frequencies).

B.2.4 Data Analysis (Inversion)

Utilize an inversion program to obtain the shear-wave velocity profile and other relevant stiffness parameters through the following steps.

1.2 Prepare Initial Input

- Develop an initial (a priori) subsurface model with layers representing the different soil types and assign each sublayer a shear-wave velocity, Poisson's ratio, and mass

density as well as thickness to each layer. The following recommendations may be helpful:

- The number of sublayers and the thickness of each layer should be determined based on the available priori information from the site, e.g., old boring log.
- The last or deepest sublayer is typically a half-space.
- The number of sublayers should be minimized (usually not more than six).
- Thick ballast layers (greater than 12 inches) should be modeled as two layers.
- The shear-wave velocity for the top layer can be estimated based on the phase velocities of the shortest wavelengths (highest frequencies).
- Limit the total thickness of the layers to one-half to one-third of the longest wavelength.

1.3 Select Control Parameters

- Set up the control parameters for the inversion process as recommended by the developer of the algorithm, i.e., review appropriate technical paper. However, the following recommendations can be helpful for a more robust inversion:
  - Specify the type of dispersion curve from its shape
    - Normal when the phase velocity increases with wavelength
    - Inverse when phase velocity decreases with wavelength
- Maintain sublayer thickness, Poison's ratio, and density of each layer constant and only vary the shear-wave velocity assumed for each layer.
- Set the maximum number of iterations (a criterion that stops the inversion when the specified cycles of iteration are exceeded).
- Maintain a reasonable convergence criterion (when the iteration stops). A 5% relative standard error is recommended for this purpose. This means the estimated dispersion is within 5% of the representative dispersion curve that was obtained from all of the measured dispersion curves.
- Set the convergence gradient (maximum percent change in the shear-wave velocity of each sublayer between iterations) to a reasonable value, a slower gradient with more number of iterations is preferred.
- Check the results for reasonableness given the non-unique nature of the inversion process.

1.4 Presentation of the Results

- At a minimum present the results in the following formats:
  - Show a graphical comparison of the measured/representative dispersion curve and matched dispersion curve (calculated from the assumed shear-wave velocity profile) to illustrate the goodness of the match (an example is shown in Figure B-8(a)).

- Show shear-wave velocity profile with depth (an example is shown in Figure B-8(b)).
- Show shear modulus and/or Young's modulus profiles, as project requires, calculated using matched dispersion curve, assumed or measured values of Poisson's ratio and mass density (see Equations 1 and 2) (an example is shown in Figure B-9).

Shear strength profile using an empirical relationship to be selected by the engineer based on the local experience. A number of relationships have been proposed in the literature based on empirical correlations. The research team cannot endorse anyone at this time due to lack of experience with the railroad structure. No such relationship exists for ballast and sub-ballast materials.

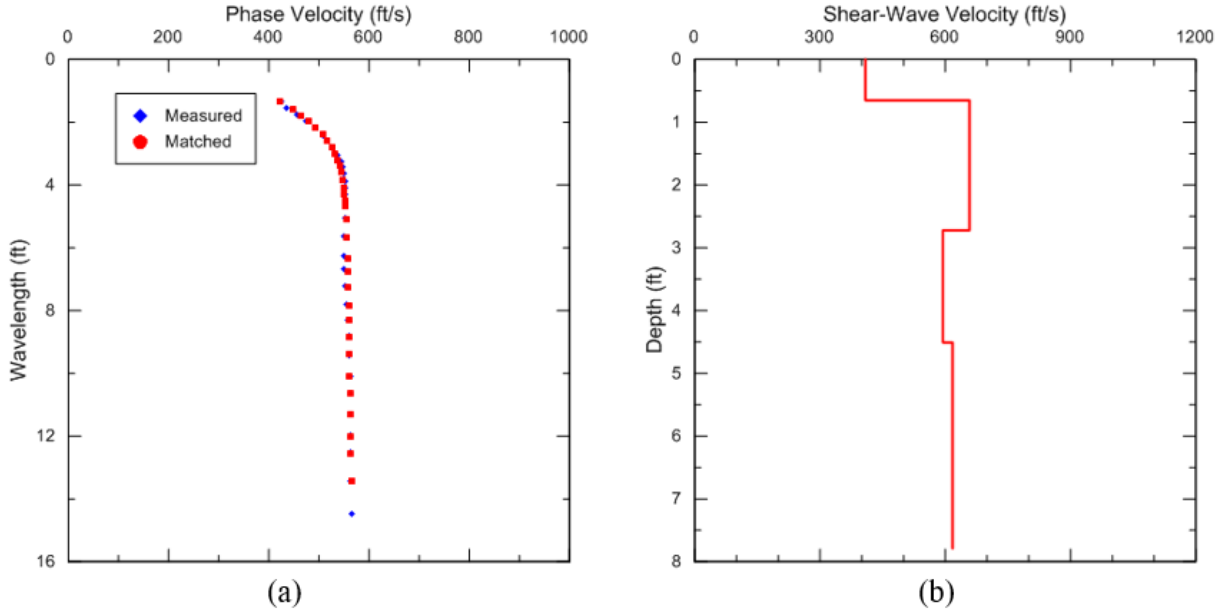

Figure B-8. Diagrams Showing: (a) Comparison of Measured (See Figure B-7(b)) and Matched Dispersion Curves and (b) Derived Shear-Wave Velocity Profile from Measured or Representative Dispersion Curve Own in Figure B-7(b)

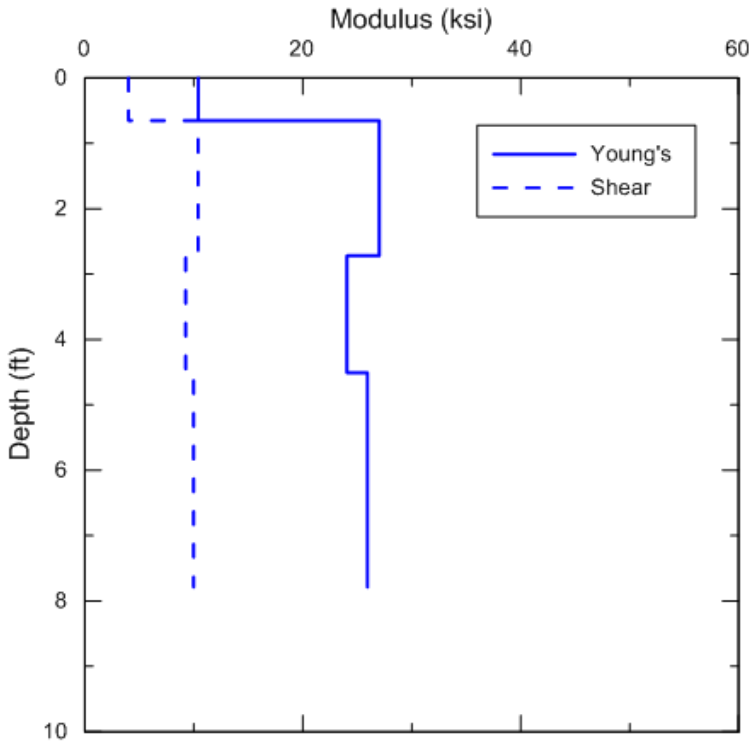

Figure B-9. Shear Modulus and Young's Modulus Profiles Computed from the Shear-Wave Velocity Profile Shown in Figure B-8

Appendix C.
Measured Modulus Profiles

Test location and date	Sites	Site Feature
El Paso, TX (Jul 2013)	Site 1 (Jobe)	

Layer	Inversion parameters			Results		
	Thickness (ft)	Density (pcf)	Poisson's ratio	V_S	G	E
Layer 1	0.5	110	0.3	669.0	10.7	27.9
Layer 2	0.5	110	0.3	757.0	13.7	35.7
Layer 3	1.4	120	0.3	975.0	24.9	64.7
Layer 4	3.8	120	0.3	768.0	15.4	40.1
Layer 5	4.5	120	0.3	840.0	18.5	48.0
Halfspace	NA	120	0.3	665.0	11.6	30.1

V_s = shear-wave velocity in ft/sec, G=shear modulus in ksi and E=Young's modulus in ksi

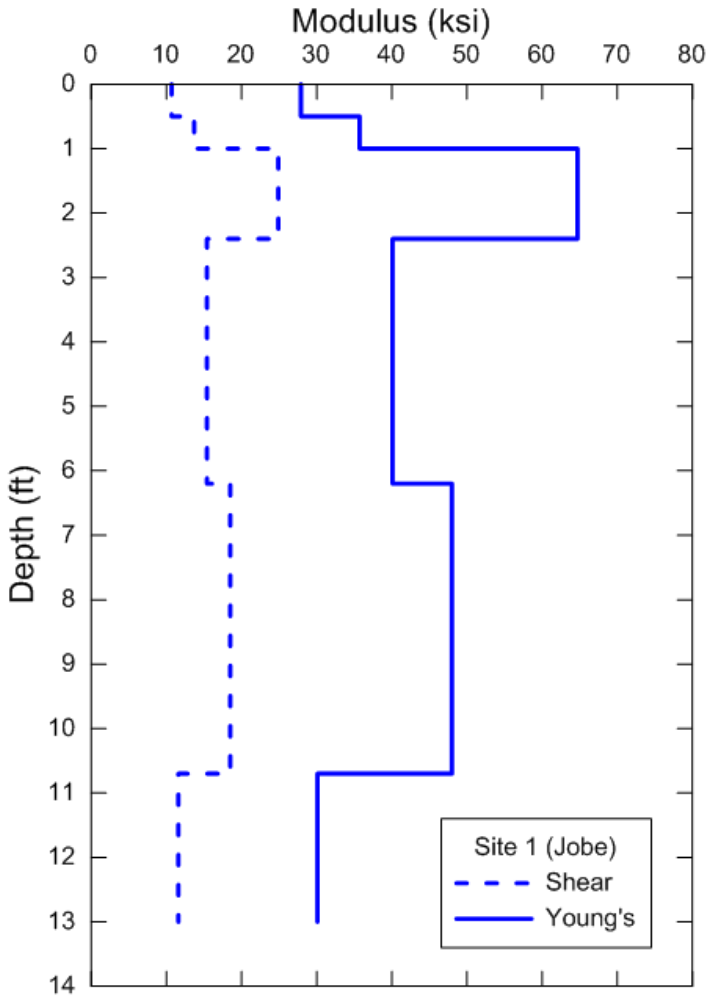

Test location and date	Site	Site Feature
Pueblo, CO (Oct 2013)	Site 9	Wet

Layers	Inversion parameters			Results		
	Thickness (ft)	Density (pcf)	Poisson's ratio	V_s	G	E
Layer 1	0.7	110	0.3	738.25	13.1	34.0
Layer 2	0.6	110	0.3	681.80	11.2	29.0
Layer 3	1.6	120	0.3	528.38	7.3	19.0
Halfspace	NA	120	0.3	514.28	6.9	18.0

V_s =shear-wave velocity in ft/sec, G=shear modulus in ksi and E=Young's modulus in ksi

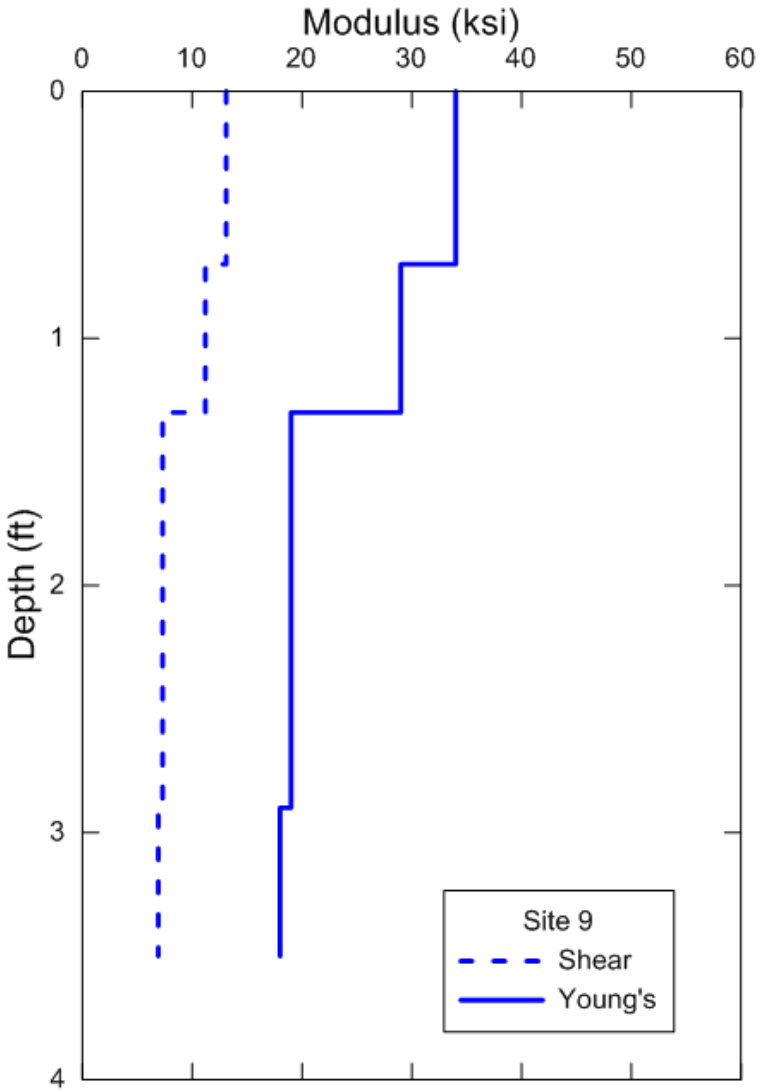

Test location and date	Site	Site Feature
Pueblo, CO (Oct 2013)	Site 8	

Layers	Inversion parameters			Results		
	Thickness (ft)	Density (pcf)	Poisson's ratio	V_s	G	E
Layer 1	0.8	110	0.3	551.87	7.3	19.0
Layer 2	1.2	110	0.3	716.20	12.3	32.0
Halfspace	NA	120	0.3	696.34	12.7	33.0

V_s =shear-wave velocity in ft/sec, G=shear modulus in ksi and E=Young's modulus in ksi

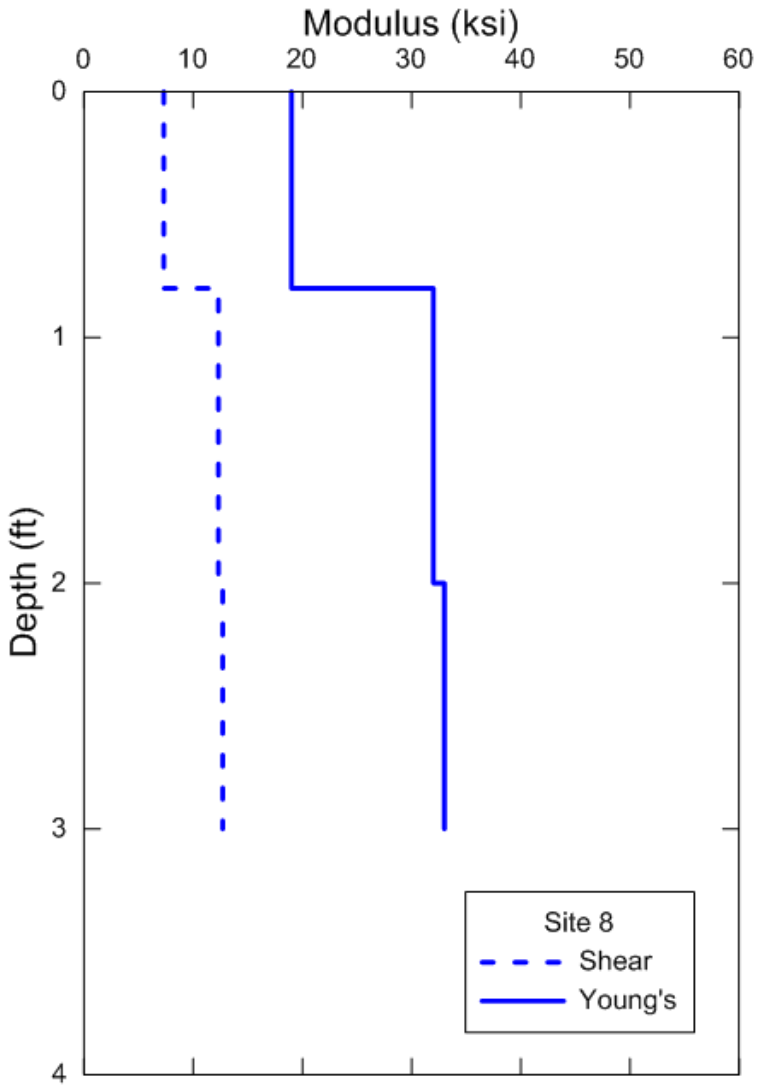

Test location and date	Site	Site Feature
Pueblo, CO (Oct 2013)	Site 29	Wood tie – Intact HMA
		Concrete tie – Failed HMA

Sections	Layers	Inversion parameters			Results		
		Thickness (ft)	Density (pcf)	Poisson's ratio	V_s	G	E
Wood tie Intact HMA	Layer 1	0.9	110	0.3	790.67	15.0	39.0
	Layer 2	1.0	110	0.3	716.20	12.3	32.0
	Layer 3	2.4	120	0.3	618.09	10.0	26.0
	Layer 4	2.9	120	0.3	618.09	10.0	26.0
	Halfspace	NA	120	0.3	629.87	10.4	27.0
Concrete tie Failed HMA	Layer 1	1	110	0.3	780.46	14.6	38.0
	Layer 2	1.1	110	0.3	657.87	10.4	27.0
	Layer 3	2	120	0.3	514.28	6.9	18.0
	Layer 4	3	120	0.3	528.38	7.3	19.0
	Halfspace	NA	120	0.3	514.28	6.9	18.0

V_s =shear-wave velocity in ft/sec, G=shear modulus in ksi and E=Young's modulus in ksi

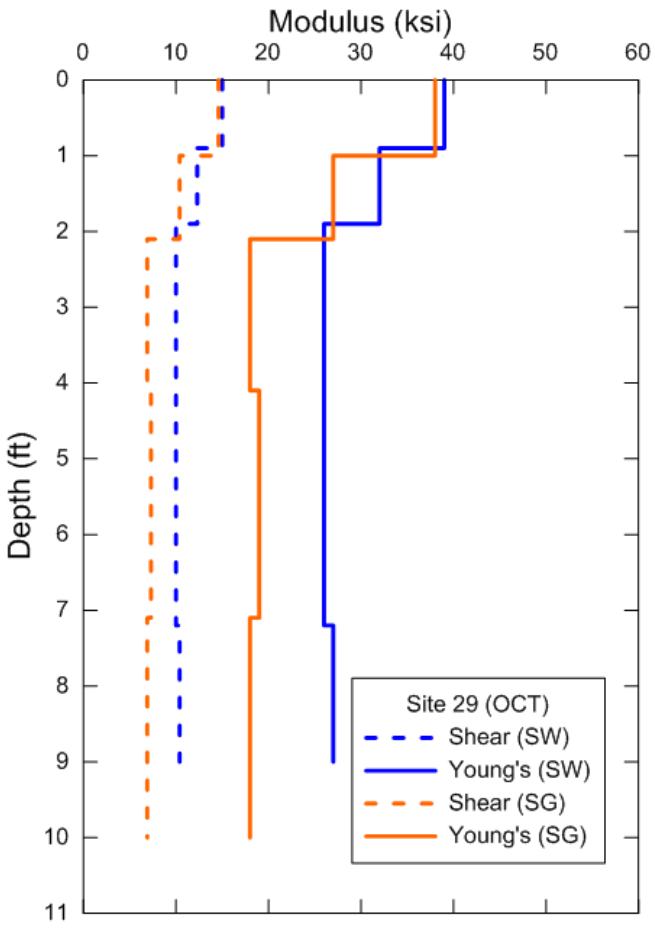
Modulus (ksi)
0
10
20
30
40
50
60
Depth (ft)
0
1
2
3
4
5
6
7
8
9
10
11
Site 29 (OCT)
Shear (SW)
Young's (SW)
Shear (SG)
Young's (SG)

Test location and date	Site	Site Feature
Pueblo, CO (Oct 2013)	Site 36	0 % Fouling
		10 % Fouling
		20 % Fouling

Sections	Layers	Inversion parameters			Results		
		Thickness (ft)	Density (pcf)	Poisson's ratio	V_s	G	E
0 % Fouling	Layer 1	0.7	110	0.3	681.80	11.2	29.0
	Layer 2	1.5	110	0.3	930.37	20.8	54.0
	Layer 3	1.2	120	0.3	907.11	21.5	56.0
	Halfspace	NA	120	0.3	674.91	11.9	31.0
10 % Fouling	Layer 1	1.0	110	0.3	490.35	5.8	15.0
	Layer 2	1.3	110	0.3	727.31	12.7	33.0
	Layer 3	1.1	120	0.3	747.24	14.6	38.0
	Halfspace	NA	120	0.3	641.42	10.8	28.0
20 % Fouling	Layer 1	0.9	110	0.3	669.95	10.8	28.0
	Layer 2	1.3	110	0.3	930.37	20.8	54.0
	Layer 3	1.0	120	0.3	785.58	16.2	42.0
	Halfspace	NA	120	0.3	663.94	11.5	30.0

V_s =shear-wave velocity in ft/sec, G=shear modulus in ksi and E=Young's modulus in ksi

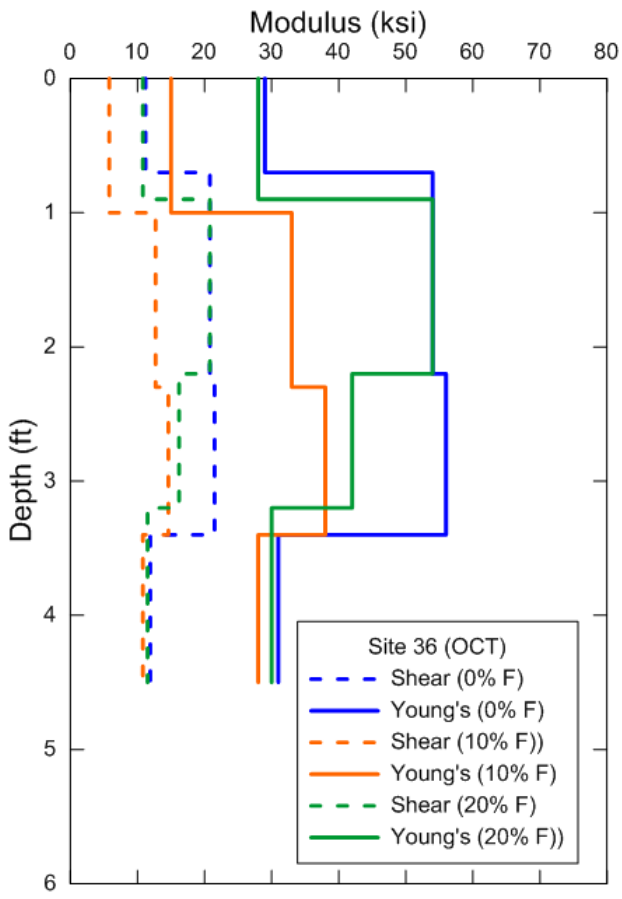

Test location and date	Site	Site Feature
Pueblo, CO (Oct 2013)	Site 3	Granite ballast

Layers	Inversion parameters			Results		
	Thickness (ft)	Density (pcf)	Poisson's ratio	V_s	G	E
Layer 1	1.2	110	0.3	566.21	7.7	20.0
Layer 2	1.7	110	0.3	727.31	12.7	33.0
Layer 3	4.2	120	0.3	785.58	16.2	42.0
Halfspace	NA	120	0.3	685.71	12.3	32.0

V_s =shear-wave velocity in ft/sec, G=shear modulus in ksi and E=Young's modulus in ksi

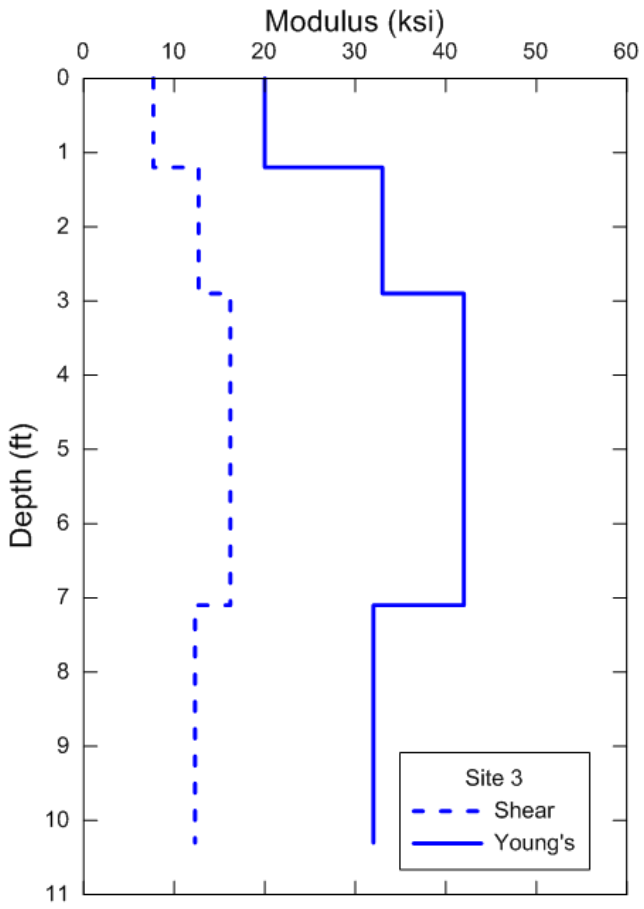

Test location and date	Site	Site Feature
Pueblo, CO (Apr 2014)	Site 36	10 % Fouling

Layers	Inversion parameters			Results		
	Thickness (ft)	Density (pcf)	Poisson's ratio	V_s	G	E
Layer 1	0.8	110	0.3	610.32	8.9	23.2
Layer 2	1.2	110	0.3	748.57	13.4	35.0
Layer 3	1.7	120	0.3	769.84	15.5	40.3
Halfspace	NA	120	0.3	749.48	14.7	38.2

V_s =shear-wave velocity in ft/sec, G=shear modulus in ksi and E=Young's modulus in ksi

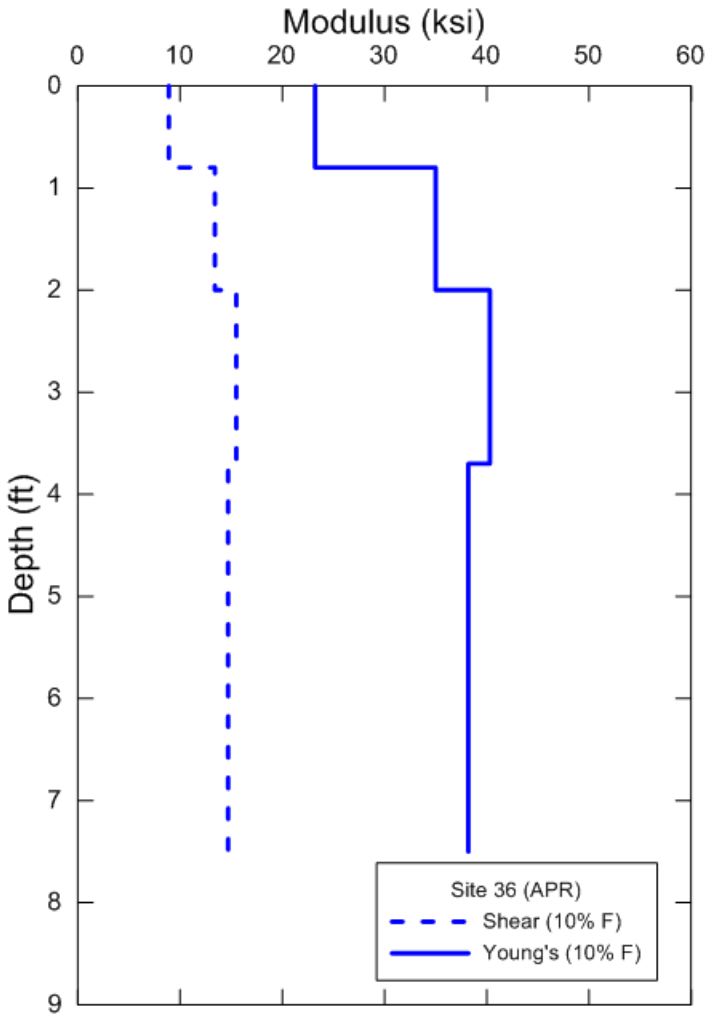
Modulus (ksi)
0
10
20
30
40
50
60
Depth (ft)
0
1
2
3
4
5
6
7
8
9
Site 36 (APR)
Shear (10% F)
Young's (10% F)

Test location and date	Site	Site Feature
Pueblo, CO (Apr 2014)	Site 29	Wood tie – Intact HMA
		Concrete tie – Failed HMA

Sections	Layers	Inversion parameters			Results		
		Thickness (ft)	Density (pcf)	Poisson's ratio	V_s	G	E
Concrete Tie Failed HMA	Layer 1	1.2	110	0.3	582.07	8.1	21.1
	Layer 2	0.8	110	0.3	816.62	16.0	41.6
	Layer 3	1.0	120	0.3	565.26	8.4	21.7
	Halfspace	NA	120	0.3	580.56	8.8	22.9
Wood Tie Intact HMA	Layer 1	0.7	110	0.3	482.70	5.6	14.5
	Layer 2	1.2	110	0.3	734.52	12.9	33.7
	Layer 3	0.7	120	0.3	762.21	15.2	39.5
	Halfspace	NA	120	0.3	626.36	10.3	26.7

V_s =shear-wave velocity in ft/sec, G=shear modulus in ksi and E=Young's modulus in ksi

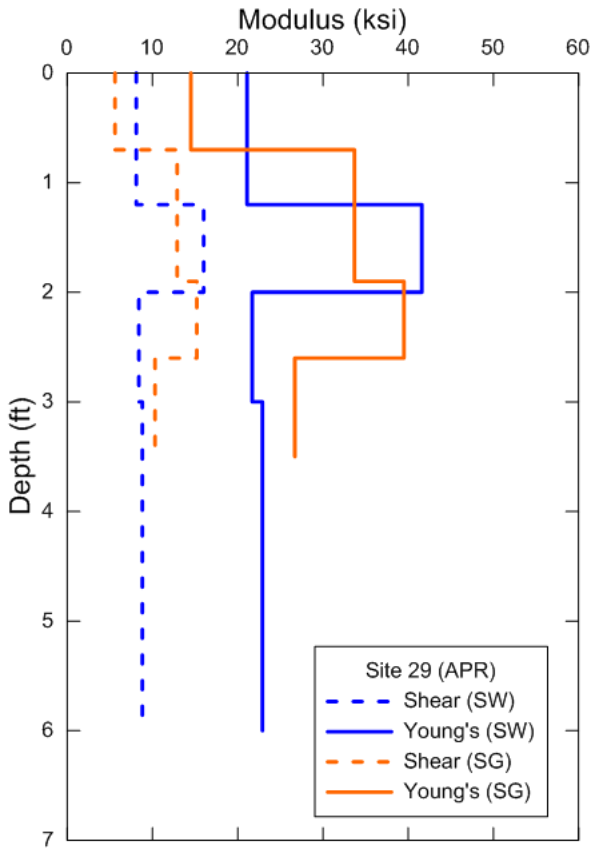

Test location and date	Sites	Site Feature
Ogallala, NE (Apr 2014)	Site 1 (Mile Post 49.75)	Clean Ballast
	Site 2 (Mile Post 62.9)	Fouled Ballast
	Site 3 (Mile Post 72)	Partially Fouled Ballast

Sections	Layers	Inversion parameters			Results		
		Thickness (ft)	Density (pcf)	Poisson's ratio	V_s	G	E
Site 1 (Mile Post 49.75)	Layer 1	0.8	110	0.3	674.34	10.9	28.4
	Layer 2	1.7	110	0.3	871.38	18.2	47.4
	Layer 3	2.5	120	0.3	838.85	18.4	47.9
	Halfspace	NA	120	0.3	816.18	17.4	45.3
Site 2 (Mile Post 62.9)	Layer 1	0.8	110	0.3	489.87	5.8	15.0
	Layer 2	1.7	110	0.3	633.81	9.6	25.1
	Layer 3	2.5	120	0.3	558.59	8.2	21.2
	Halfspace	NA	120	0.3	612.45	9.8	25.5
Site 3 (Mile Post 72)	Layer 1	0.8	110	0.3	668.18	10.7	27.9
	Layer 2	1.7	110	0.3	802.96	15.5	40.2
	Layer 3	2.5	120	0.3	728.92	13.9	36.2
	Halfspace	NA	120	0.3	783.59	16.1	41.8

V_s =shear-wave velocity in ft/sec, G=shear modulus in ksi and E=Young's modulus in ksi

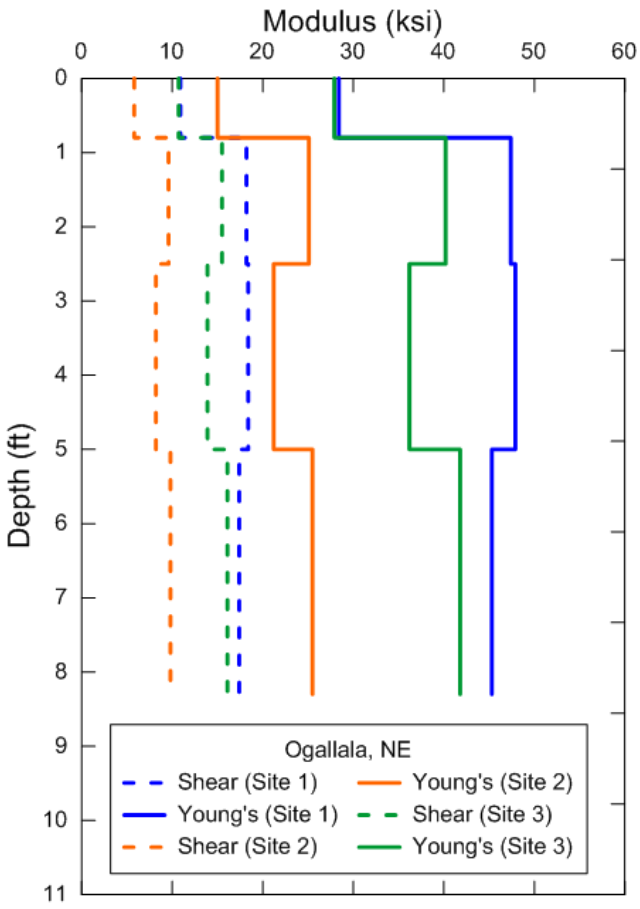
Modulus (ksi)
0
10
20
30
40
50
60
Depth (ft)
0
1
2
3
4
5
6
7
8
9
10
11
Ogallala, NE
Shear (Site 1)
Young's (Site 1)
Shear (Site 2)
Young's (Site 2)
Shear (Site 3)
Young's (Site 3)

Test location and date	Sites	Site Feature
Gilbertsville, KY (June 2014)	Site A (about 50 ft west of the bridge)	
	Site B (next to the bridge)	

Sections	Layers	Inversion parameters			Results		
		Thickness (ft)	Density (pcf)	Poisson's ratio	V_s	G	E
Site A	Layer 1	1.0	110	0.3	592.22	8.4	21.9
	Layer 2	0.7	110	0.3	723.99	12.6	32.7
	Layer 3	1.3	120	0.3	654.69	11.2	29.2
	Halfspace	NA	120	0.3	671.86	11.8	30.7
Site B	Layer 1	1.0	110	0.3	658.60	10.4	27.1
	Layer 2	0.7	110	0.3	896.15	19.3	50.1
	Layer 3	1.3	120	0.3	779.57	15.9	41.4
	Halfspace	NA	120	0.3	725.39	13.8	35.8

V_s =shear-wave velocity in ft/sec, G=shear modulus in ksi and E=Young's modulus in ksi

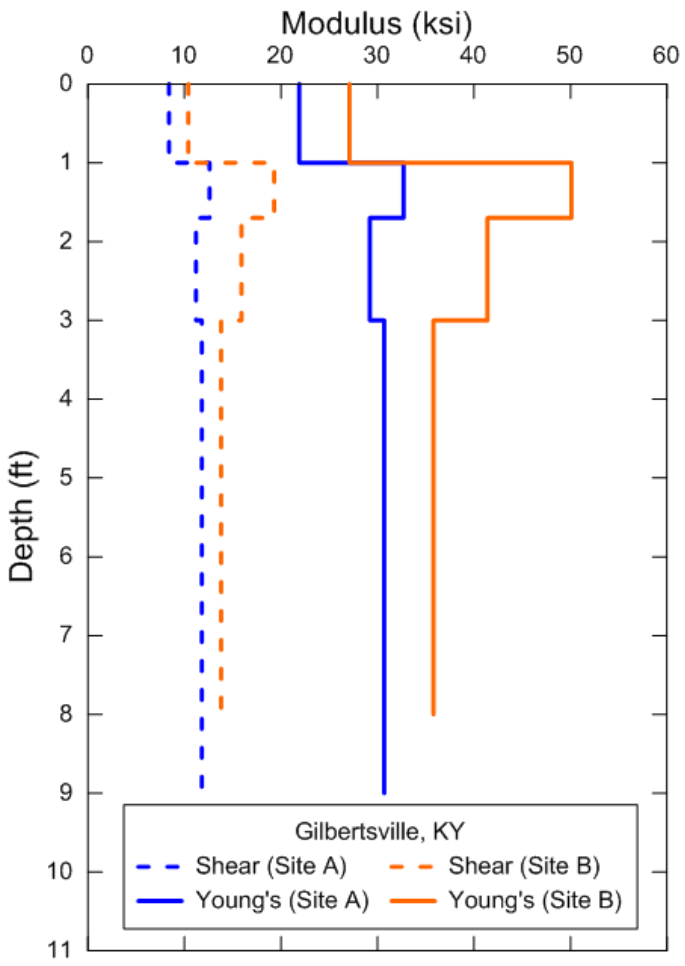
Modulus (ksi)
0
10
20
30
40
50
60
Depth (ft)
0
1
2
3
4
5
6
7
8
9
10
11
Gilbertsville, KY
Shear (Site A)
Shear (Site B)
Young's (Site A)
Young's (Site B)

Abbreviations and Acronyms

BSPA	Ballast Seismic Property Analyzer
CBR	California Bearing Ratio
CF	Concrete Tie – Failed HMA
FAST	Facility for Accelerated Service Testing
FLAC	Fast Lagrangian Analysis of Continuum
DCP	Federal Motor Vehicle Safety Standards
FEM	Finite Element Method
HTL	High Tonnage Loop
NI	National Instrument
PFC	Particle Flow Code
PSPA	Pavement Property Seismic Analyzer
ν	Poisson's Ratio
Pcf	Pounds Per Cubic Foot
G	Shear Modulus
V_s	Shear-Wave Velocity
SASW	Spectral Analysis of Surface Waves
WI	Timber Tie – Intact HMA
TTCI	Transportation Technology Center, Inc.
UIUC	University of Illinois at Urbana-Champaign
USW	Ultrasonic Surface Wave
UTEP	University of Texas at El Paso